

University of California, Los Angeles  
Mechanical, Aerospace and Nuclear Engineering Department

**LABORATORY SIMULATION OF THE  
EFFECT OF ROCKET THRUST ON  
A PRECESSING SPACE VEHICLE**

**FINAL REPORT**

*Participating Students:*

Oscar Alvarez  
Henry Bausley  
Sam Cohen  
Miguel Falcon-Martin  
Gary Furumoto, Report Editor  
Asikin Horio  
David Levitt  
Amy Walsh

*Instructor:*

R. X. Meyer, Adjunct Professor

Sponsored by NASA/USRA

May 22, 1990

(NASA-CR-186681) LABORATORY SIMULATION OF  
THE EFFECT OF ROCKET THRUST ON A PRECESSING  
SPACE VEHICLE Final Report (California  
Univ.) 118 p

N90-25182

CSCL 21H

Unclas  
0289178

G3/20

## Abstract

Ground tests of solid propellant rocket motors have shown that metal-containing propellants produce various amounts of slag (primarily aluminum oxide) which is trapped in the motor case, causing a loss of specific impulse. Although not yet definitely established, the presence of a liquid pool of slag also may contribute to nutational instabilities that have been observed with certain spin-stabilized, upper-stage vehicles. Because of the rocket's axial acceleration--absent in the ground tests--estimates of in-flight slag mass have been very uncertain. Yet such estimates are needed to determine the magnitude of the control authority of the systems required for eliminating the instability. A test rig with an eccentrically mounted hemispherical bowl was designed and built which incorporates a "follower" force that properly aligns the thrust vector along the axis of spin. A program that computes the motion of a point mass in the spinning and precessing bowl was written. Using various RPMs, friction factors, and initial starting conditions, plots were generated showing the trace of the point mass around the inside of the fuel tank. The apparatus will be used extensively during the 1990-1991 academic year and incorporate future design features such as a variable nutation angle and a film height measuring instrument. Data obtained on the nutational instability characteristics will be used to determine order of magnitude estimates of control authority needed to minimize the sloshing effect.

## Introduction

Many rocket motor solid propellants in current use contain a significant amount of aluminum which, when burned, produces a slag consisting of aluminum oxide and elemental aluminum. Most of this material is expelled throughout the rocket motor nozzle and adds to the thrust, but some remains trapped in the motor case. The melting point of the  $\alpha$ -form of  $\text{Al}_2\text{O}_3$  is about  $2050^\circ\text{C}$ , below the temperature of the combustion gas. The liquid slag, in the form of small droplets, is subject to a combination of forces that include the drag from the combustion gas, the inertial force resulting from the axial acceleration of the rocket, and (for spin-stabilized vehicles) the centrifugal force resulting from the vehicle spin.

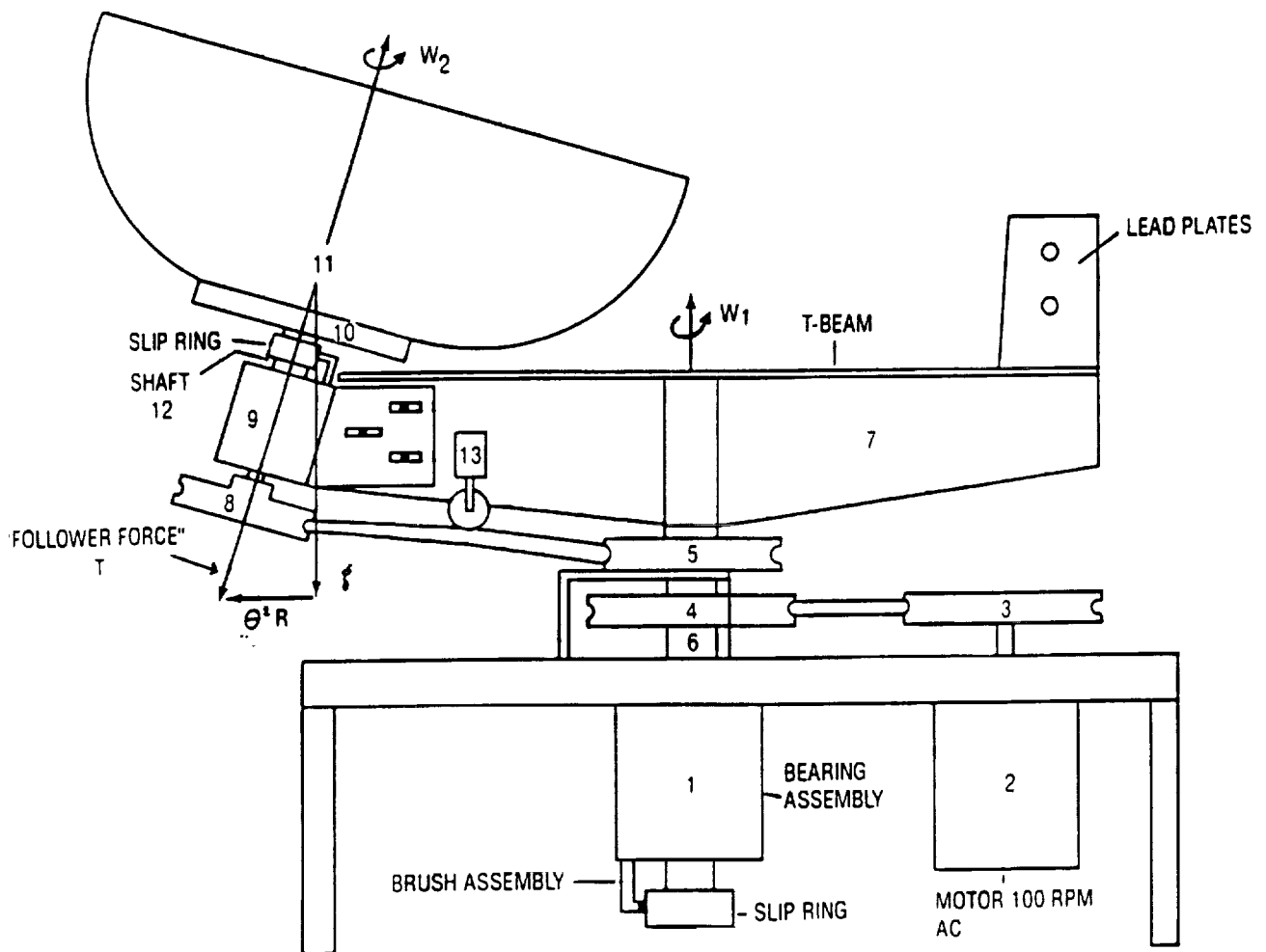
The present analysis postulates that, because of the high level of turbulence in the motor, slag droplets entering the gas stream are ejected, and that trapped slag is formed primarily by liquid slag flowing along the surfaces toward the point of minimum potential energy in the accelerating and spinning motor. Also, the present analysis concludes that slag will accumulate to some degree in all spinning or accelerating rocket motors with aluminum-containing propellants and submerged nozzles.

A number of spin-stabilized vehicles that use aluminized propellant have shown a marked tendency for a "coning" instability; i.e., a precession with steadily increasing nutation angle. These motors have a submerged nozzle geometry, resulting in a downstream annular pocket which is likely to favor slag retention. It has been surmised, therefore, that the sloshing motion of a liquid slag pool may be a contributing cause of the observed flight instability. The effects of liquid slag on the stability of spinning vehicles is similar to the effects produced by fuel slosh in spacecraft. Slag retention also requires examination because of its potentially deleterious effect on specific impulse.

Through installation of witness plates downstream of the nozzle, where some of the (now solid) slag particles are deposited, estimates of the size distribution and total mass of the expelled particles have been made. Ground tests of this type, however, take no account of the processing of the droplets in the nozzle.

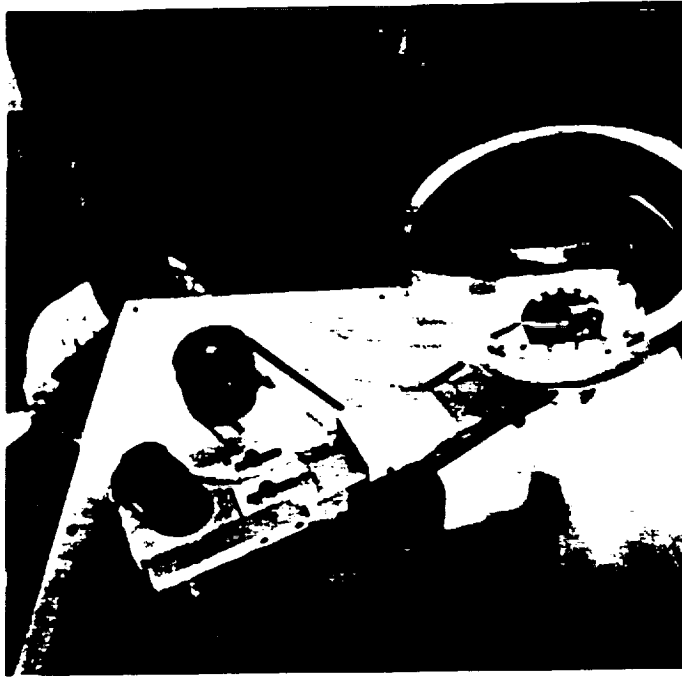
This report consists of a mechanical design that simulates the motion of a spherical fuel tank in a thrusting spacecraft. A true simulation of the thrust was thought to be impossible due to the gravitational support forces present in the laboratory. However, through the means of an eccentrically mounted spacecraft model on the top of a turntable, the simulation of thrust aligned with the vehicle axis is possible. The mechanical design was finished during the 1990 winter quarter and the test rig was built in the spring. The comparison of the initial description (see figure 1) with the design actually built (see figure 2) shows the evolution of the design concept. Qualitative analysis will be provided by photographs of fluid profiles at given time intervals and quantitative analysis by correlation of film thickness from capacitance measurements between two platinum wires located in the bowl. This sensor will be designed, built, and incorporated into the test rig slip-ring assembly during the 1990-1990 academic year. From these data, nutational instability characteristics and order of magnitude estimates of control authority needed to eliminate the instability will be determined.

A computer program was written to simulate the shape of a fluid in a spinning and precessing container with a nutation angle equal to zero. The fluid was assumed to be in hydrostatic equilibrium. The fluid depth as a function of position along with the shoreline of the fluid was determined. A more general code was written which computes the motion of a point mass in a spinning and precessing hemispherical container. Using various RPMs and friction factors, plots were generated to compare the motion of the point mass and validate the theoretical model (see figure 4).



- |                                  |                                  |
|----------------------------------|----------------------------------|
| 1. general bearing assembly      | 8. bowl pulley                   |
| 2. AC motor (variable rpm)       | 9. bowl bearing housing assembly |
| 3. pulley for motor shaft        | 10. bowl mounting flange         |
| 4. main drive pulley             | 11. hemispherical bowl (lucite)  |
| 5. secondary pulley (stationary) | 12. bowl support shaft           |
| 6. main shaft                    | 13. idler guide                  |
| 7. control arm                   |                                  |

**Figure 1: Apparatus Diagram (Not to scale)**



ORIGINAL PAGE IS  
OF POOR QUALITY

**Figure 2: Completed Test Rig**  
**(a) top view showing liquid sloshing in bowl**  
**(b) front view showing dual motor assembly**

## **Viscous Dissipation:**

The degree of instability of a thrusting, spin stabilized spacecraft depends strongly on the amount of internal energy dissipation. The dominant energy dissipation mechanism is thought to be caused by the sloshing of liquid slag at the bottom of the solid motor casing which directly influences the body's motion. Oscillatory, and sometimes violent, motion of the fluid induce corresponding oscillations of the body. Viscous effects in the fluid also influence the body causing the nutation angle to change thereby affecting the stability. It is, therefore, important to estimate the energy losses in the fluid.

Once these energy losses are estimated, one can predict the body motion by reducing its kinetic energy at the same rate. This approach is known as the "energy sink" procedure. Due to the growing nutation angle from energy dissipation, thrust corrections need to be fired to stabilize the craft. This requires more fuel to be included for stabilization during launch which ultimately increases launch mass. Having to fire these correcting thrusters at the right time creates yet another problem in the attitude dynamics and control of the spacecraft. Ideally, nutational instability characteristics and order of magnitude estimates of control authority needed to eliminate the instability would allow designers to provide the lightest control system necessary to minimize this phenomenon.

## **Scale Model Principles**

Many different models have been developed to test sloshing and its effect on spacecraft. Most of these models, however, are made to simulate the sloshing of a spacecraft in which thrust is absent. One of the recent problems is that an instability evidenced by a growing nutation angle has been observed during the firing of liquid and solid perigee and apogee motors. A new model to simulate this motion was needed which properly aligns the "thrust" vector with the model axis.

A simple design of a spacecraft model mounted eccentrically on a turntable can be used. This rig simulates the thrust as a "follower" force (see figure 3). Previous models were subjected to gravity forces acting at the center of mass. But the new model produces a resultant of gravity and inertial forces that remains aligned at all times with the vehicle axis. Hence, this thrust "follows" the model as it spins and precesses around on the turntable.

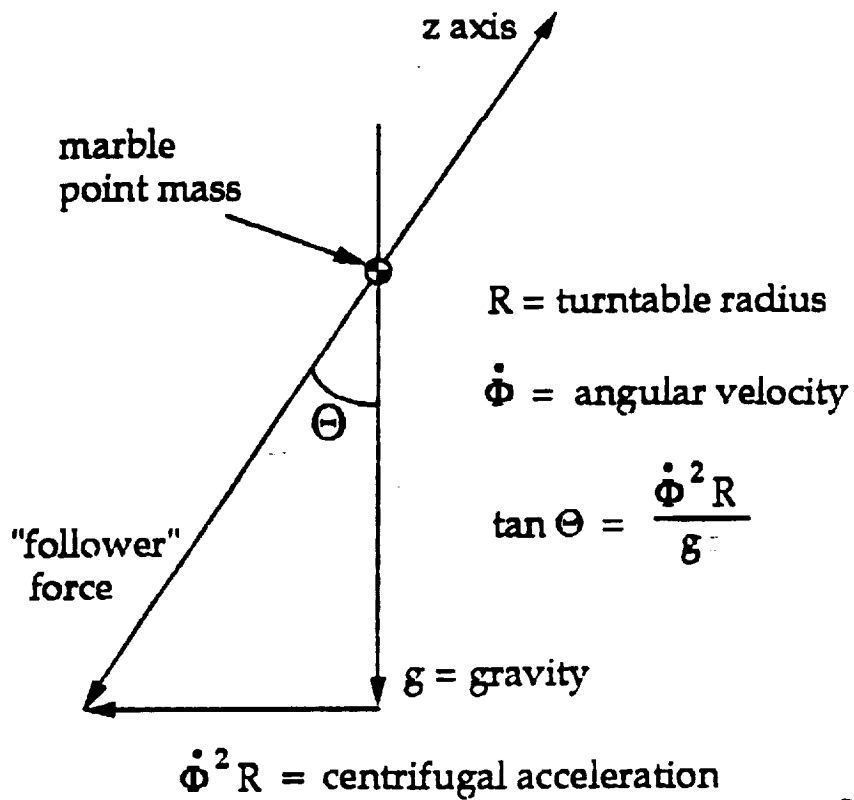


Figure 3: "Follow Force Diagram"

## 10 Second Marble Trace

40 RPM, friction factor = 0.5

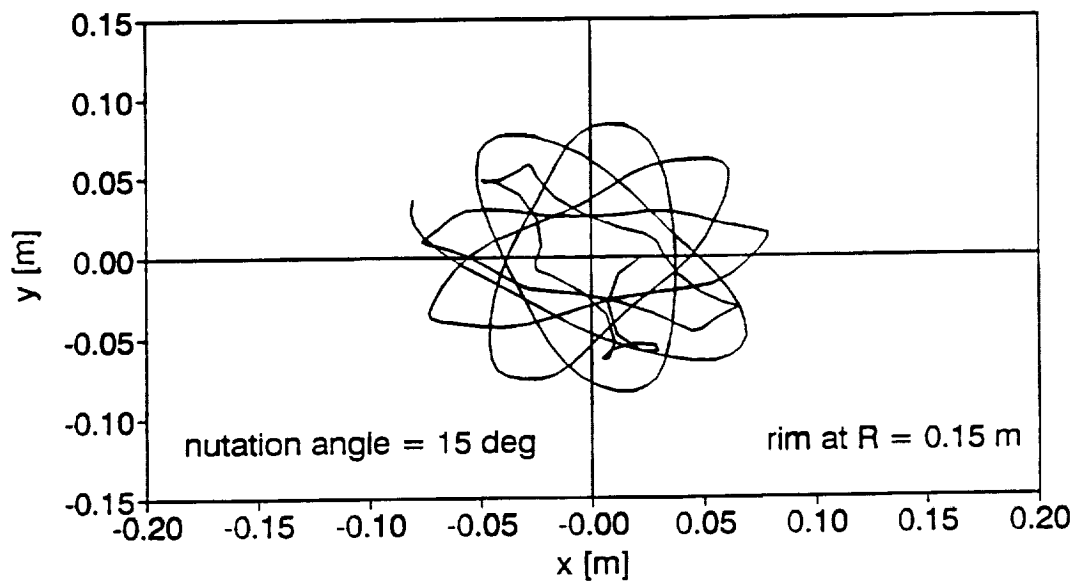


Figure 4: Computer Code Results

Because of space and cost constraints, it is necessary to have a model that is not full scale. It must then be shown that the model behaves in the same way as the spacecraft. Therefore, it is required for the model to have the same inertia ratio as the spacecraft:

$$\left[ \frac{I_s}{I_p} \right]_{\text{model}} = \left[ \frac{I_s}{I_p} \right]_{\text{spacecraft}}$$

It also follows that the ratio of the precession rate to the spin rate be the same in both the model and the full scale model. To simulate the dynamics of the sloshing requires that the Froude numbers of the model and spacecraft be the same:

$$\text{Froude number} \equiv \left[ \frac{Rt(d\Phi/dt)^2}{g/\cos\theta} \right]_{\text{model}} = \left[ \frac{Rt(d\Phi/dt)^2}{T/M} \right]_{\text{spacecraft}}$$

Solving for  $(d\Phi/dt)_{\text{model}}$ :

$$(d\Phi/dt)_{\text{model}} = (d\Phi/dt)_{\text{spacecraft}} \sqrt{\frac{(Rt)_{\text{spacecraft}} g M}{(Rt)_{\text{model}} T \cos\theta}}$$

Using these equations, a good approximation to a thrusting spacecraft can be made in the laboratory.

### Mechanical Design:

A distinct design evolution was experienced in attempting to construct a test rig which would adequately simulate the conditions present during the burn of a solid propellant rocket motor. As a preliminary experiment it was primarily designed to provide a qualitative analysis of fuel and slag sloshing and aid in the development of future experimentation.

The design problem was to simulate rotation about the rocket's own axis and the subsequent precession about an associated axis, both of which are effects of spin stabilization. It was initially agreed that dual rotating shafts were best fitted to produce the kinematics of the situation, and subsequently the design problem was limited to developing a system that would drive the two shafts with correct direction and rates of spin. In order to achieve this effect several proposals were made, first of which entailed using a set of belts and pulleys driven by a single electric motor. Succeeding designs included such elements as a planetary gear system, a set of rubber wheels, or a set of dual motors. In the end, the initial concept of belts and pulleys was adopted for their availability and ease of use.

The rig is mounted on a half inch thick aluminum table, approximately one meter square and held up by four nine inch long aluminum legs. The main shaft is positioned vertically through the middle of the table, housed by a bearing assembly which is mounted to the under face of the table. This shaft is driven by a belt, connected to a variable RPM electric motor also mounted from beneath the table. To the top of the main shaft is mounted a control arm made from an aluminum T beam. On one side of the control arm is the fuel tank assembly and on the other, an equal counter weight made of lead plates.

The hemispherical bowl, turned from a Lucite block, is mounted to a second shaft which rotates within the bearing housing mounted to the control arm. Positioned on the main shaft and on the bottom of the second shaft are two pulleys. The pulley on the main shaft is secured and remains stationary with respect to the table. The other pulley is secured to the second shaft and produces the rotation of the bowl about its own axis. A crossing belt connects the two pulleys, and as the main shaft rotates at an average rate of forty RPM, the second shaft rotates twice as fast in the opposite direction. In order to keep an adequate tension in the belt, the bearing assembly housing the shaft, can shift horizontally by  $\pm 0.5$  inch. In addition, an idler is included on the control arm to guide the belt and maintain its tension.

During the next academic year (1990-1991) a sensor will be designed which determines the film thickness by measuring the capacitance between two platinum wires. This will hopefully provide a means to quantify the force and momentum produced by the rotating liquid in the bowl at various RPMs. In order to incorporate this instrument, an electric connection to the bowl is needed through a set of slip rings in the rotating mechanism. Just below the bowl and above the bearing assembly is mounted the first slip ring. And at the bottom of the main shaft below the bearing assembly is mounted the second slip ring. To connect the wires from the control arm to the second ring, a hole is drilled down the center and through the entire length of the shaft. Through this hole the wires are run to the slip ring.

### **Computer Simulation:**

A theoretical analysis which approximates the fluid in the bowl with a point mass was developed. The result was a system of two ordinary differential equations which can be solved numerically by Heun's method for initial value problems. A code was generated which determines the x, y, and z coordinates of a "marble" rolling around inside the bowl given a friction factor, initial starting coordinates, bowl RPM, and nutation angle. The friction factor was varied to simulate the effects of fluid viscosity and friction of the point mass. The larger the friction value, the more of a damping effect the marble exhibited. For smaller values, the marble took longer to stabilize and rose higher in the bowl (see figures). When the actual experiments begin this fall, the code can be properly validated with better estimates of the friction factor, RPM, and nutation angles necessary to demonstrate a valid theoretical model and test rig.

ORIGINAL PAGE IS  
OF POOR QUALITY

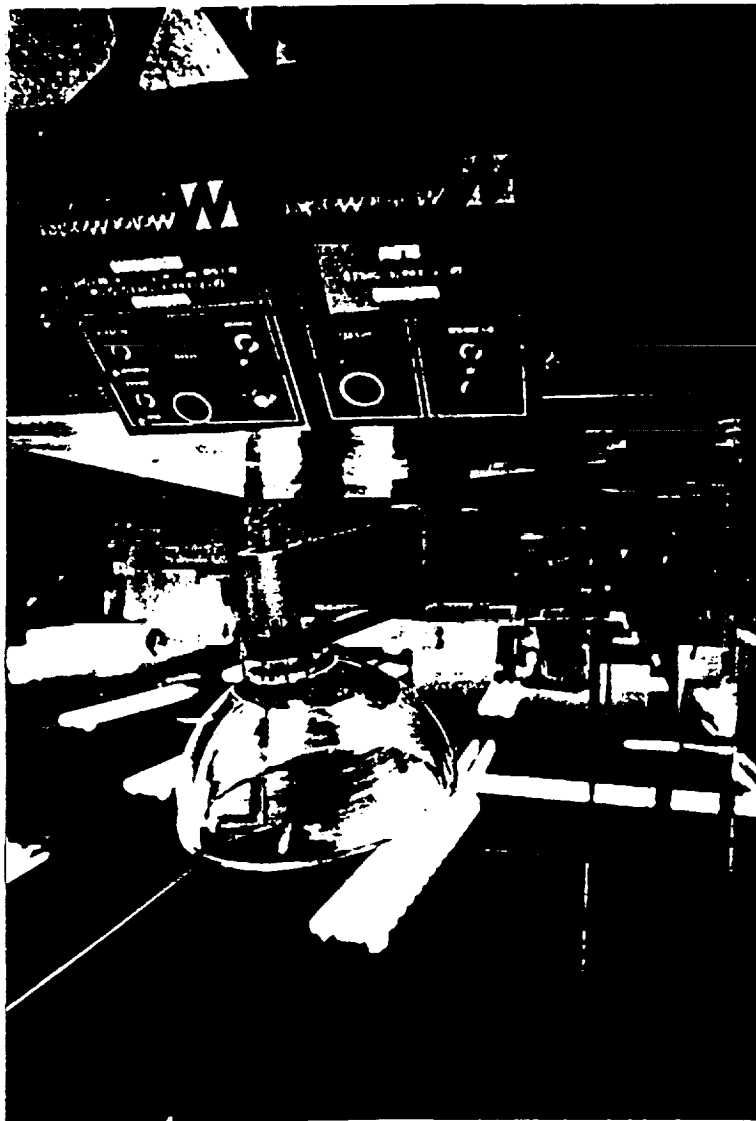


## TABLE OF CONTENTS

INTRODUCTION.....	1
LIST OF SYMBOLS.....	3
REFERENCE FRAMES.....	4
STABILIZATION PRINCIPLES.....	5
SCALE MODEL PRINCIPLES.....	8
MECHANICAL DESIGN.....	13
DESIGN SKETCHES.....	16
COMPUTER ANALYSES - A. SIMULATION OF FLUID SHAPE.....	35
B. SIMULATION OF POINT MASS MOTION.....	42
HOT TUNGSTEN WIRE ANALYSIS.....	47
LIST OF MATERIALS.....	61
CONCLUSION.....	64
APPENDIX A: PRELIMINARY DESIGN.....	65
APPENDIX B: CALCULATION FO FLUID SHAPE SIMULATION.....	76
APPENDIX C: POINT MASS MOTION HANDOUT.....	80
APPENDIX D: POINT MASS MOTION COMPUTER PROGRAM LISTING.....	85
APPENDIX E: VELOCITY CALCULATIONS FOR HOT WIRE.....	98
REFERENCES.....	105
BIBLIOGRAPHY.....	106

## INTRODUCTION

In theory, the definition of a rigid body does not permit any energy dissipation. However, it is known that all spacecraft and rockets have some non-rigid entities including elastic structural deflection and the liquid motion of fuel in its tanks, otherwise known as slosh. Since Explorer I, it has been known that these properties can have a major effect on the motion, that is, there can be instabilities that depend largely on the internal energy dissipation. In most spinning spacecraft and rockets, the largest amount of energy dissipation comes from the liquid slosh.

This report consists of a mechanical design that simulates the motion of a spherical fuel tank in a thrusting spacecraft. A true simulation of the thrust was thought to be impossible due to the gravitational support forces present in the laboratory. However, through the means of an eccentrically mounted spacecraft model on the top of a turntable, it was discovered in reference 1, that the simulation of thrust aligned with the vehicle axis was indeed possible. The mechanical design is scheduled to be built and tested during the next summer. Results will be in the form of pictures and data collected about the depth of water at certain points. The results will then be qualitatively presented with conclusions drawn about the sloshing of the fuel. A background on the design and a list of materials needed for the design are included.

Also presented in this report is a theory on the possibility of using a heated tungsten wire to measure the depth of liquid in the model. By relating the heat loss of the wire to the depth of fluid inside the cup, it was thought that an accurate reading of the depth could be obtained. However, after many calculations it was found that there were too many uncertainties for the hot wire to be an accurate device. Nevertheless, these calculations are valuable and therefore included.

A computer program was written to simulate the shape of a fluid in a spinning and precessing container with a nutation angle equal to zero. The fluid was assumed to be in hydrostatic equilibrium. The fluid depth as a function of position along with the shoreline of the fluid were determined. A program that determined the motion of a point mass in a spinning and precessing hemispherical container was also written. Using different conditions, i.e., different RPMs and friction factors, plots were generated to compare the motions of the point mass.

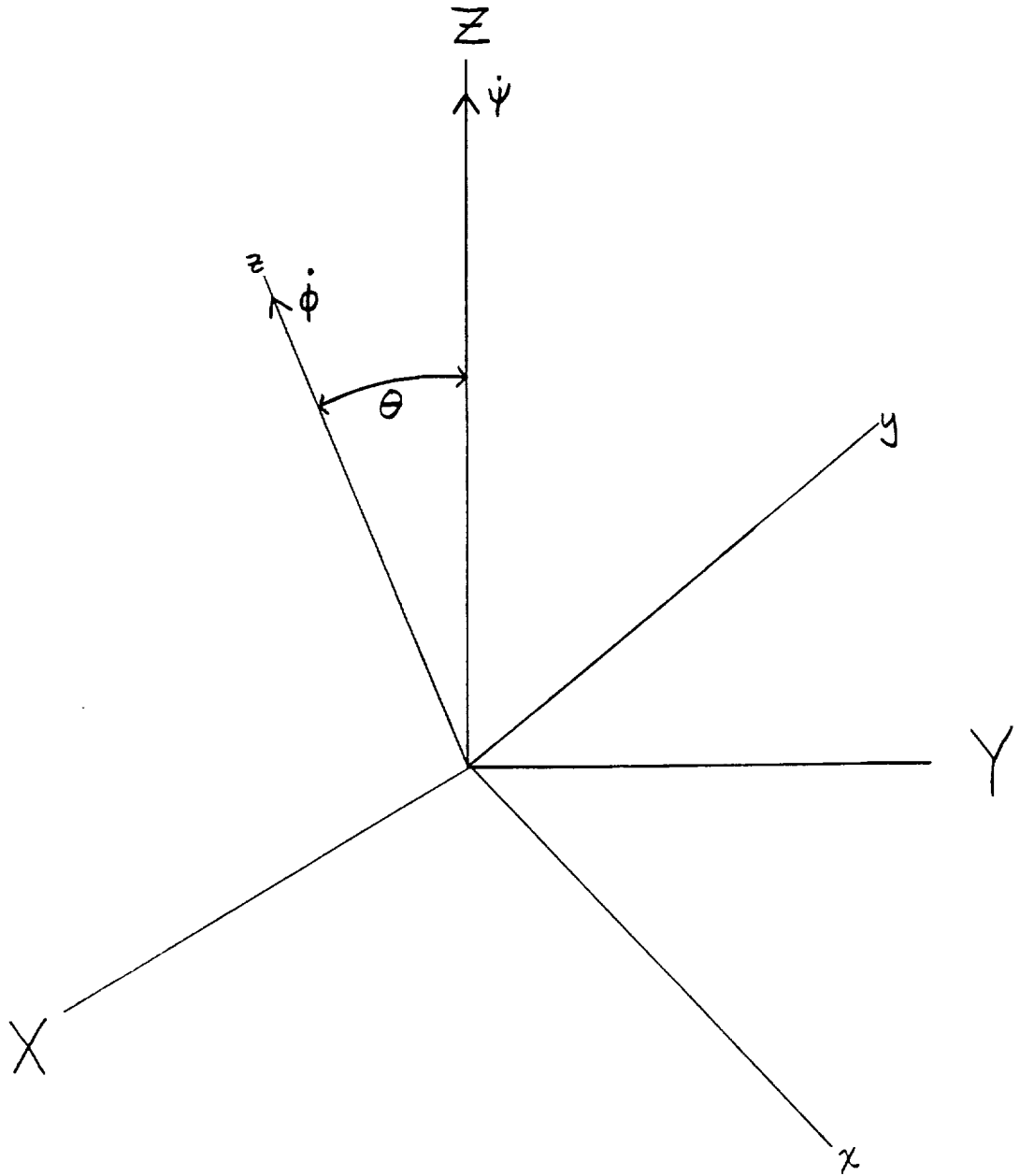
ORIGINAL PAGE IS  
OF POOR QUALITY

LIST OF SYMBOLS

$(X,Y,Z)$	Inertial reference frame
$(x,y,z)$	Body-fixed frame
$\dot{\psi}$	Precession rate
$\dot{\phi}$	Spin rate
$\Theta$	Nutation angle
$M$	Total mass including fuel
$m$	Fluid mass
$\nu$	Kinematic viscosity
$r$	Radius
$a$	Centripetal acceleration
$\rho$	Density
$g$	Acceleration of gravity
$I$	Moment of inertia
$T$	Thrust
$Re$	Reynolds number
$Fr$	Froude number
$C_{Dsk}$	Pertaining to spacecraft
$C_{Dm}$	Pertaining to model
$h$	Height
$p$	Pressure
$\omega$	Angular velocity (subscripts obvious)
$Pr$	Prandtl number
$Gr$	Grashof number
$Nu$	Nusselt number

ORIGINAL PAGE IS  
OF POOR QUALITY

# Reference Frames



12 381 50 SHEETS 3 SQUARE  
12 380 100 SHEETS 3 SQUARE  
12 379 200 SHEETS 3 SQUARE  
NATIONAL

ORIGINAL PAGE IS  
OF POOR QUALITY

## STABILIZATION PRINCIPLES

There are primarily two different stabilization techniques currently in use. They are spin stabilization and three-axis stabilization, each of which has its advantages and disadvantages. Since we are concerned with rockets and thrusting spacecraft, we will be most interested in spin stabilization.

Spin stabilization is based on the gyroscopic stiffness produced due to the rotation of the rocket or spacecraft. Dual-spin, which involves two types of spinning and also precessing of the rocket is the most common stabilization technique as opposed to single-spin. Since spacecraft and rockets carry much of their fuel in the form of a liquid, the motion of this fuel due to the spin stabilization and the presence of thrust is of great interest. This motion from its nominal position is what is known as "liquid sloshing".

The degree of instability of the spinning body depends strongly on the amount of internal energy dissipation. The most dominant energy dissipation mechanism is the fuel sloshing which influences the body's motion immediately and directly. Oscillatory, and sometimes violent, motion of the fluid induce corresponding oscillations of the body. Viscous effects in the fluid also influence the body causing the nutation angle to change thereby affecting the stability. It is, therefore, important to estimate the energy losses in the fluid.

The energy dissipation rate is assumed to be a function of the many spacecraft parameters as follows,

$$\dot{E} = g(\theta, I_x, I_y, M, m, r_T, r_f, \dot{\phi}, \dot{\psi}, \rho, \nu, g, a, R)$$

where,

$M$  = total mass including fuel

$m$  = fluid mass

$\nu$  = kinematic viscosity

$R$  = radial distance of tank center from spin axis

$r_T$  = radius of tank

$r_f$  = radius to free surface

$a$  = centripetal acceleration,  $r(\dot{\phi} + \dot{\psi})^2$

etc.

expanding in an infinite series representation,

$$\dot{E} = \sum_{i=1}^{\infty} (K_i \theta^{e_{\theta i}} I_x^{e_{I_x i}} I_y^{e_{I_y i}} M^{e_{M i}} m^{e_{m i}} r_T^{e_{r_T i}} r_f^{e_{r_f i}} \dot{\phi}^{e_{\dot{\phi} i}} \dot{\psi}^{e_{\dot{\psi} i}} \rho^{e_{\rho i}} \nu^{e_{\nu i}} g^{e_{g i}} a^{e_{a i}})$$

where  $e_{ij}$  = exponents,  $j = 1, 2, \dots, 12$ ,  $i = 1, 2, \dots, \infty$

Using the non-dimensionalization process using the "Buckingham Pi Theorem" (see reference 2) and writing the result in the original form (where terms of like exponents have been brought together and the exponents dropped),

$$\dot{E} = \rho r_T^5 \dot{\phi}^3 f\left(\theta, \frac{\rho r_T^5}{I_x}, \frac{\rho r_T^5}{I_y}, \frac{\rho r_T^3}{M}, \frac{\rho r_T^3}{m}, \frac{r_f}{r_T}, \frac{\dot{\psi}}{\dot{\phi}}, \frac{r_T^2 \dot{\phi}}{\nu}, \frac{r_T^2 \dot{\phi}}{g}, \frac{a}{r_T \dot{\phi}^2}\right)$$

some of these terms can be invented to show their more familiar form,

$$\begin{aligned} \frac{r_T^2 \dot{\phi}}{\nu} &= \text{Reynolds number} \\ \frac{r_T^2 \dot{\phi}}{g} &= \text{Froude number} \\ \frac{m}{\rho r_T^3} &= \text{fraction fill} \end{aligned}$$

Once these energy losses are estimated, one can then predict the body motion by reducing its kinetic energy at the same rate. This approach known as the "energy sink" procedure is beyond the scope of the class. A more detailed discussion of it and energy dissipation can be found in reference 3 and reference 4.

One of the results of this growing nutation angle from energy dissipation is that correcting thrusts will have to be fired to restabilize the craft. This will use up more fuel and shorten the life of the craft. Having to fire these correcting thrusts at the right time creates yet another problem in the attitude dynamics and control. The simplicity of spin stabilization means that liquid sloshing will still remain a challenging problem.

## SCALE MODEL PRINCIPLES

Many different models have been developed to test sloshing and its effect on spacecraft. Most of these models, however, are made to simulate the sloshing of a spacecraft in which thrust is absent. One of the recent problems is that an instability evidenced by a growing nutation angle has been observed during the firing of liquid perigee and apogee rocket motors (reference 1). Therefore, a new model to simulate the motion had to be found.

As seen in reference 1, an intricate model need not be made. Instead, a rather simple design of a spacecraft model mounted eccentrically on a turntable can be used. This rig simulates the thrust as a "follower force" (figure 1). As opposed to figure 2, where the model is subject to gravity reacting forces acting at its center of mass, figure 3 shows the design where the model lies eccentrically on a turntable. This produces a resultant of gravity and inertial forces that remains aligned at all times with the vehicle axis. Hence, this thrust is of the type referred to as a "follower force".

Because of space and cost constraints, it is necessary to have a model that is not full scale. It must then be shown that the model behaves in the same way as the spacecraft. Therefore, it is required for the model to have the same inertia ratio as the spacecraft,

$$\frac{(I_s)_m}{(I_{\perp})_m} = \frac{(I_s)_{s/c}}{(I_{\perp})_{s/c}}$$

It also follows that the ratio of the precession rate to the spin rate be the same in both the model and the full scale model. To simulate the dynamics of the sloshing requires that the Froude numbers of the model and spacecraft be the same,

$$Fr = \frac{\dot{\phi}_m^2 (r_T)_m}{(g/\cos\theta_m)} = \frac{\dot{\phi}_{s/c}^2 (r_T)_{s/c}}{(T/M)_{s/c}}$$

From this it is seen that

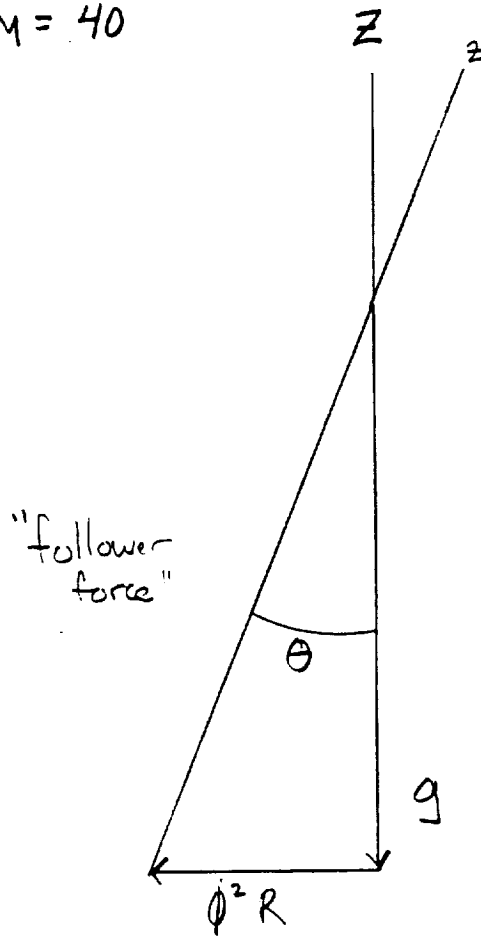
$$\dot{\phi}_m = \dot{\phi}_{s/c} \sqrt{\frac{(r_T)_{s/c} g M}{(r_T)_m T \cos\theta_0}}$$

Using these equations, a true simulation of a thrusting spacecraft can be made.

## Calculation of Nutation Angle

$$R = 150 \times 10^{-3} \text{ m}$$

$$\text{RPM} = 40$$



$$\begin{aligned} g \sin \theta &= \phi^2 R \cos \theta \\ \tan \theta &= \frac{\phi^2 R}{g} \\ &= \frac{\left(\frac{2\pi(40)}{60 \text{ s}}\right)^2 (150 \times 10^{-3} \text{ m})}{9.8 \text{ m/s}^2} \end{aligned}$$

$$\theta = 15.0^\circ$$

Figure 1

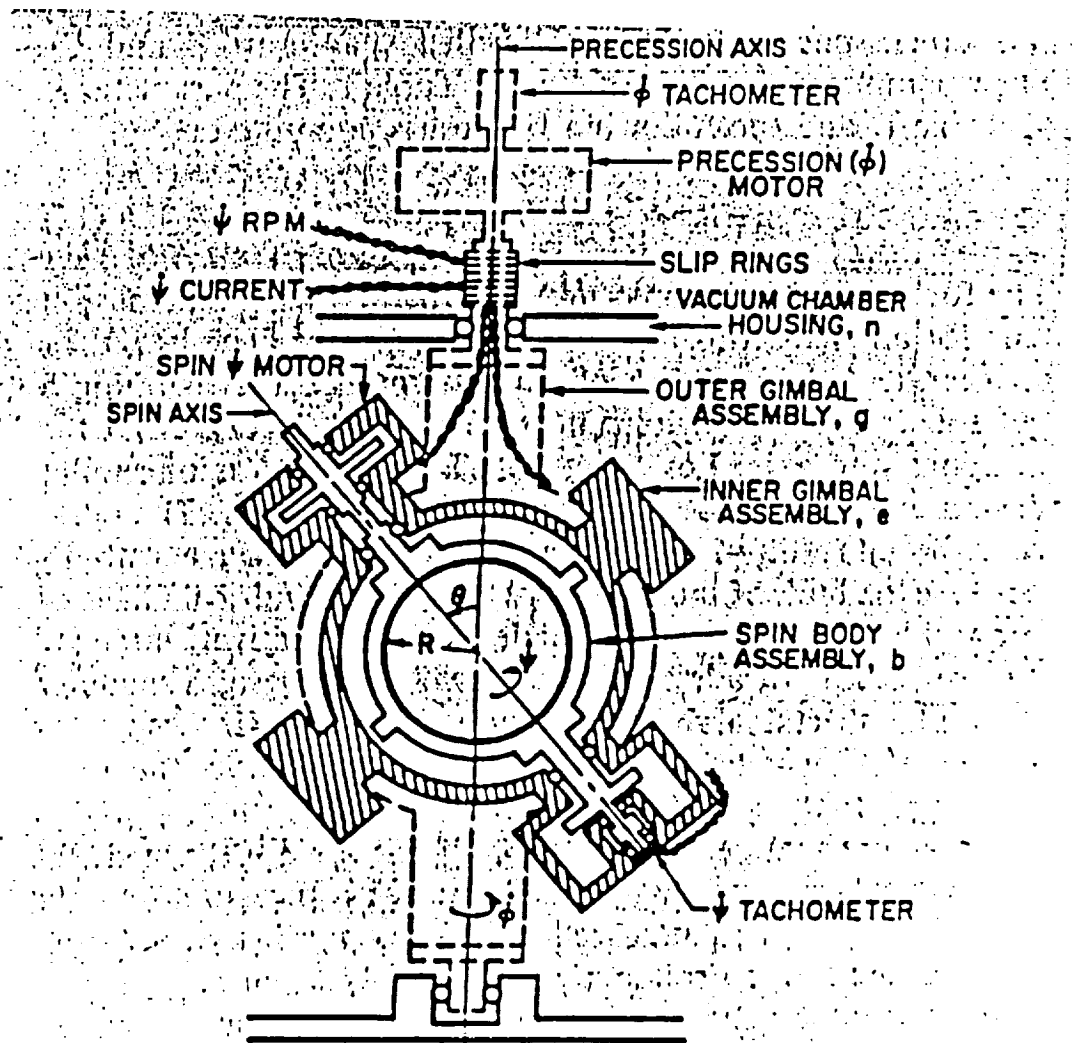


Figure 2

NOT TO SCALE.

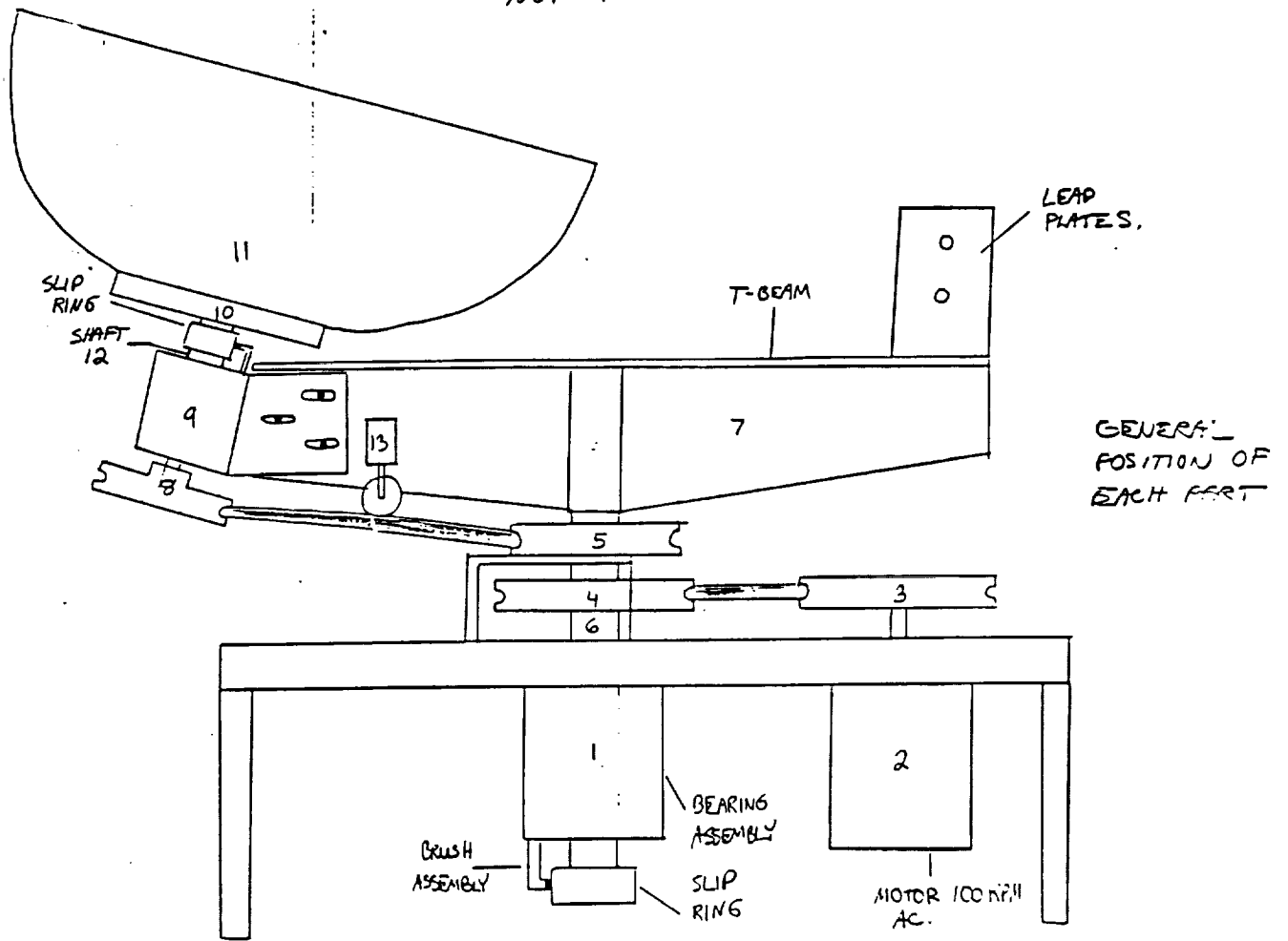


Figure 3

ORIGINAL PAGE IS  
OF POOR QUALITY

## MECHANICAL DESIGN

A distinct design evolution was experienced in attempting to construct a test rig, which would adequately simulate the conditions present during the burn of a liquid propellant rocket engine. As a preliminary experiment it was primarily designed to provide a qualitative analysis of fuel sloshing and aid in the development of future experimentation.

The design problem was to simulate rotation about the rocket's own axis and the subsequent precession about an associated axis, both of which are effects of spin stabilization. It was initially agreed that dual rotating shafts were best fitted to produce the kinematics of the situation, and subsequently the design problem was limited to developing a system that would drive the two shafts with correct direction and rates of spin. In order to achieve this effect several proposals were made, first of which entailed using a set of belts and pulleys driven by a single electric motor. Succeeding designs included such elements as a planetary gear system, a set of rubber wheels, or a set of dual motors. In the end, the initial concept of belts and pulleys was adopted for their availability and ease of use. The details of test rig's design are the following:

The rig is mounted on a half inch thick aluminum table, approximately one meter square and held up by four nine inch long aluminum legs. The main shaft is positioned vertically through the middle of the table, housed by a bearing assembly which is mounted to the under face of the table. This shaft is driven by

a belt, connected to a variable RPM electric motor also mounted from beneath the table. To the top of the main shaft is mounted a control arm made from an aluminum T beam. On one side of the control arm is the fuel tank assembly and on the other, an equal counter weight made of lead plates.

The hemispherical fuel tank, turned from a lucite block, is mounted to a second shaft which rotates within the bearing housing mounted to the control arm. Positioned on the main shaft and on the bottom of the second shaft are two pulleys. The pulley on the main shaft is secured and remains stationary with respect to the table. The other pulley is secured to the second shaft and produces the rotation of the fuel tank about its own axis. A crossing belt connects the two pulleys, and as the main shaft rotates at an average rate of forty RPM, the second shaft rotates twice as fast in the opposite direction. In order to keep an adequate tension in the belt, the bearing assembly housing the shaft, can shift horizontally by + or - half an inch. In addition, an idler is included on the control arm to guide the belt and maintain its tension.

If a feasible means of determining the depth of the fluid could be produced, an electric connection to the fuel tank would be necessary. For this purpose, incorporated into the design is a set of slip rings to make possible electric connections to the rotating mechanisms. Just below the fuel tank and above the bearing assembly is mounted the first slip ring. And at the bottom of the main shaft below the bearing assembly is mounted the second slip ring. To connect the wires from the control arm

to the second ring, a hole is drilled down the center and through the entire length of the shaft. Through this hole the wires are run to the slip ring.

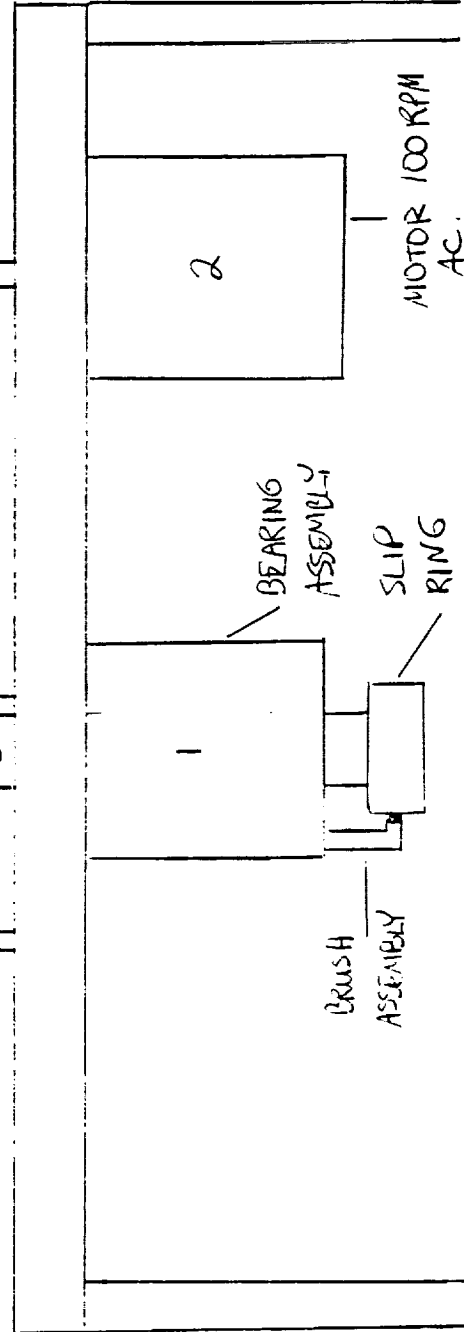
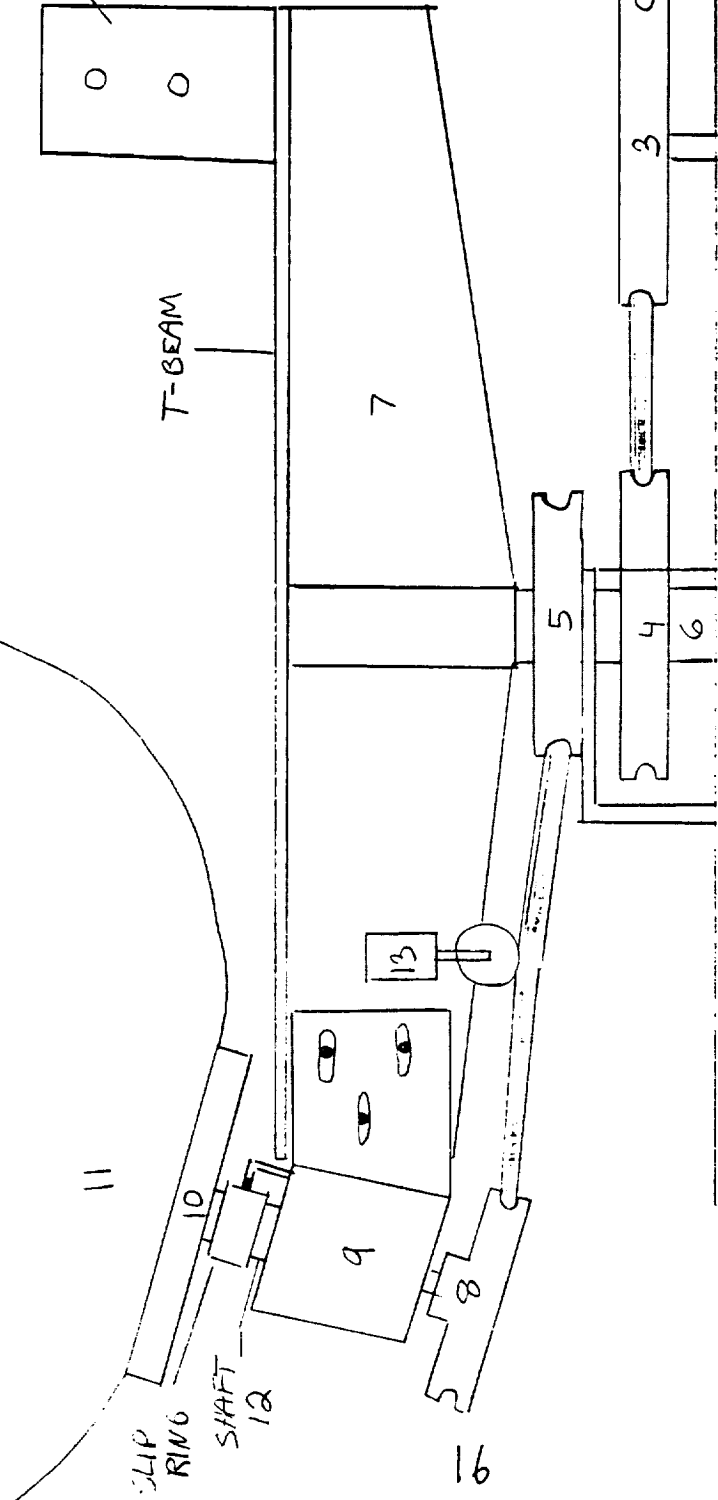
The following are detailed drawings of the individual parts.

# Design Sketches

GENERAL OF POSITION OF EACH PART

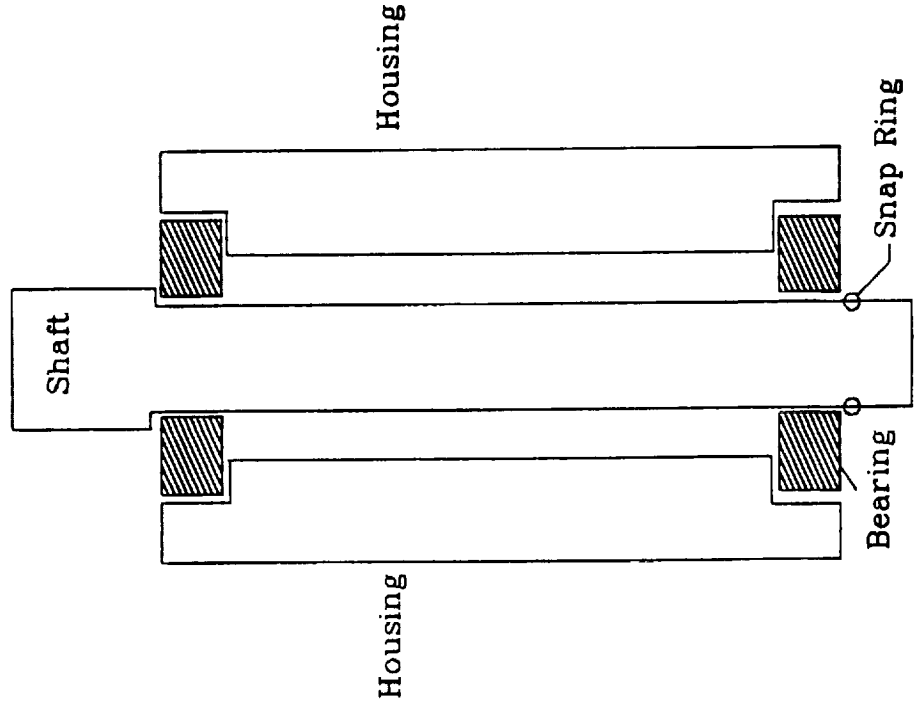
NOT TO SCALE.

LEAD PLATES.



# Part#1. General Bearing Assembly

Side Cut View



PART # 1

# MAIN BEARING HOUSING

TURN FROM ALUMINUM  $4\frac{1}{4}$ " DIA  
STOCK CYLINDER.

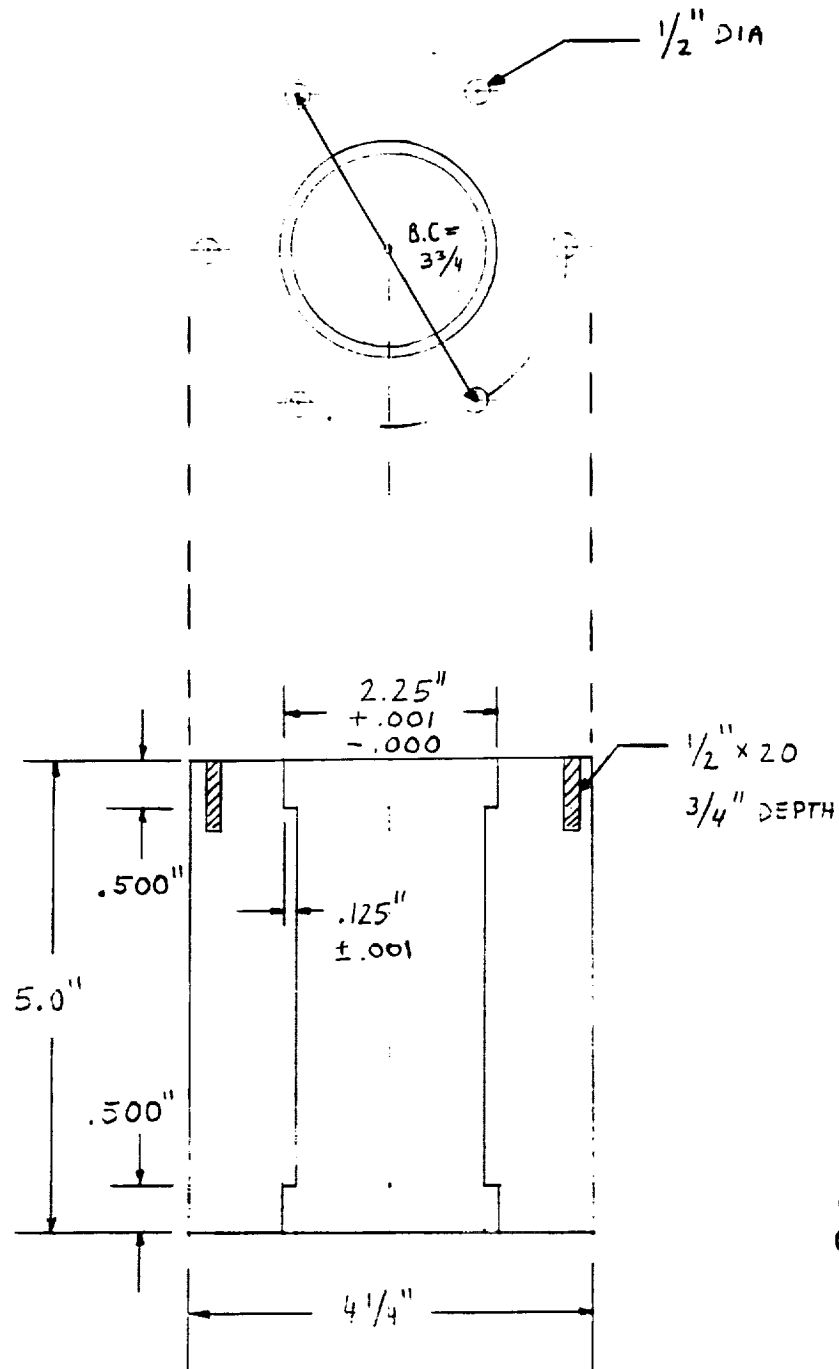
DIMENSIONS  $\pm 0.010$ "

HOUSING FOR USE WITH TWO  
SEALED BEARINGS

$1\frac{1}{4}$ " I.D

$2\frac{1}{4}$ " O.D

$\frac{1}{2}$ " WIDTH



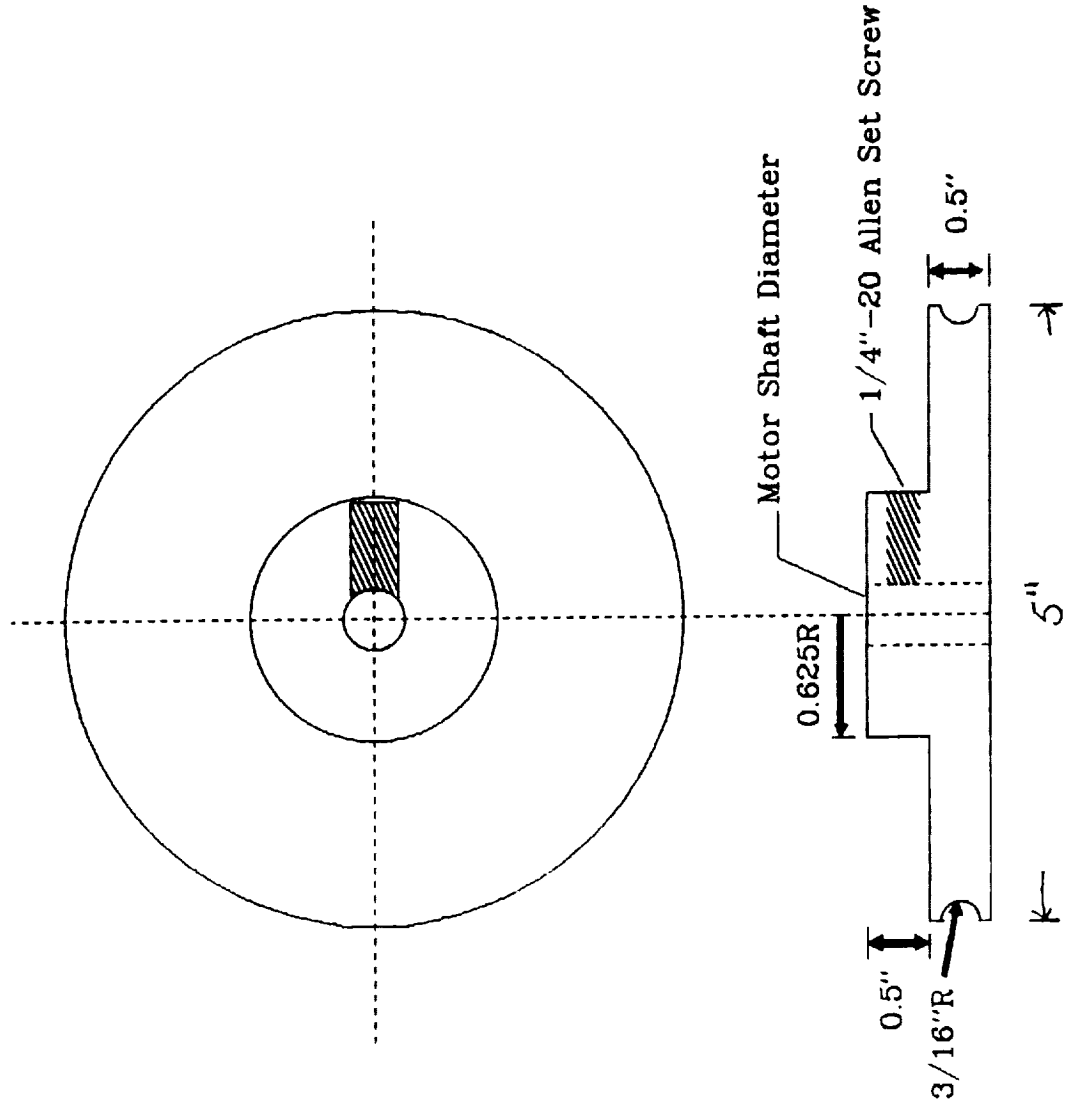
ORIGINAL PAGE IS  
OF POOR QUALITY

SCALE 1:2

# Part #3. Pulley for Motor Shaft

Turned From Aluminum Stock

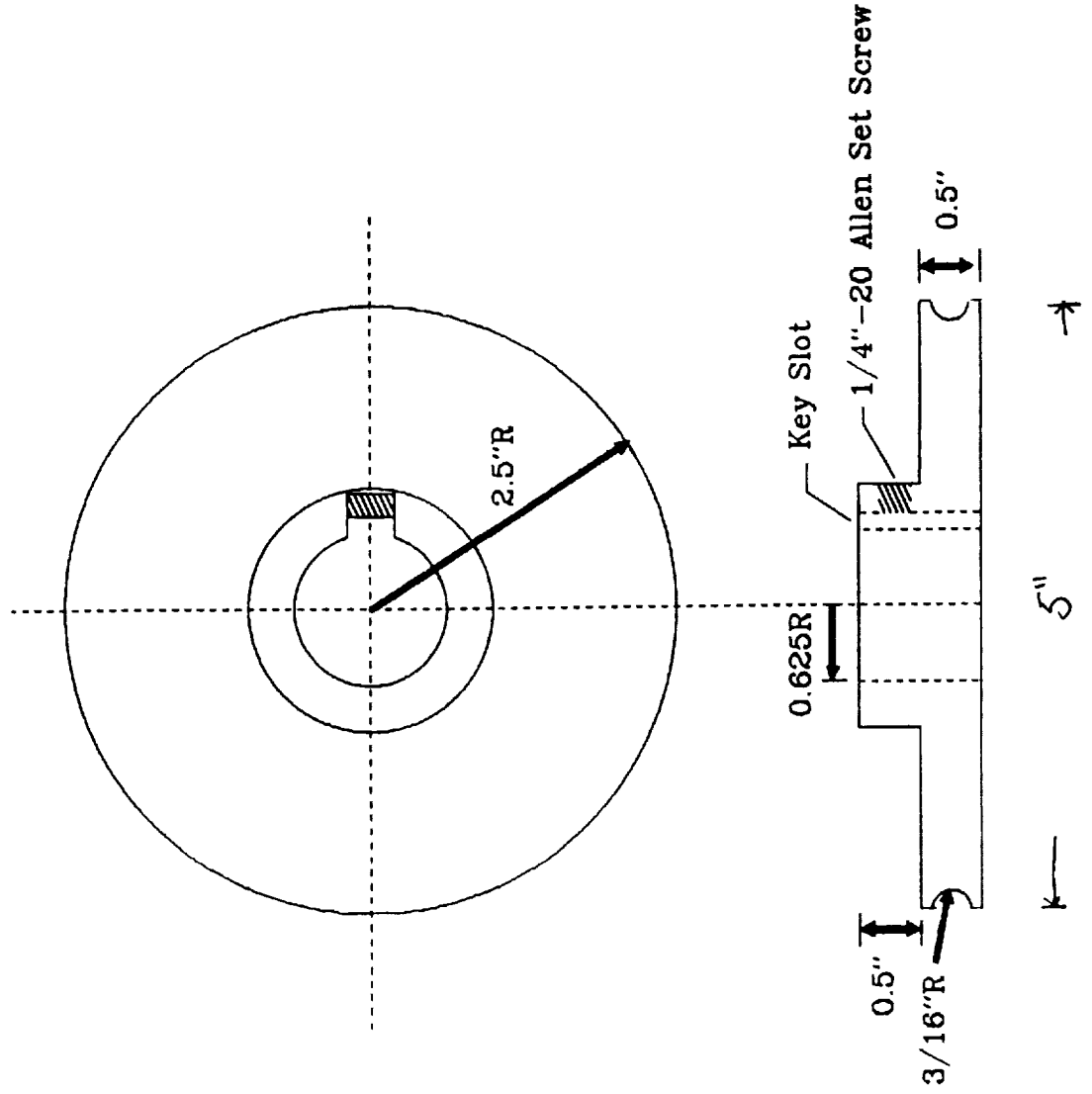
All dimensions  $\pm 0.02$ "



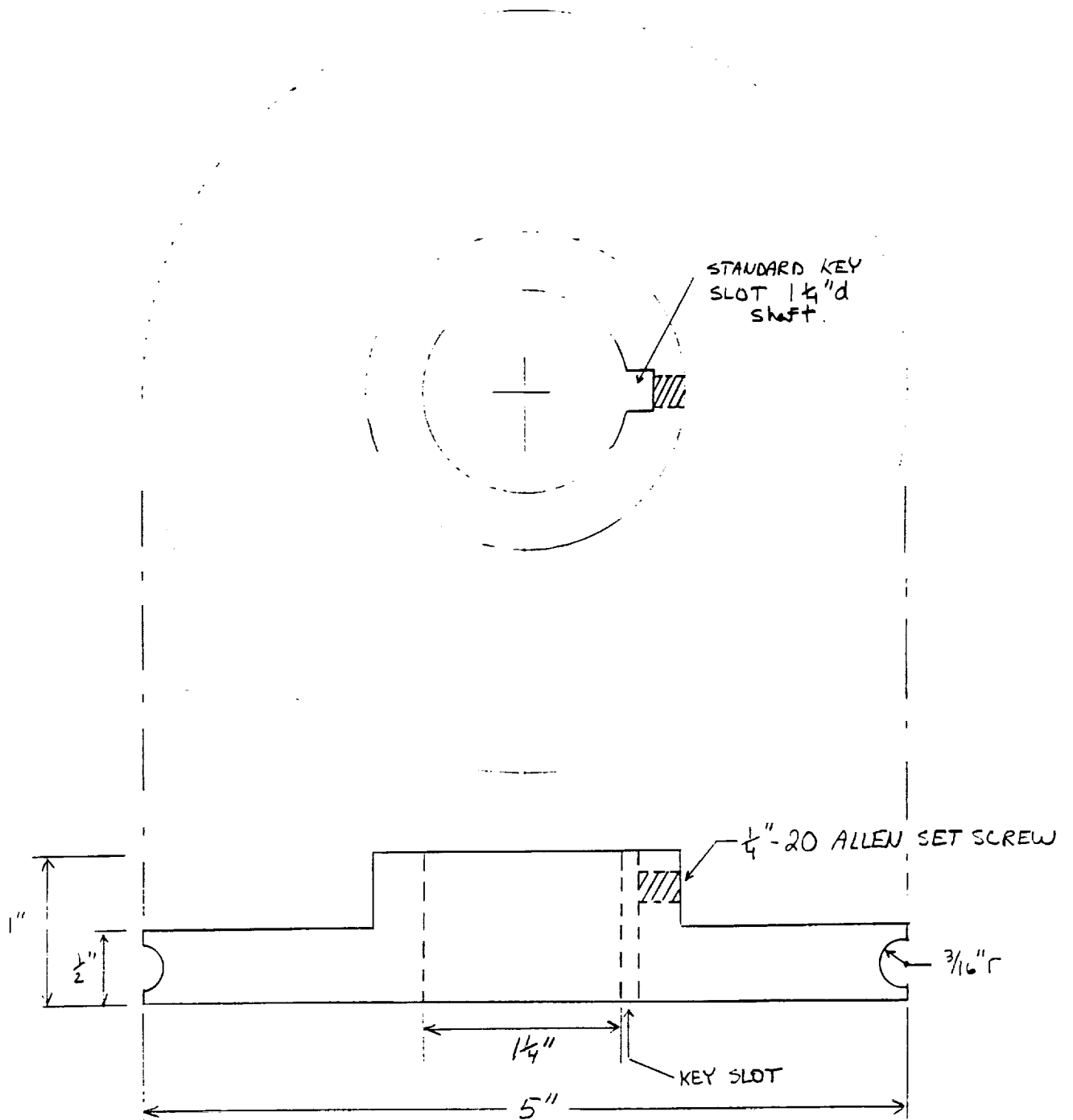
# Part #4. Main Drive Pulley

Turned From Aluminum Stock

All dimensions  $+/- 0.02"$



PART #4

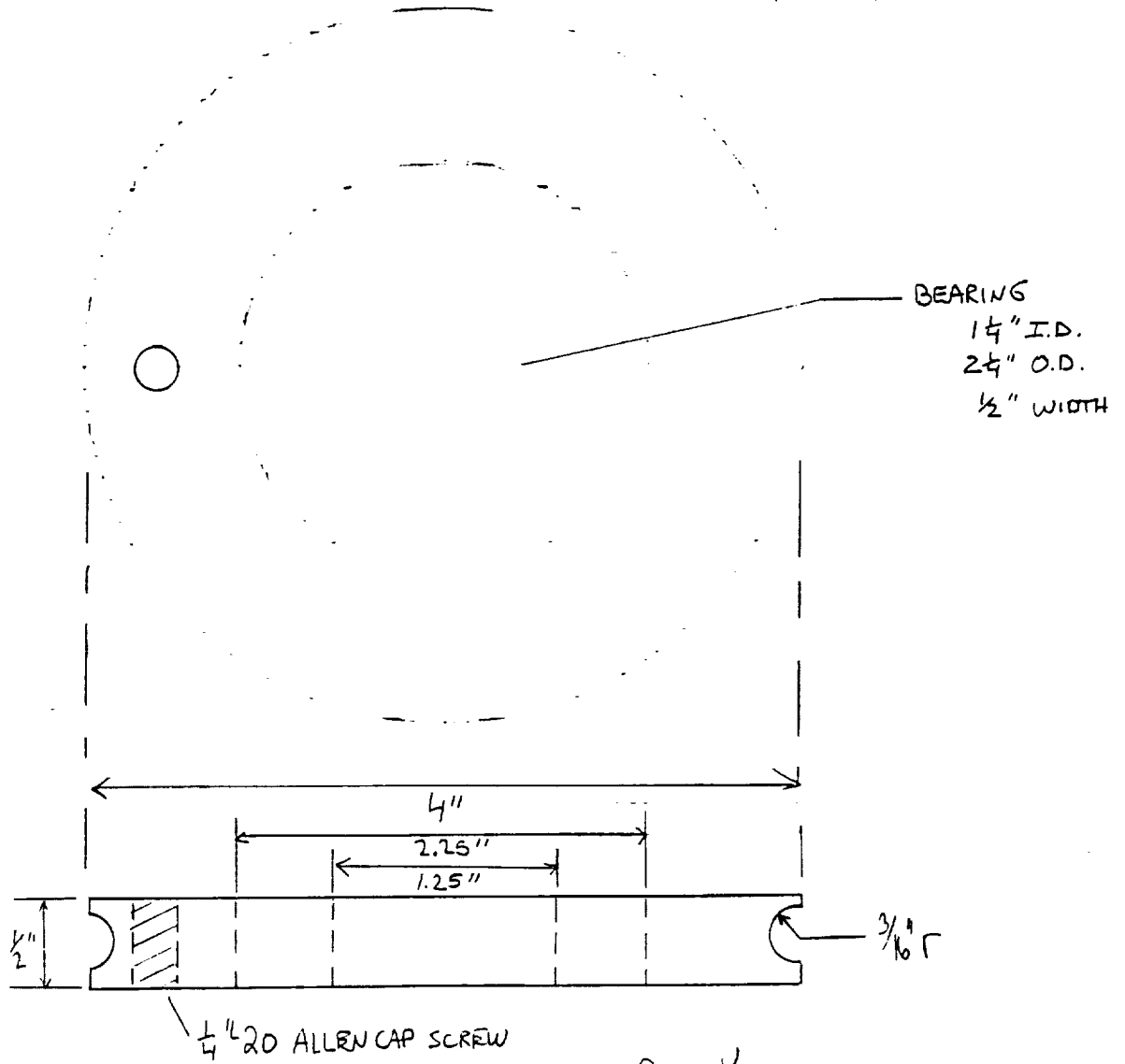


ORIGINAL PAGE IS  
OF POOR QUALITY

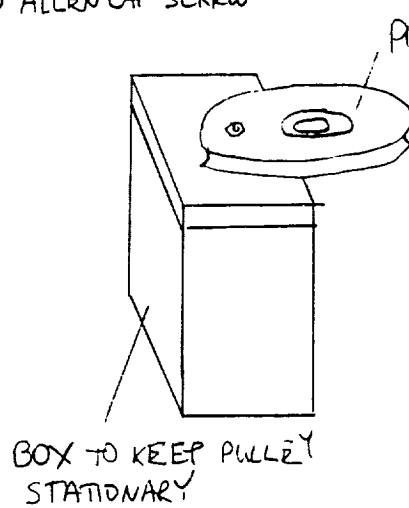
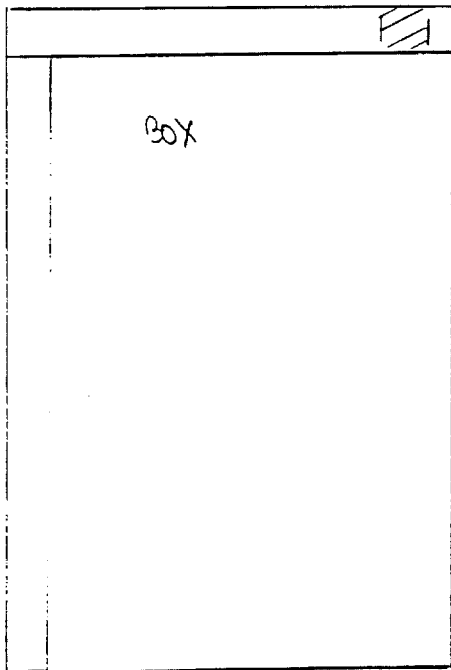
MAIN PULLEY FOR  
PRIMARY SHAFT  
TURNED FROM ALUMINUM  
CYLINDER - 5" d.

ALL DIMENSIONS = .01

PART #5



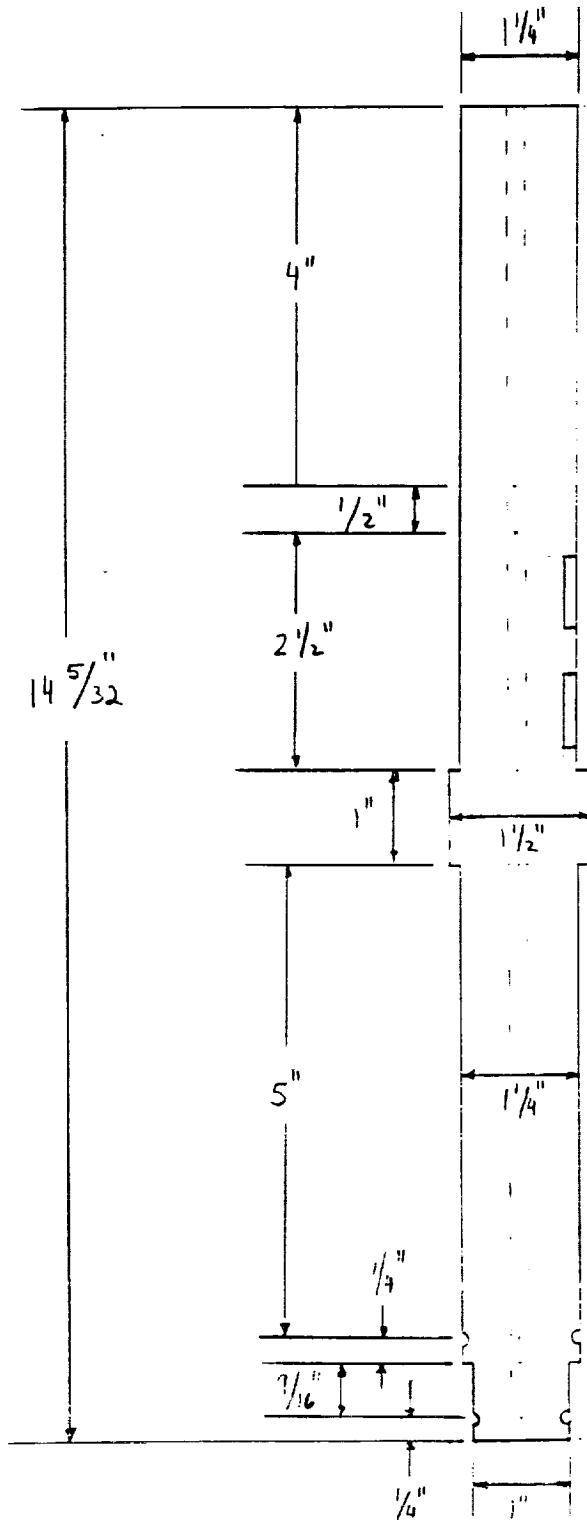
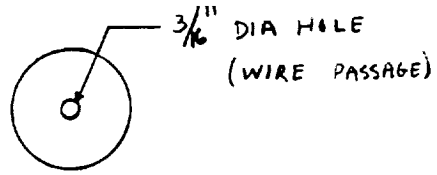
ORIGINAL PAGE IS OF POOR QUALITY



SECONDARY PULLEY TURNED FROM ALUMINUM STOCK.

DIMENSIONS ± .01

PART # 6

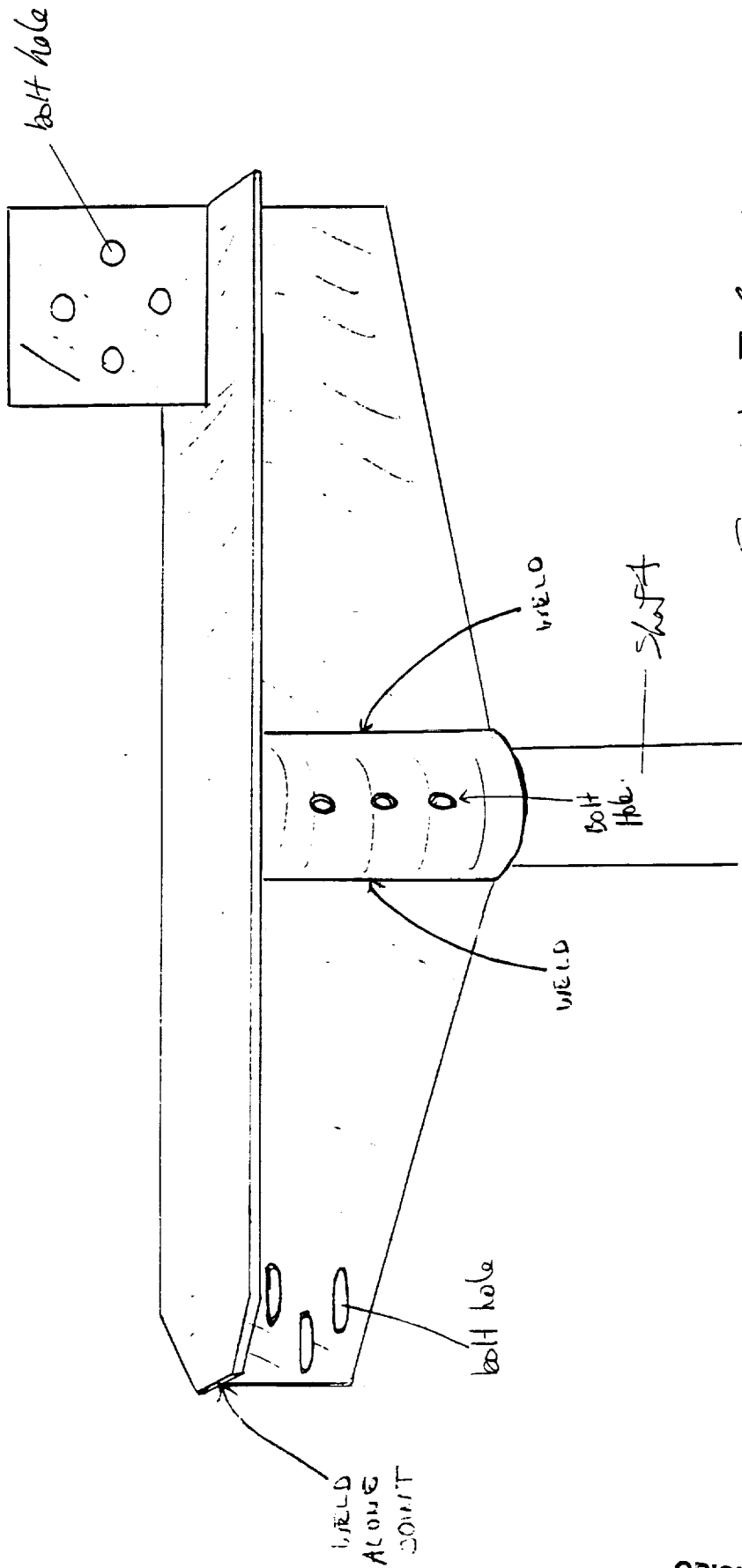


MAIN SHAFT  
TURNED FROM 1.5" DIA  
1020 COLD ROLLED STEEL.  
ALL DIMENSIONS ± 0.010"

ORIGINAL PAGE IS  
OF POOR QUALITY

SCALE 1:2

PART # 7



SKETCH OF CONTROL ARM

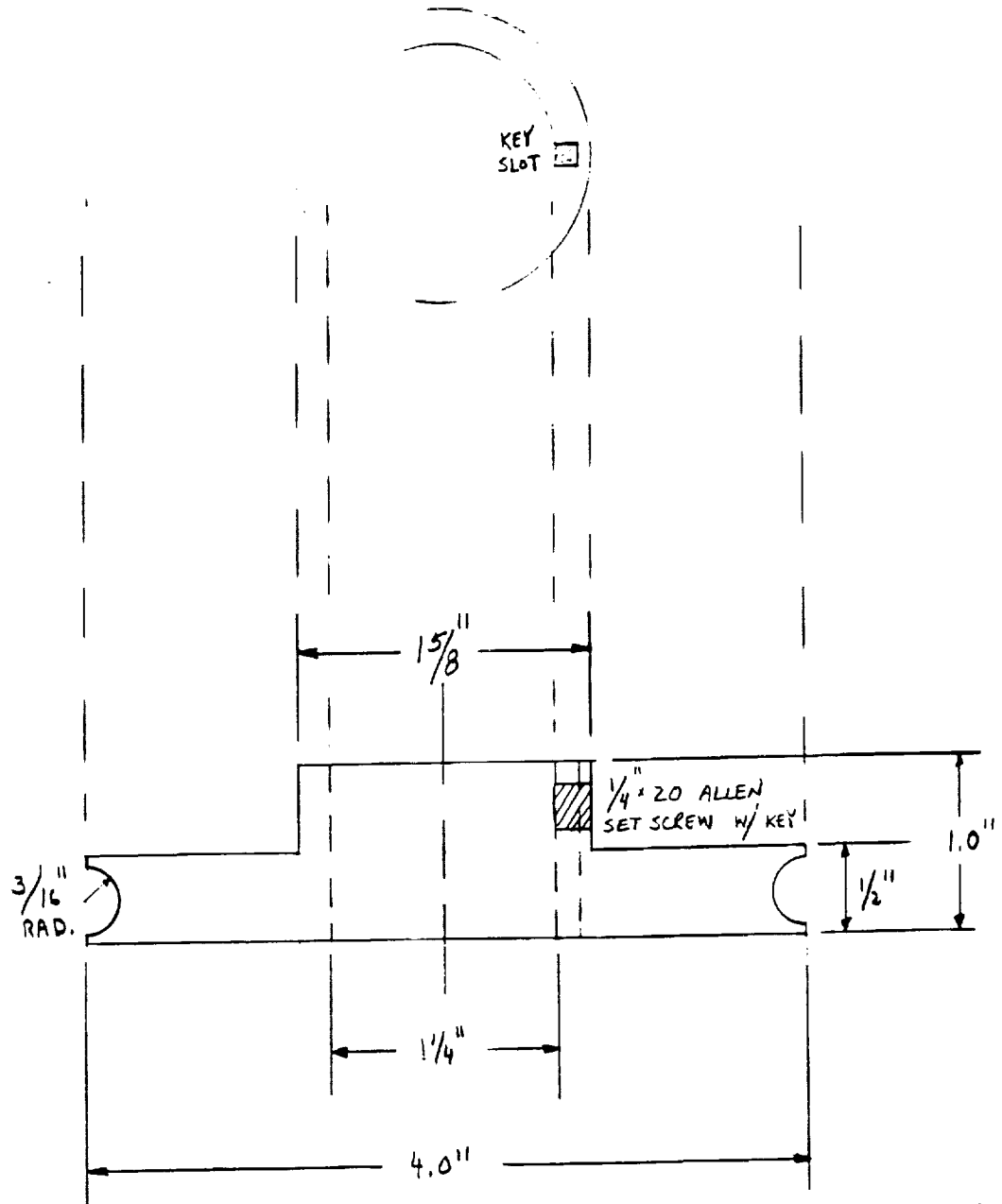
FROM 3 - 1/4" ALUMINUM PLATES  
& ALUMINUM TUBE.

ORIGINAL PAGE IS  
OF POOR QUALITY



PART # 8

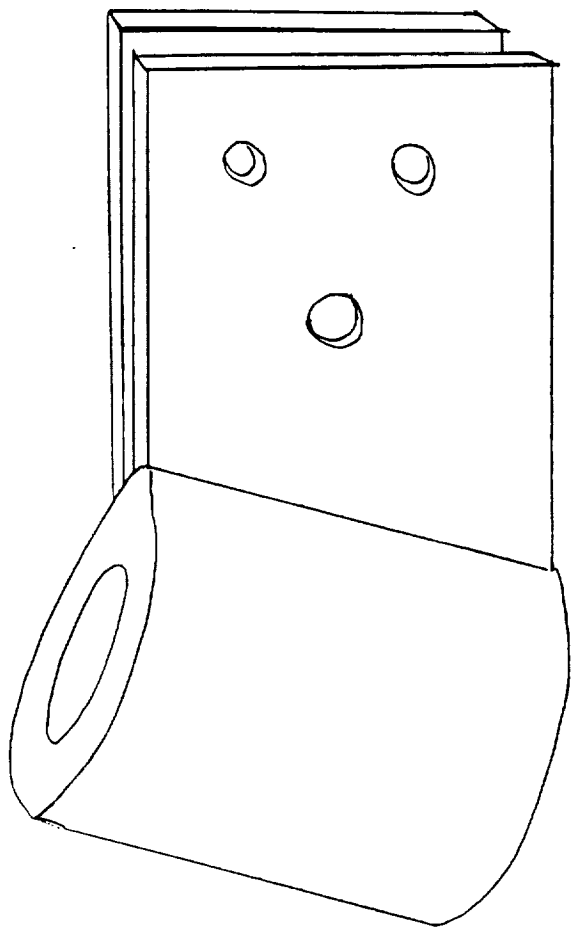
ALUMINUM STOCK



ORIGINAL PAGE IS  
OF POOR QUALITY

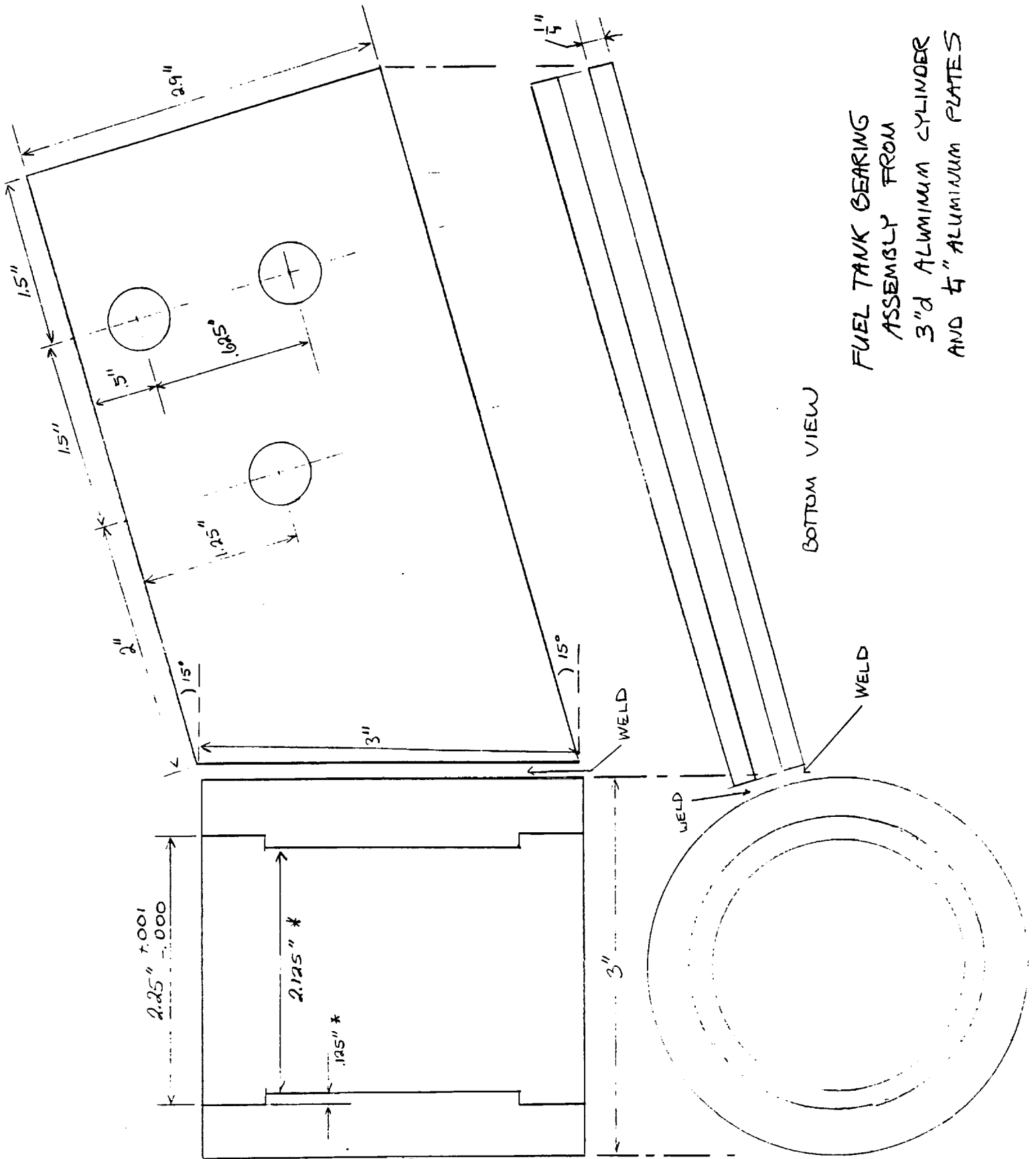
SCALE 1:1

PART 449



SKETCH OF FUEL TANK  
BEARING HOUSING

PART # 9 TOP VIEW

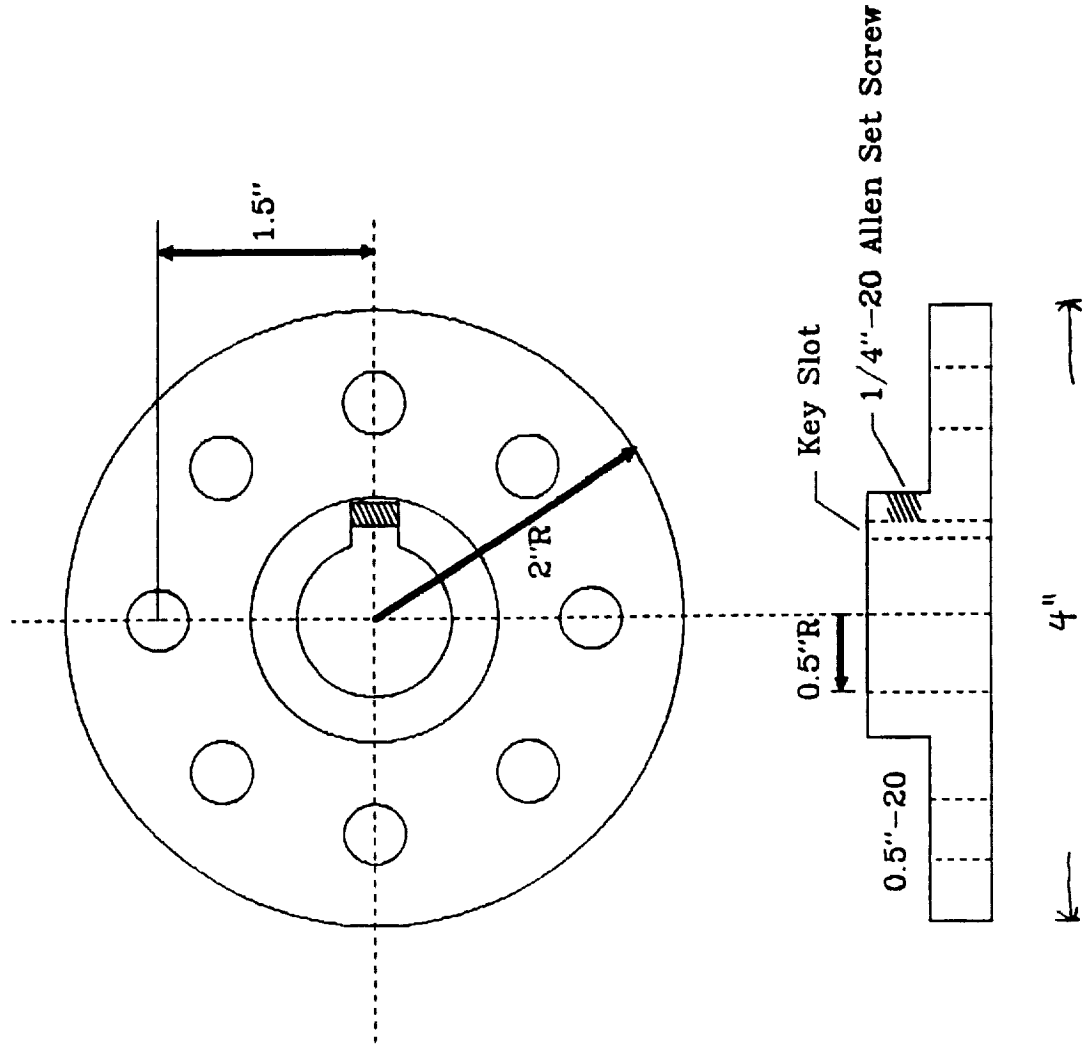


STOCK AS RECEIVED

# Part #10. Fuel Tank Mounting Flange.

Turned From Stainless Steel Cylinder

All dimensions  $+/- 0.02$ "

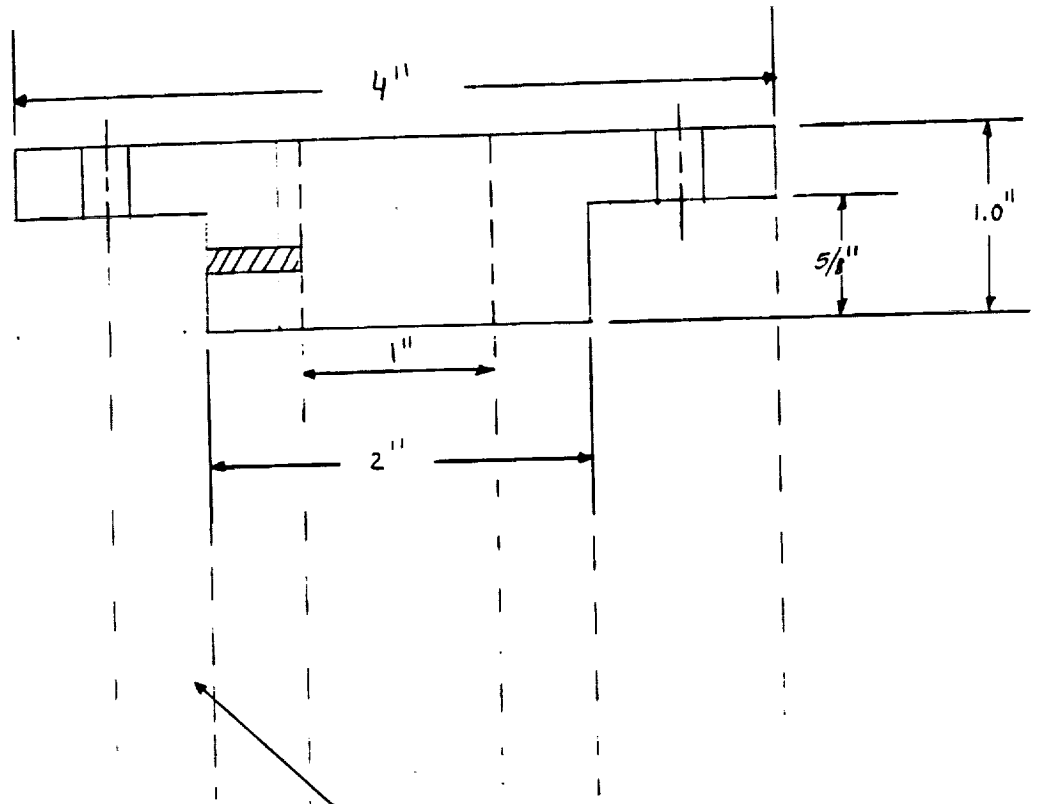


PART # 10

FUEL TANK MOUNTING  
FLANGE.

TURNED FROM STAINLESS  
STEEL STOCK CYLINDER

ALL DIMENSIONS  $\pm 0.010$



$\frac{1}{2}$ " DIA HOLE  
FOR ALLEN CAP SCREWS

12 HOLES WITH  
B.C = 3.0"

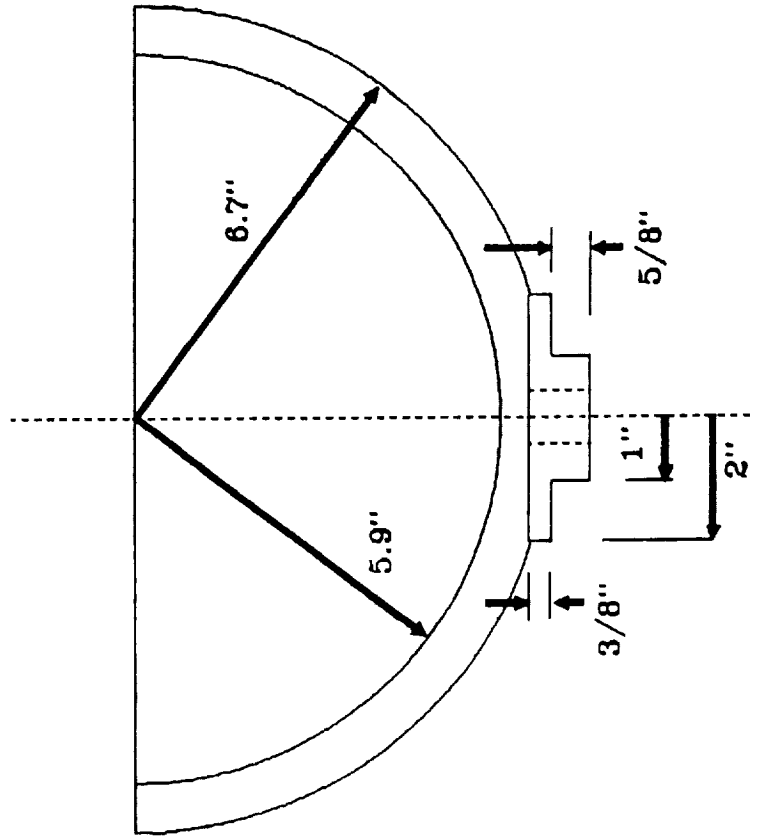
KEY  
SLOT

B.C = 3.0"

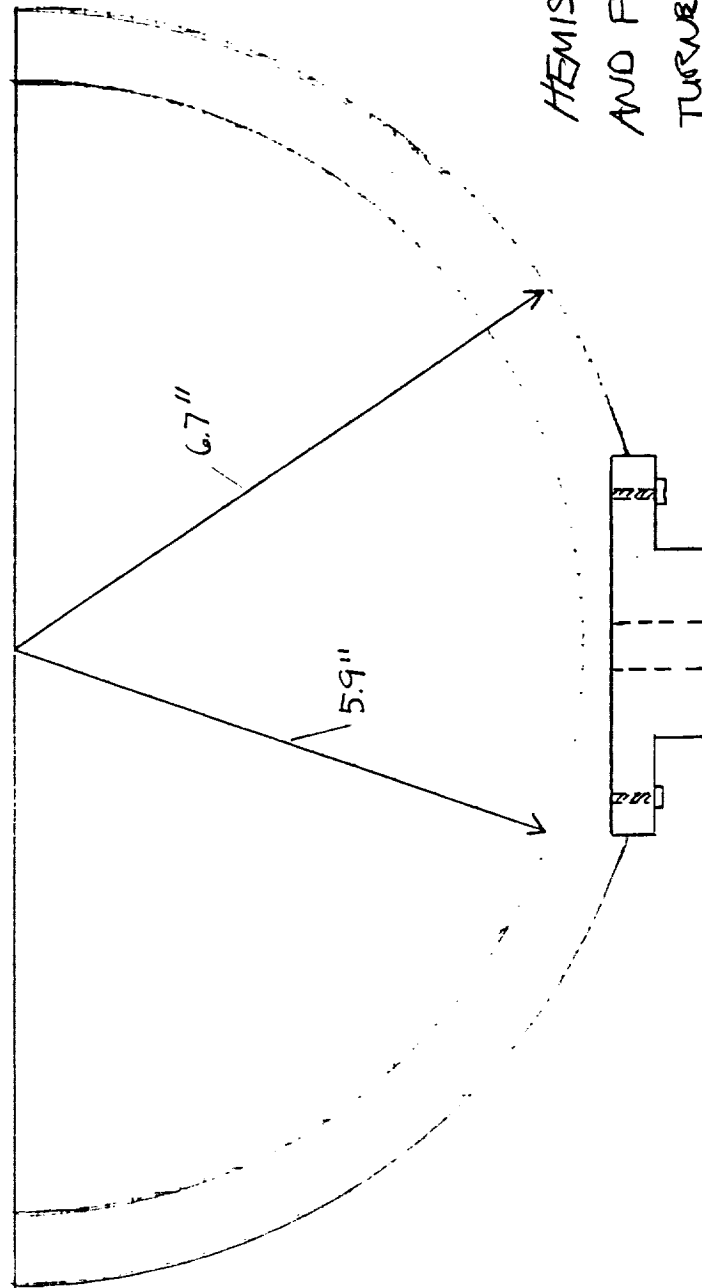
ORIGINAL PAGE IS  
OF POOR QUALITY

SCALE 1:1

Parts 10&11. Hemispherical tank and flange



PART #11



HEMISPHERICAL TANK  
AND FLANGE.

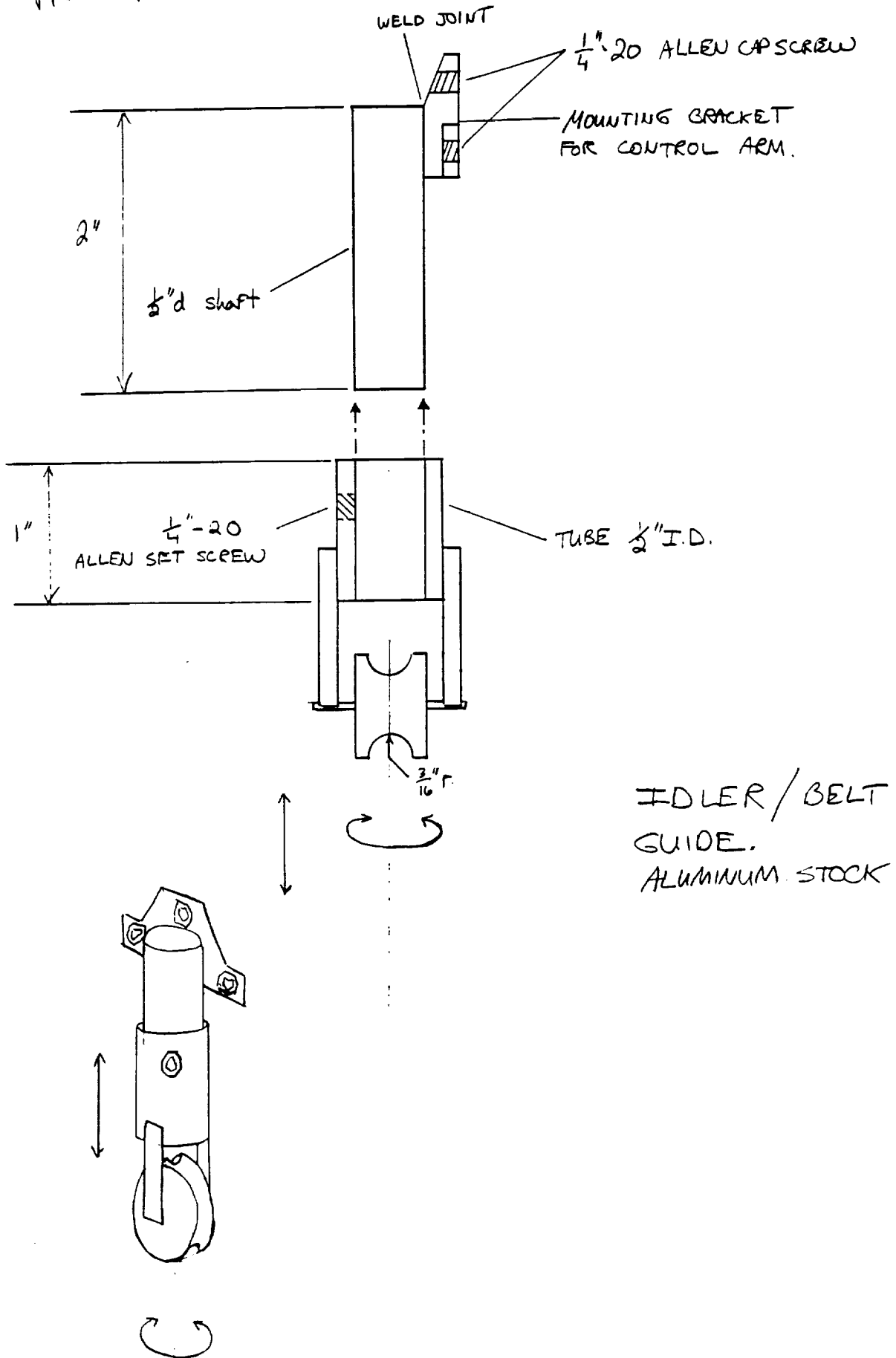
TURNED FROM LUCITE  
BLOCK MADE FROM 1"  
THICK SLABS.

TURN INSIDE AND OUTSIDE  
WITH CLEAR FINISH

ORIGINAL PAGE IS  
OF POOR QUALITY



PART # 13



## Simulation of Fluid Shape

In order to gain insight into the instability of a spacecraft due to liquid slag, a simple study of a liquid under simulated static forces should be made. This study can be made by applying Bernoulli's Equation (1) for both spherical and Cartesian coordinate systems in 3 dimensions.

$$-(\nabla \cdot P + \rho \cdot g \cdot \nabla \cdot h) = \rho \cdot a \quad (1)$$

If applied properly a shoreline--the line where the fluid meets the cup--can be graphed to obtain a top view of the cup. Moreover a cross-section of the front view may also be obtained. Due to the difficulty that the actual spacecraft precession poses with its nutation angle, a simplified study shall be made using a cup without a nutation angle.

Before the detailed study of the fluid shape under static forces is made, it is useful to conduct a qualitative examination of the fluid shape. Since the cup is spinning about its own axis, as well as about a point located at a fixed distance from the cup's center, one can assume that the fluid's actual shape is the superposition of the shapes caused by each motion separately. Figure 1 shows a picture of the posed problem while figures 2,3 and 4 are purely qualitative drawings of the fluid's shape before any calculations were done.

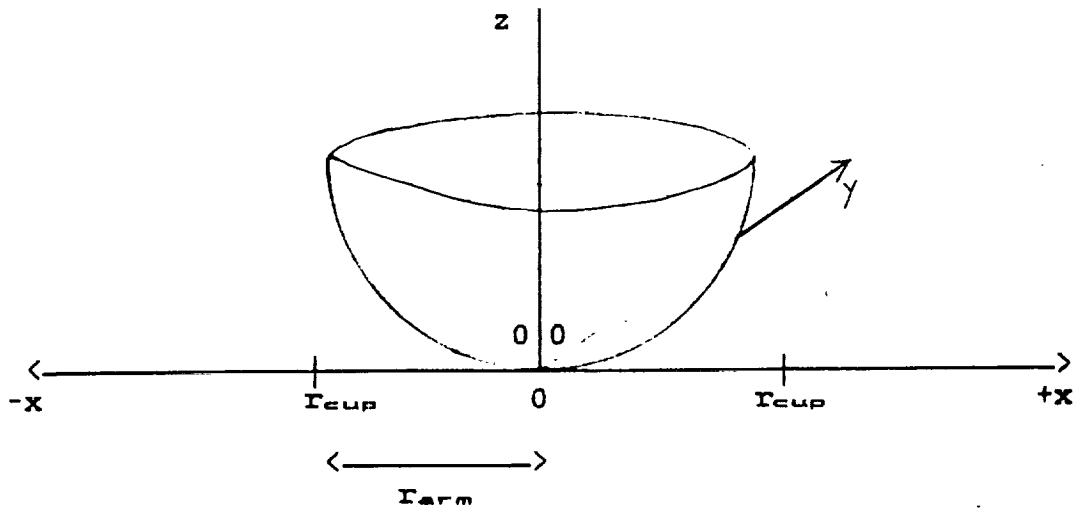


Figure 1.

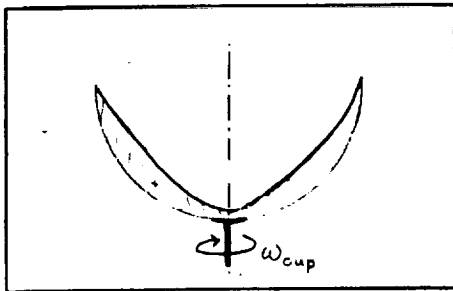


Fig.2 rotation about the cups center.

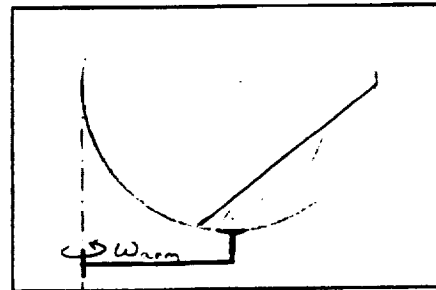


Fig.3 rotation about a fixed point.

Summing figures 1 and 2 figure 3 is obtained.

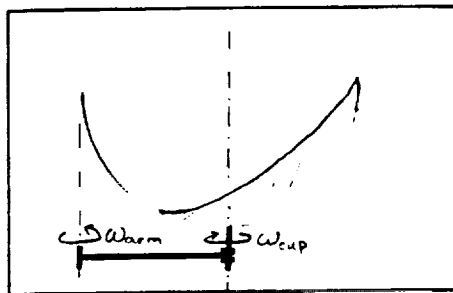


Fig.3 superposition of shapes in Fig. 2 and 3.

Now that a qualitative understanding of the situation

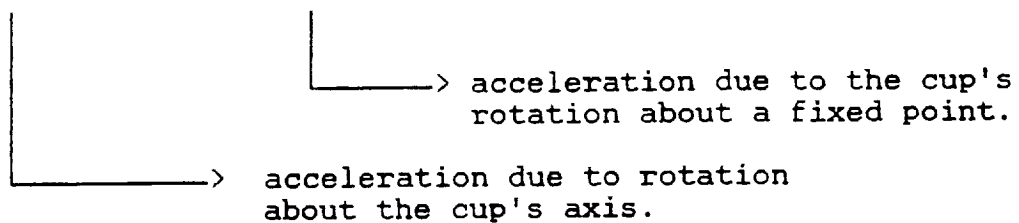
has been made, a theoretical solution should be constructed using equation (1) applied to our posed problem of fig. 1.

Applying Bernoulli's equation in the x direction, eqn. (1) reduces to eqn. (2):

$$-\frac{d}{dx} [P + \rho \cdot g \cdot h] = \rho a_x \quad (2)$$

where  $a_x$  is :

$$a_x = \omega_{cup}^2 \cdot x + \omega_{arm}^2 \cdot (r_{arm} + x) \quad \text{where: } -r_{cup} \leq x \leq r_{cup}$$



After integrating and assuming zero gauge pressure outside of the cup, equation (3) is obtained in the xy-plane:

$$z(x) = \frac{\omega_{cup}^2 + \omega_{arm}^2}{2 \cdot g} \cdot x^2 + \frac{\omega_{arm}^2 \cdot r_{arm}}{g} \cdot x + z(0) \quad (3)$$

Similarly applying eqn. (1) in the y direction, the following is obtained (4):

$$-\frac{d}{dy} [P + \rho \cdot g \cdot h] = \rho a_y \quad (4)$$

where  $a_y$  is :

$$a_y = \omega_{cup}^2 \cdot y$$

$$\text{where: } -r_{cup} \leq y \leq r_{cup}$$

Note that there is only acceleration due to the cup's rotation about its own axis in the yz-plane at the instant time we apply eqn. (1). Following the same integrating procedure used to obtain equation (3), equation (5) can easily be shown:

$$z(y) = \frac{\omega_{cup}^2}{2 \cdot g} \cdot y^2 + z(0) \quad (5)$$

Combining equations (3) and (5) we get a general three-dimensional expression for the height of the fluid in Cartesian and spherical coordinates (6a) & (6b). See appendix for the definition of spherical coordinates used.

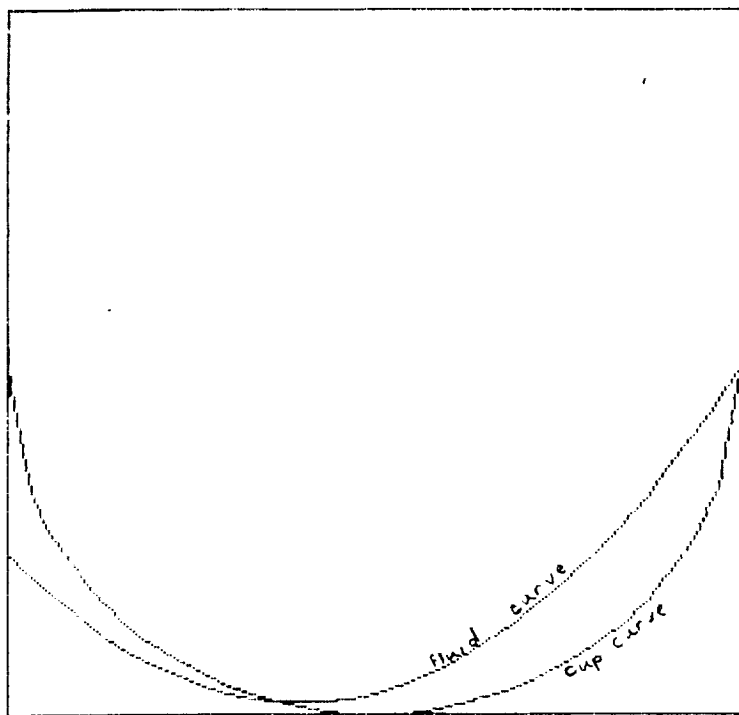
$$z(x,y) = \frac{\omega_{cup}^2 + \omega_{arm}^2}{2 \cdot g} \cdot x^2 + \frac{\omega_{arm}^2 \cdot r_{arm}}{g} \cdot x + \dots$$

$$\dots + \frac{\omega_{cup}^2}{2 \cdot g} \cdot y^2 + z(0,0) \quad (6a)$$

$$z(R, \phi, \theta) = \left[ \frac{\omega_{cup}^2 + \omega_{arm}^2}{2 \cdot g} \cdot R \cdot \cos(\phi) \cos(\theta) + \omega_{arm}^2 \cdot r_{arm} \right] \cdot R \cdot \cos(\phi) \cos(\theta) + z(0,0) \quad (6b)$$

In the xz-plane (front view,  $z(x,y=0)$ ), we obtain a

parabolic equation. By adjusting the constant  $z(0,0)$  one can determine how high the fluid may be at the middle of the cup before it would spill out. A quantitative plot was made and the initial height of the fluid determined to be 0.91cm using MathSoft's MathCad program. The following graph, constructed for the xz-plane, indicates the qualitative drawing for the final fluid shape in the xz-plane was indeed correct .



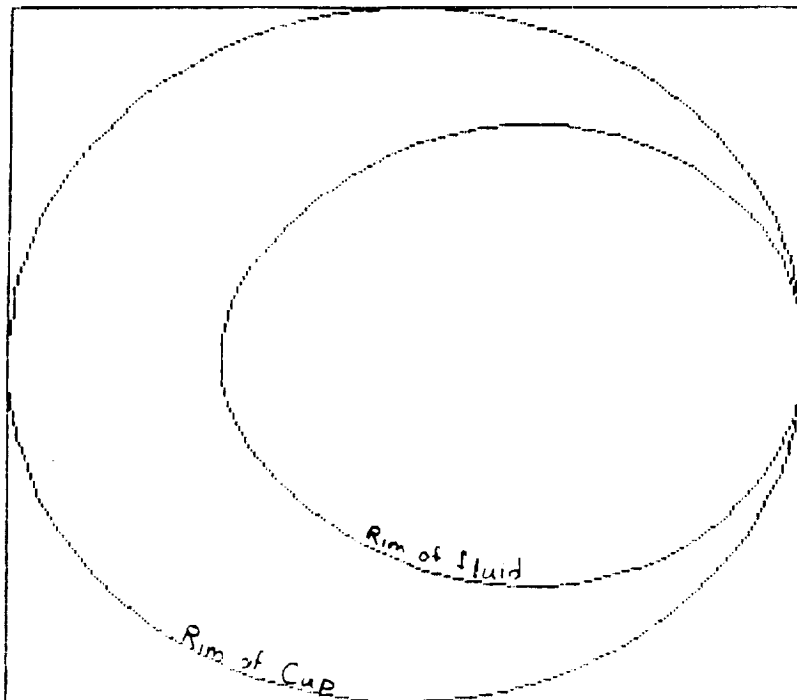
To obtain a shoreline of the fluid (xy-plane, top view) one must combine the equations for the height of the cup with the equation obtained for the height of the fluid shape (6b).

The since the cup is a sphere, the equation of the cup may be described by equation (7a) or (7b).

$$z^2 + x^2 + y^2 = R^2 \quad (7a)$$

$$z = \sqrt{R^2 - x^2 - y^2} \quad (7b)$$

Combining equations (7b) and (6b) then letting MathCad handle the algebra and plotting, we get the following graph.



If we examine equation (6a) we see that the form of the equation for the  $xy$ -plane is that of an ellipse displaced some distance from the origin (8).

$$A \cdot x^2 + B \cdot x + C \cdot y^2 = D$$

or

$$A' \cdot (x + b)^2 + C \cdot y^2 = D \quad (8)$$

where  $A, A', B, C, D$  are constants.

This form of our equation certainly agrees with the plot of the shoreline performed on MathCad as one can easily see by inspection. Thus we may conclude that the plot agrees with

the equation obtained for the fluid shape.

One may attempt to dispute the validity of the equations; however, recall that the problem of the actual fluid sloshing was not solved but rather a simplification of the problem. The solution though is still useful in gaining insight to the degree of fluid sloshing under the simulated conditions that have been chosen.

## COMPUTER SIMULATION OF A POINT MASS

A theoretical analysis representing a fluid by a displaced mass point has been developed by reference 5. Using this knowledge to validate our efforts, it was desired to track the motion of a point mass in a spinning and precessing hemispherical container with a nutation angle equal to zero. This was done in reference 6, (see appendix B), resulting in the following governing equations:

$$\frac{\partial^2 \theta}{\partial t^2} = (\psi_c)^2 \sin \theta \cos \theta + \frac{1}{r} (g_\theta - a_{\theta r}) - \gamma \theta_c - \omega_{sp} (\omega_{sp} - 2\psi_c \sin \theta) - (\omega_{sp})_c$$

$$\frac{\partial^2 \psi}{\partial t^2} = \frac{1}{\sin \theta} \left[ -2\theta_c \psi_c \cos \theta + \frac{1}{r} (g_\psi - a_{\psi r}) - \gamma \psi_c \sin \theta - \omega_{sp} (\omega_{sp} + 2\theta_c) + (\omega_{sp})_c \right]$$

where  $( )_c = \frac{\partial ( )}{\partial t}$

Using Heun's method for solving ordinary differential equations, as in reference 6, and noting that the quantities  $\omega$ ,  $g$ , and  $a$  are nearly constant, the position of the point mass as a function of time was found. A computer program was written to generate the data needed to develop a plot of the motions (see appendix C).

Several initial conditions were used (i.e. 20, 40, and 80 RPMs; and friction factors of 0.50, 0.75, 1.50) and plots were made for each of the nine conditions. It was found that no matter what value the friction factor had, the point mass flew out of the cup at 80 RPM. In fact, barely a difference in motion was observed (see figures 1-3).

However, at 40 RPM, the size of the friction factor influenced the motion in two distinct ways, see figures 4-6.

At a lower value, the motion rose higher in the cup as expected. Also as expected because of the greater motion, the point mass in the case of lower friction factor took much longer to stabilize and have a smooth motion.

In the case of spinning at 20 RPM, see figures 7-9, much less is obvious. Since the spin rate is so low, the point mass stays much closer to the bottom of the cup. The most interesting observation is that again the friction factor plays a large role in compactness of the motion.

This theoretical analysis, though it is valid, will not have much of an influence in the report except that it shows that a stable motion can be achieved. Applying this to our problem we can hope that an equilibrium of the fluid motion can be found.



142 381 30 SHEETS 3 SQUARE  
100 SHEETS 3 SQUARE

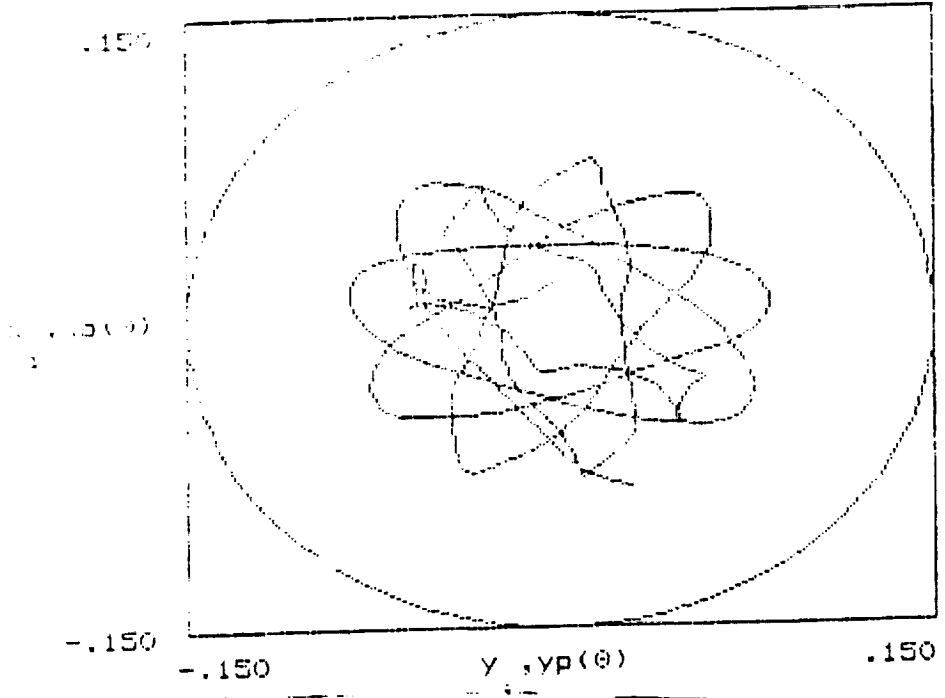


fig. 4

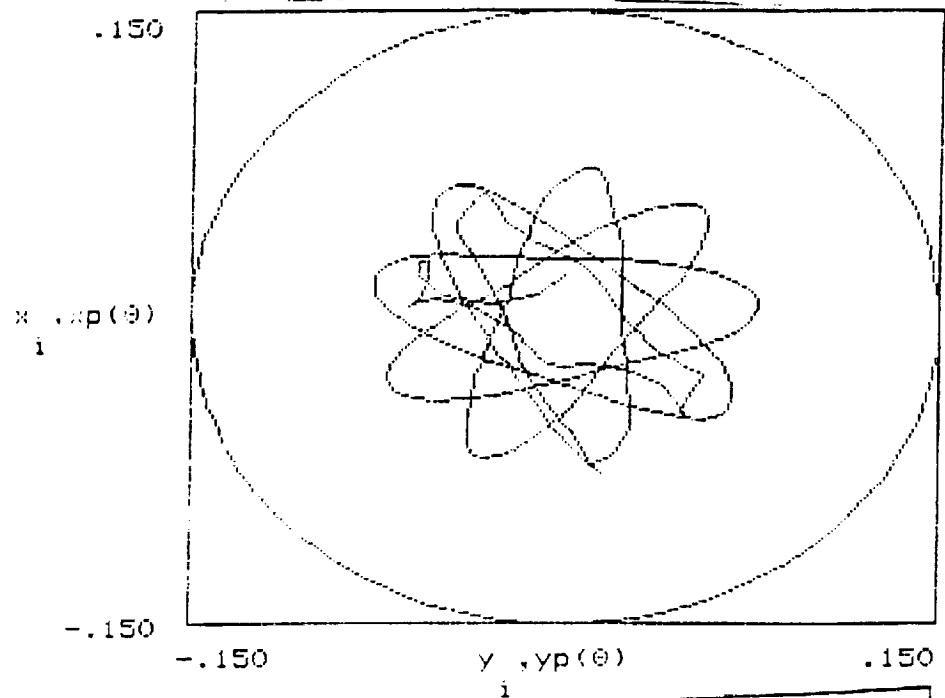


fig. 5

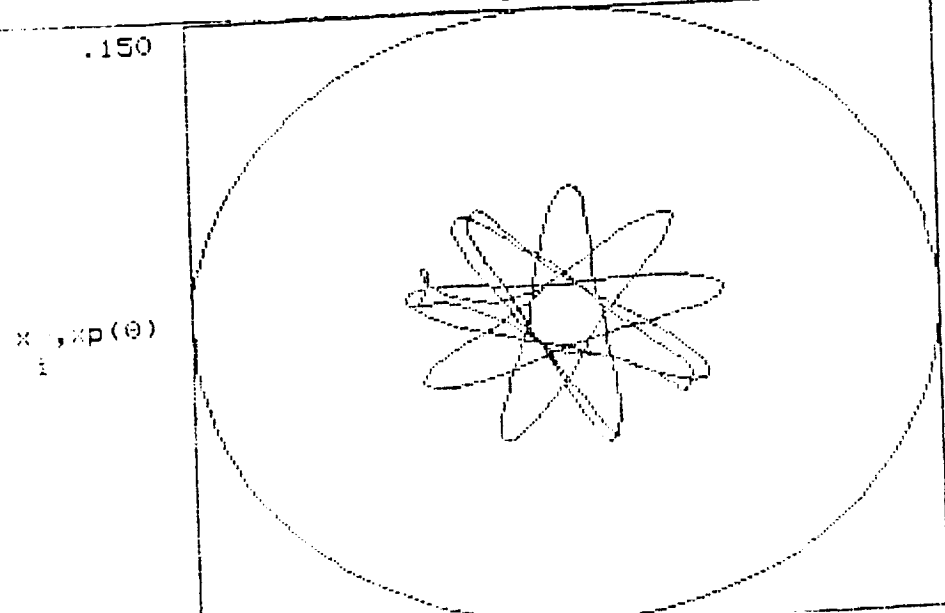


fig. 6

ORIGINAL PAGE IS  
OF POOR QUALITY

GF, 4

3 381 30 SHEETS 3 SQUARE  
42 389 300 SHEETS 3 SQUARE

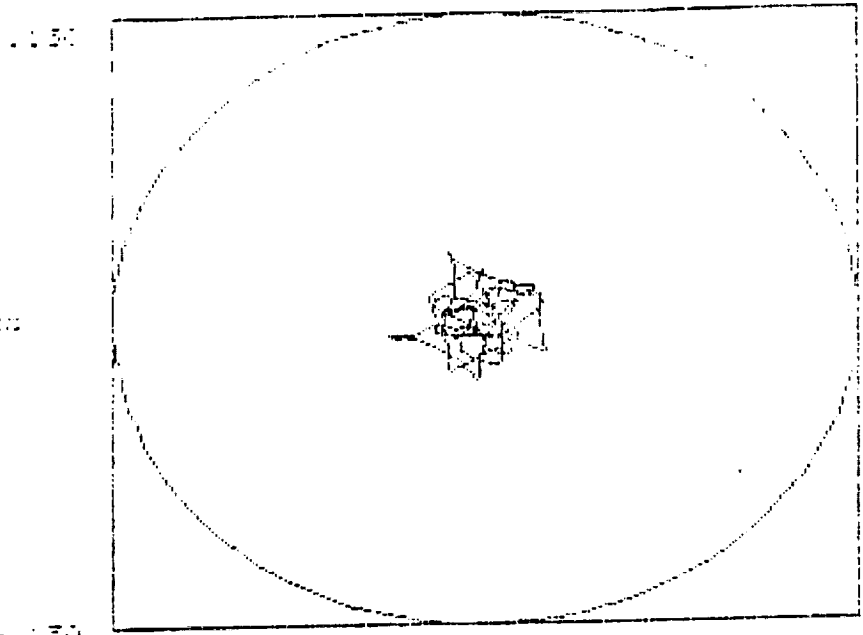


fig. 7

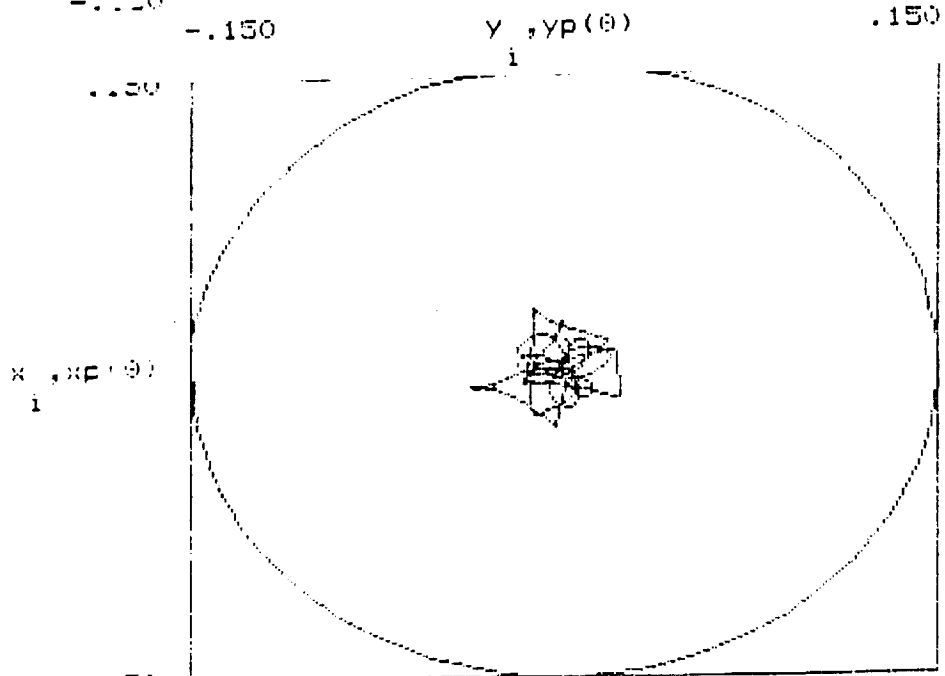


fig. 8

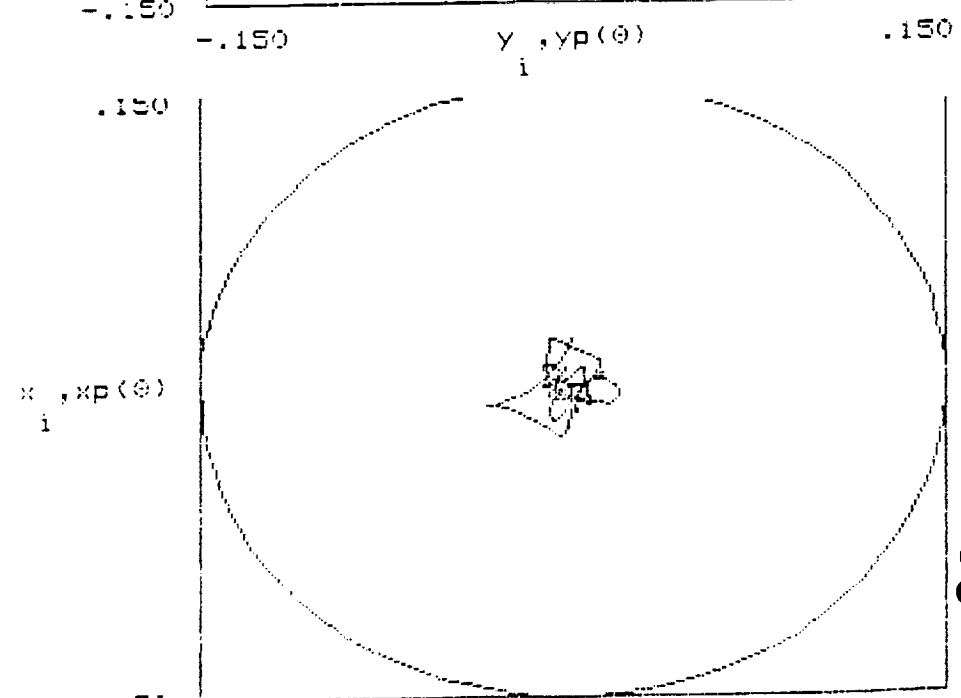


fig. 9

ORIGINAL PAGE IS  
OF POOR QUALITY

## HOT WIRE

In the process of designing the experimental fluid sloshing machine, the question of how to measure the depth of fluid in the sloshing container turned out to be a very challenging project. Professor Meyer proposed the use of a heated tungsten wire inside of the fluid container (cup). The heat loss of the wire would in turn be related to the depth of fluid inside of the cup. Other proposals, like pressure tabs and simple capillary tubes, were also considered and thoroughly discussed.

Since the hot wire proposal seemed to be the most promising path, several calculations were done to relate the heat loss of the tungsten wire to the actual depth of fluid in the cup.

The hot-wire was intended to be an application of the Hot-Wire Anemometer commonly used in measuring the speed of fluids. The hot wire anemometer is basically a thermal transducer. An electric current is passed through a fine filament which is exposed to a cross flow. (This fine wire is actually one of the resistances in a Wheatstone bridge circuit). As the flow rate varies, the heat transfer from the wire to the flowing fluid varies (increases with increasing velocity and decreases with decreasing velocity). This variation occurs because the electrical resistivity of the wire is

a very strong function of temperature. Hence, when the wire loses heat (it cools) its electric resistivity goes down (true for metals).

There are basically two techniques to monitor flow conditions with the hot wire: constant temperature and constant current flowing through the wire. When the current in the wire is kept constant, the changes in its electrical resistivity unbalance the Wheatstone Bridge. This is recorded as a voltage drop across the bridge. On the other hand, when the temperature of the wire is kept constant, then a feed-back control will have to be part of the Wheatstone bridge. This feed-back control will sense the increase or decrease of heat transferred by the wire to its surroundings, and will adjust the amount of current flowing through the wire in order to keep the temperature constant.

The problem with the hot wire proposal is not one but many. For example, it is necessary to determine whether the wire is losing heat through a free convection process or a forced convection process. Moreover, it is critical to determine how much heat is lost to the sloshing fluid, and how much is lost to the surrounding air. This is important because if the difference between the heat lost to air and to water is not very significant then the recorded datum would be misleading.

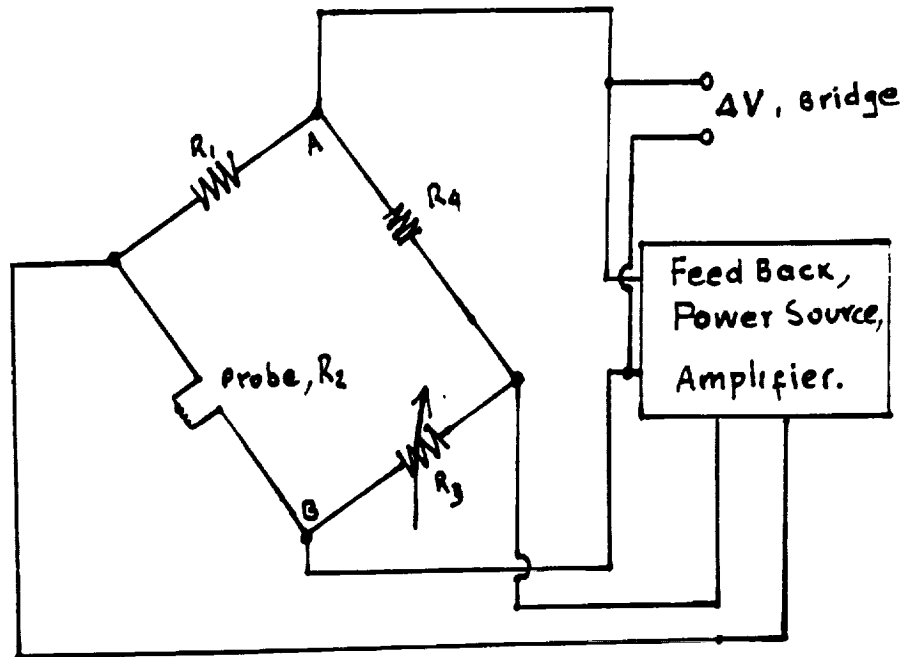


Fig. A Block diagram of a constant temperature anemometer. The hot wire is the probe acting as one of the resistors in the Wheatstone Bridge circuit. The feed back control adjusts the current to keep the bridge balanced.

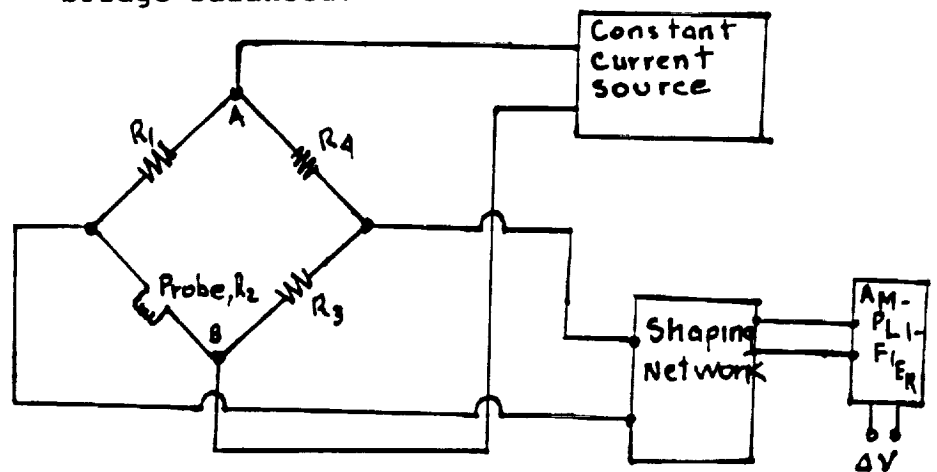
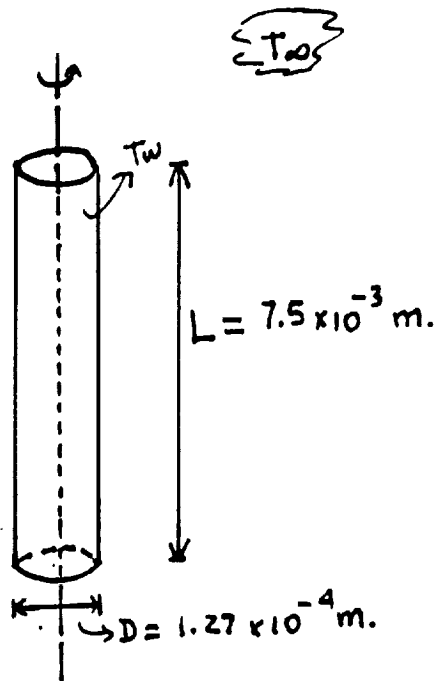


Fig. B The block diagram of a constant current anemometer. The probe is one of the resistors in the Wheatstone Bridge circuit. The voltage across the bridge is shaped and amplified before being recorded.

The following calculations will show that, in view of all the "forced" assumptions to idealize the process, the hot wire is not the most reliable method to determine the depth of fluid in the cup.



$T_w = \text{Wire's wall Temp}$   
 $= 50^\circ\text{C}$

$T_{\infty} = \text{Fluid's Temp.}$   
 $= 21.11^\circ\text{C}$   
 $= \text{Air Temp.}$

$\beta = 3.51 \times 10^{-4} \text{ } 1/^\circ\text{K}$

$\mu_f = 6.82 \times 10^{-4} \text{ kg/m. sec}$

$\rho_f = 993 \text{ kg/m}^3$

$C_p = 4.174 \text{ J/kg } ^\circ\text{C}$

$K_f = 0.630 \text{ W/m } ^\circ\text{C}$

To be treated as a vertical cylinder, the necessary condition is, [1]\*\*

$10^{-1} < Gr Pr < 10^{12}$ , so,

$Pr = 4.53$

$Gr = \frac{g \beta (T_w - T_{\infty}) L^3 \rho_f^2}{\mu_f^2}$

(9-A)

$= 88,941$

And:

$Gr Pr = 402,904 \checkmark$

\* ( )<sub>f</sub> implies that the given material property is valid for the "film temperature",  $T_f = \frac{T_w + T_{\infty}}{2}$

\*\* Free Convection Heat transfer is Assumed.

See Appendix E

Now, from [1],

$$\bar{Nu}^{1/2} = 0.825 + \frac{0.387 (Gr Pr_f)^{1/6}}{\left[1 + \left(\frac{0.492}{Pr_f}\right)^{9/16}\right]^{8/27}} \quad (1-B)$$

$$\bar{Nu}^{1/2} = \frac{\bar{h} D}{k_f} = 1.38178 \quad (1-C)$$

$$\bar{h} \cong 6854 \text{ W/m}^2\text{°C}$$

To get the heat Lost,

$$q_{\text{water}} = \bar{h} A_{\text{surf}} (T_w - T_\infty) \quad (1-D)$$

$$= 6854 \text{ W/m}^2\text{°C} \left[1.27 \times 10^{-4} \pi 7.5 \times 10^{-3}\right] \text{m}^2 (\Delta T)$$

$$\underline{\underline{Q_{\text{water}} = 5.927 \times 10^{-1} \text{ W}}}$$

Now if the same wire were exposed only to air, the air could not be assumed stagnant with respect to the wire since the cup is rotating about a point ten inches away. (see fig.C)

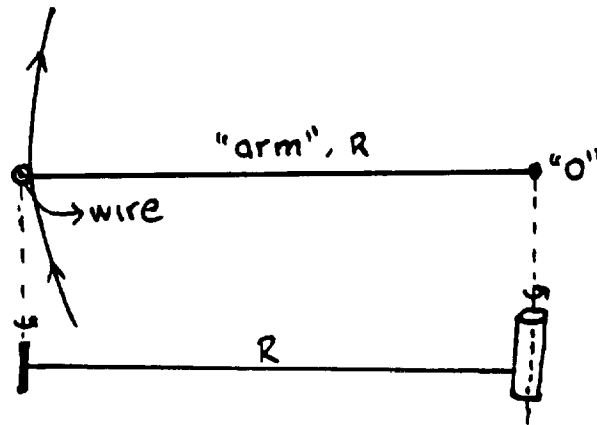


Fig. C Wire rotates about point "o"

Hence, the velocity of the air hitting the vertical wire is approximately given by the tangential velocity of the wire:

$$V_{ar} = R \cdot \omega_1 \quad (2-A)$$

However, this velocity indicated by eq. ( ) does not take into account the fact that the wire is also rotating about its own axis. So, the absolute velocity of a point on the surface of the wire is the sum of  $V$  given by eq. ( ) and the velocity of the point with respect to the center of the wire:

$$V_{or} = r \cdot \omega_2 \quad (2-B)$$

So:

$$V_{o,abs.} = r \cdot \omega_2 + R \omega_1 \quad (2-C)$$

So:

$$V_{\theta} = 0.00027 \text{ m/sec} + 1.0640 \text{ m/sec.}$$

$$V_{\theta} = 1.0643 \text{ m/sec.}$$

And:

$$\left. \begin{array}{l} T_{\infty} = 21.11 \\ T_w = 50.00 \end{array} \right\} T_f = 36 = 310^{\circ}\text{K}$$

$$\mu_f = 1.89196 \times 10^{-5} \text{ kg/m}\cdot\text{sec.}$$

$$\rho_f = 1.14152 \text{ — kg/m}^3$$

$$K_f = 0.026998 \text{ W/m}\cdot^{\circ}\text{K}$$

$$Pr = 0.7058$$

$$\beta = \frac{1}{T_{\infty}} = 0.0034$$

$$\begin{aligned} Re &= \frac{V_{\theta} D \rho_f}{\mu_f} && (2-d) \\ &= 8.1553 \end{aligned}$$

From Ref [1], p. 292,

$$\bar{Nu} = (0.43 + 0.50 Re^{0.5}) Pr^{0.38} \quad (2-e)$$

when,  $1 < Re < 1000$

So,

$$\bar{Nu} = \frac{\bar{h} D}{K_f} = 1.6275$$

And

$$\bar{h} = 346 \text{ W/}^{\circ}\text{K m}^2$$

So; from eq (1-d)

$$\underline{\underline{q_f = Q_{air} = 2.99 \times 10^{-2} \text{ W}}}$$

The ratio of  $Q_{\text{air}}$  to  $Q_{\text{water}}$  when the wire is in air only and water only respectively is:

$$\frac{Q_{\text{water}}}{Q_{\text{air}}} = \underline{\underline{19.81}}$$

This ratio is very likely to go down when more of the wire is exposed to air as it would be the case during an actual experiment. So,

$L_1 = \text{Length of wire in H}_2\text{O} : \overset{\textcircled{A}}{0.0025 \text{ m}} / \overset{\textcircled{B}}{0.0010 \text{ m}}$   
 $L_2 = \text{Length of wire in Air} : 0.0050 \text{ m} / 0.0065 \text{ m}$

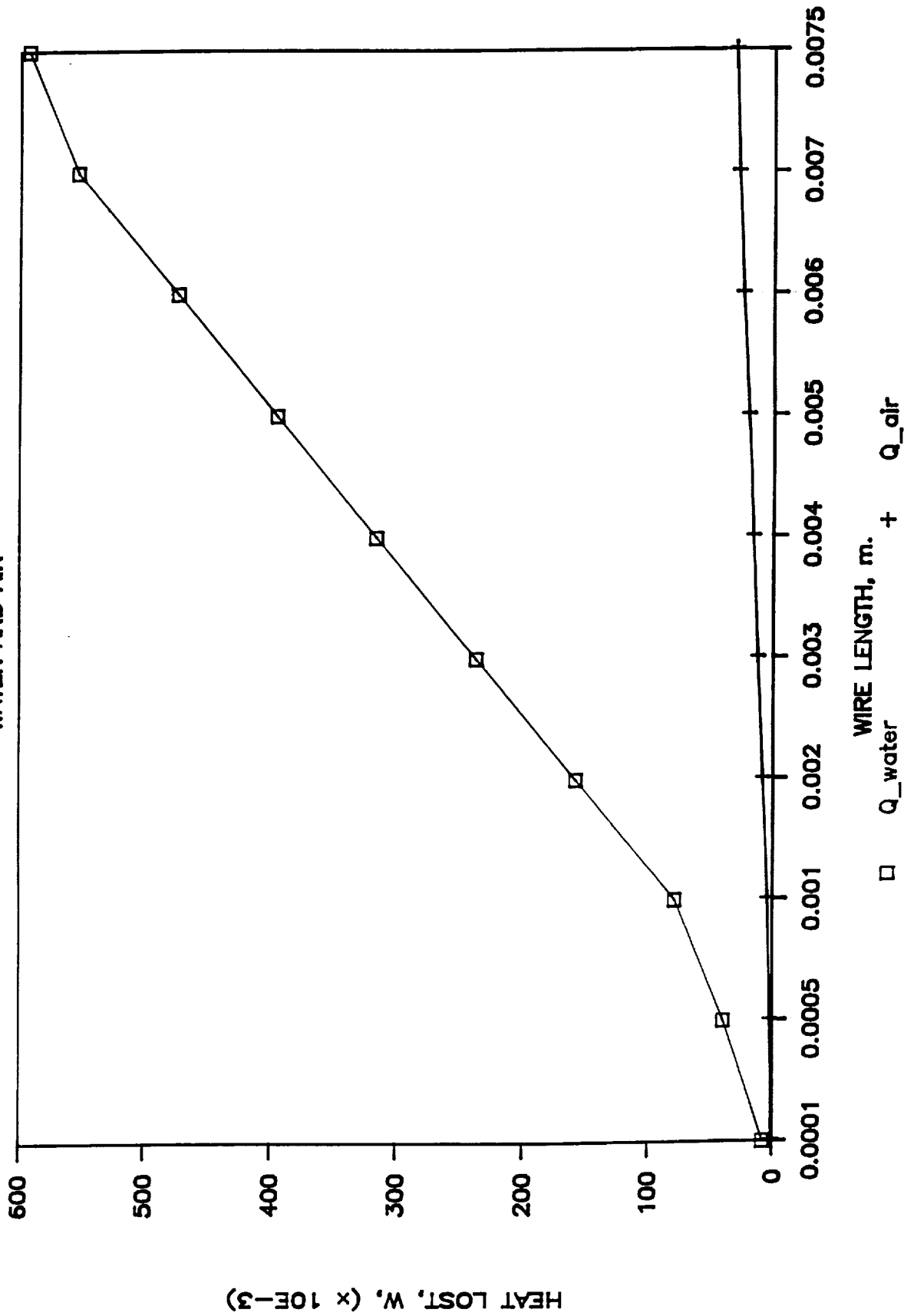
$$\textcircled{A} \quad \frac{Q_{\text{water}}}{Q_{\text{Air}}} = \underline{\underline{9.90}}$$

$$\textcircled{B} \quad \frac{Q_{\text{water}}}{Q_{\text{Air}}} = \underline{\underline{3.04}}$$

In view of all the assumptions and of the given sample ratios, this proposal of the hot wire presents too many uncertainties. For this reason no experimental work was carried on and the proposal had to be turned down. However, there is another proposal that is likely to give more precise results in a simpler manner. This proposal, given by James Marcollesco (TA), will be explored further this Spring.

# HEAT LOST BY WIRE VS. LENGTH IN

WATER AND AIR



The purpose of these calculations is to demonstrate that the heat loss of tungsten wire is greater in water than in air and hence the voltage drop is also greater in water.

However, a very simplified version of calculating the heat transfer of the hot-wire probe is as follows:

A tungsten wire of length,  $L = 7.5\text{mm}$  and diameter,  $D = 1.27 \times 10^{-3}\text{mm}$  is used. There are two cases where this tungsten wire is either exposed to the air or water in the rotating cup with no nutation angle. Several assumptions are made due to the complexity of these problems, such as forced convection heat transfer of wire, the wire is entirely exposed to the air or submerged in water, the temperature of wire is below the boiling-point of water, and both wire and cup have equal angular velocity (or constant velocity) on the stationary arm.

The sample calculations of these two cases are as follows:

I. To find the velocity of water in the cup using Navier-Stokes equation.

Assume that wire and cup are two long cylinders and rotating at  $\omega$ , with water as incompressible liquid.

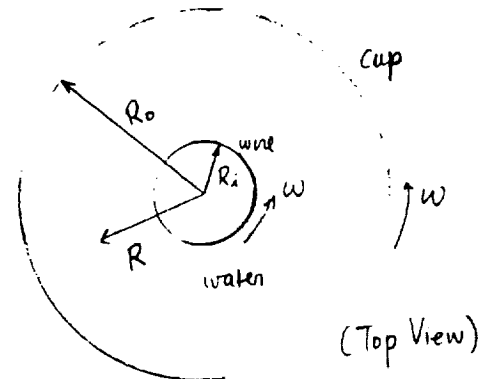
$$R = \frac{1}{2} R_o = 0.07493\text{m}, \quad \omega = 80\text{rpm} = 8.38\text{rad/s}$$

$$\text{Boundary conditions: } \begin{aligned} V_\theta(R_i) &= \omega R_i \\ V_\theta(R_o) &= \omega R_o \end{aligned}$$

Using Navier-Stokes (neglecting pressure and hydrostatic effects, and at steady-state):

$$\theta: \quad \left\{ \frac{D V_\theta}{dr} + \frac{V_r V_\theta}{r} \right\} = -\frac{\gamma}{r} \left[ \frac{\partial h}{\partial \theta} - \frac{\partial P}{\partial \theta} \right] + \mu \left[ \nabla^2 V_\theta - \frac{V_\theta}{r^2} + \frac{2}{r^2} \frac{\partial V_r}{\partial \theta} \right]$$

$$0 = \mu \left[ \frac{\partial^2 V_\theta}{\partial r^2} + \frac{\partial}{\partial r} \left( \frac{V_\theta}{r} \right) \right]$$



(Top View)

$$\frac{d^2 V_r}{dr^2} + \frac{d}{dr} \left( \frac{V_r}{r} \right) = 0$$

$$\Rightarrow V_r(r) = \frac{C_1 r}{2} + \frac{C_2}{r}$$

Applying b.c's :

@  $r = R_i \Rightarrow \omega R_i^2 = \frac{C_1 R_i^2}{2} + C_2$  — ①

@  $r = R_o \Rightarrow \omega R_o^2 = \frac{C_1 R_o^2}{2} + C_2$  — ②

Solving ① & ②,  $C_1 = 2\omega$  and  $C_2 = 0$

$$V_r(r) = \frac{2\omega r}{2} = \omega r$$

Then, at  $r = R$ , the assumed velocity of water in the cup is

$$V_r(R) = \omega R = 0.63 \text{ m/s}$$

## II. Forced convection of wire in air.

Let  $T_{\text{wire}} = 80^\circ\text{C} = 353 \text{ K}$ ,  $T_\infty = T_{\text{air}} = 25^\circ\text{C} = 298 \text{ K}$

Film temperature,  $T_f = \frac{T_{\text{wire}} + T_\infty}{2} = 326 \text{ K}$

Air properties evaluated at  $T_f$ :  $\nu = 18.41 \times 10^{-6} \text{ m}^2/\text{s}$ ,  $Pr = 0.7035$ ,  $k = 22.15 \times 10^{-3} \text{ W/mK}$

a. @  $V_r = 0.63 \text{ m/s}$ ,

$$Re_D = \frac{V_r D}{\nu} = 4.334$$

and  $Re_D Pr = 3.05 > 0.2$

Using Churchill & Bernstein correlation:

$$\overline{Nu}_D = \frac{\overline{h} D}{k} = 0.3 + \left[ \frac{0.62 Re_D^{1/2} Pr^{1/3}}{(1 + (0.4/Pr)^{1/4})^{1/4}} \right] \left( 1 + \left( \frac{Re_D}{28200} \right)^{5/8} \right)^{4/5}$$

$$\frac{\overline{h} D}{k} = 1.311$$

$\Rightarrow \therefore \overline{h} = \text{average heat transfer coefficient} = 2.906 \times 10^2 \text{ W/m}^2 \cdot \text{K}$

Since, heat loss =  $q = \overline{h} A [T_{\text{wire}} - T_\infty]$ ,  $A = 2\pi R_i L$

$$= 2.906 \times 10^2 [2\pi] \left[ \frac{0.0127 \times 10^{-2}}{2} \right] [7.5 \times 10^{-3}] \quad (55)$$

$$\therefore q = 4.78 \times 10^{-2} \text{ Watt}$$

But  $q = I^2 R = \frac{V^2}{R}$

$$(R_{\text{tungsten}} = \frac{54 \times 10^{-8} \Omega \cdot \text{m}}{7.5 \times 10^{-3} \text{ m}^2} = 7.2 \times 10^{-6} \Omega)$$

$$V = \sqrt{qR} = 3.44 \times 10^{-7} \text{ Volt}$$

b) @  $V_0 = 0.5 \text{ m/s}$ ,

$$Re_D = 3.449 \quad \text{and} \quad Re_D Pr = 2427 > 0.2$$

Using the same correlation:

$$\overline{Nu}_D = \frac{\bar{h}D}{K} = 1.201$$

$$\therefore \bar{h} = 266.3 \text{ W/m}^2 \cdot \text{K}$$

$$\therefore q = \bar{h}A [T_{\text{wire}} - T_{\infty}] = 4.38 \times 10^{-2} \text{ Watt}$$

$$\text{and, } V = 3.16 \times 10^{-7} \text{ Volt}$$

III. Forced convection of wire in water.

$$\text{Let } T_{\text{wire}} = 353 \text{ K}, \quad T_{\infty} = T_{\text{H}_2\text{O}} = 298 \text{ K}$$

$$\therefore \text{Film temperature, } T_f = \frac{T_{\text{wire}} + T_{\text{H}_2\text{O}}}{2} = 326 \text{ K}$$

Water properties evaluated at  $T_f$

$$\nu = 5.35 \times 10^{-7} \text{ m}^2/\text{s}, \quad Pr = 3.42, \quad K = 645 \times 10^{-3} \text{ W/m} \cdot \text{K}$$

1) @  $V_0 = 0.63 \text{ m/s}$ ,

$$Re_D = \frac{V_0 D}{\nu} = 149.55 \quad \text{and} \quad Re_D Pr = 511466 > 0.2$$

Using Churchill & Bernstein correlation:

$$\overline{Nu}_D = \frac{\bar{h}D}{K} = 11.4528$$

$$\therefore \bar{h} = 58165.82 \text{ W/m}^2 \cdot \text{K}$$

$$\therefore q = \bar{h}A [T_{\text{wire}} - T_{\text{H}_2\text{O}}] = 9.573 \text{ Watt}$$

$$\text{And, } V = 6.89 \times 10^{-5} \text{ Volt}$$

b @  $V_0 = 0.5 \text{ m/s}$ ,

$$Re_D = 118.69 \quad \text{and} \quad Re_D Pr = 405.93 > 0.2$$

Using the same correlation:

$$\overline{Nu_D} = \frac{\overline{h}D}{K} = 10.1967$$

$$\therefore \overline{h} = 51786.41 \text{ W/m}^2\cdot\text{K}$$

$$\dots q = 8.523 \text{ Watt}$$

$$\text{and } V = 6.14 \times 10^{-5} \text{ Volt}$$

We can observe that the heat loss of wire in the air is much less compared to the heat loss of wire in the water. It can therefore be argued that the heat loss in air is quite negligible.

After performing these sample calculations, we still need to examine the effects of heat loss and also the voltage difference of tungsten wire having a different height submerged in water. Let us make several assumptions for this case by:

1. neglecting heat loss of tungsten wire in the air (as shown earlier where heat loss in air is much smaller than in water).
2. having the temperature of wire below the boiling-point of water.
3. having constant velocity (at  $V_0 = 0.63 \text{ m/s}$ ).

We have the same conditions for wire and water temperatures, except that the height of wire submerged in water is 5.0mm. This sample calculation follows:

IV. Forced convection of wire in water.

The same calculation procedure as of case II(a).

$$\begin{aligned}\Rightarrow q &= \bar{h} A [T_{wire} - T_{H_2O}] \\ &= 58165.8 [2\pi] \left[ \frac{0.0127 \times 10^{-2}}{2} \right] [5 \times 10^{-3}] \quad (55) \\ &= 6.382 \text{ Watts.}\end{aligned}$$

$$\text{Since, } q = \frac{V^2}{R}$$

$$\therefore V = \sqrt{qR}$$

$$= 1.82 \times 10^{-5} \text{ Volt}$$

Examining these three cases, we can argue that for smaller values of tungsten wire height being submerged in water, we will obtain lower heat transfer coefficients, lower values of heat loss and thus, lower voltage differences. So, based on these "rough" assumptions that as the convection heat transfer coefficient decreases, so will the voltage differences, and we can try to correlate these to give  $\bar{h} = \bar{h}(V)$ .

Material Request

Part #	Quantity	Description
1	1	Aluminum cylinder O.D. = $4\frac{1}{4}$ " , I.D. = 2" , H = 5"
2	1	Bodine capacitor motor (100 rpm)
3	1	Aluminum pulley (sheave) O.D. = 4" , I.D. = $1\frac{1}{4}$ " , H = 1" , $r = \frac{3}{16}$ "
4	1	Aluminum pulley (sheave) O.D. = 5" , I.D. = $1\frac{1}{4}$ " , H = 1" , $r = \frac{3}{16}$ "
5	1	Aluminum pulley (sheave) O.D. = 4" , I.D. = $1\frac{1}{4}$ " , H = $\frac{1}{2}$ " , $r = \frac{3}{16}$ "
	1	Aluminum box ( $\frac{1}{4}$ " thick plate) L = $1\frac{1}{2}$ " , W = 6" , Depth = 8"
6	1	Shaft (1020 Cold rolled steel) O.D. = $1\frac{1}{2}$ " , I.D. = $\frac{3}{16}$ " , H = $14\frac{5}{32}$ "
7	1	Top : (Aluminum $\frac{1}{4}$ " thick plate) L = 11.8" , W = 3"
	1	Bottom : (Aluminum $\frac{1}{4}$ " thick plate) L = 18" , W = 4"
	1	Aluminum tube O.D. = 2" , I.D. = $1\frac{1}{4}$ " , H = 4"

Part #	Quantity	Description
8	1	Aluminum pulley (sheave) O.D. = 4", I.D. = 1 $\frac{1}{4}$ ", H = 1", r = $\frac{3}{16}$ "
9	1	Aluminum cylinder O.D. = 3", I.D. = 2 $\frac{1}{8}$ ", H = 3"
	2	Aluminum plates ( $\frac{1}{4}$ " thick) L = 5.776", W = 3"
10	1	Stainless steel cylinder O.D. = 4", I.D. = 1", t = 1"
11	14 slabs	Lucite blocks (1" thick slabs) L = W = 13.4"; O.D. = 13.4", I.D. = 11.8"
12	1	Shaft (1020 Cold rolled steel) O.D. = 1 $\frac{1}{2}$ ", H = 5.8125"
13	1	Aluminum cylinder O.D. = $\frac{1}{2}$ ", H = 2"
	1	Aluminum cylinder O.D. = 1", I.D. = $\frac{1}{2}$ ", H = 1"
	1	roller r = $\frac{3}{16}$ "

ORIGINAL PAGE IS  
OF POOR QUALITY

Part #	Quantity	Description
	5	Sealed bearings O.D. = $2\frac{1}{4}$ " , I.D. = $1\frac{1}{4}$ " , $t = \frac{1}{2}$ "
	2	Rubber belts $r = \frac{3}{16}$ "
	20 lb or as needed	Lead plates ( $\frac{1}{4}$ " thick) $L = 3$ " , $H = 3.5$ "
	as needed	Plexiglass cover $L = 40$ " , $W = 40$ " , $H = 35$ "
	1	Aluminum table with legs ( $\frac{1}{2}$ " thick) Table $L = 40$ " , $W = 40$ "
	4	Legs $H = 10$ "
	1	Speed Controller for AC motor (Dayton brand), 10 max. amperes
	as needed	$\frac{1}{4}$ " - 20 Allen set screws $\frac{1}{2}$ " - 20 Allen set screws
	as needed	electrical cables

## CONCLUSION

Although three-axis stabilization presents few sloshing effects, the ease of spin stabilization means that liquid sloshing still remains a problem. Nutational stability characteristics have generally been established by costly, full scale tests. By use of the "follower force" method, results will be more easily obtained and just as accurate. Two different simplified methods for the observation of liquid slosh will be used in this design. Pictures will be taken for qualitative analysis and the depth of fluid at various points in the cup will be used for quantitative analysis. It is hoped that after the model is built, the results will be helpful in gaining an insight into the problem of liquid sloshing.

ORIGINAL PAGE IS  
OF POOR QUALITY

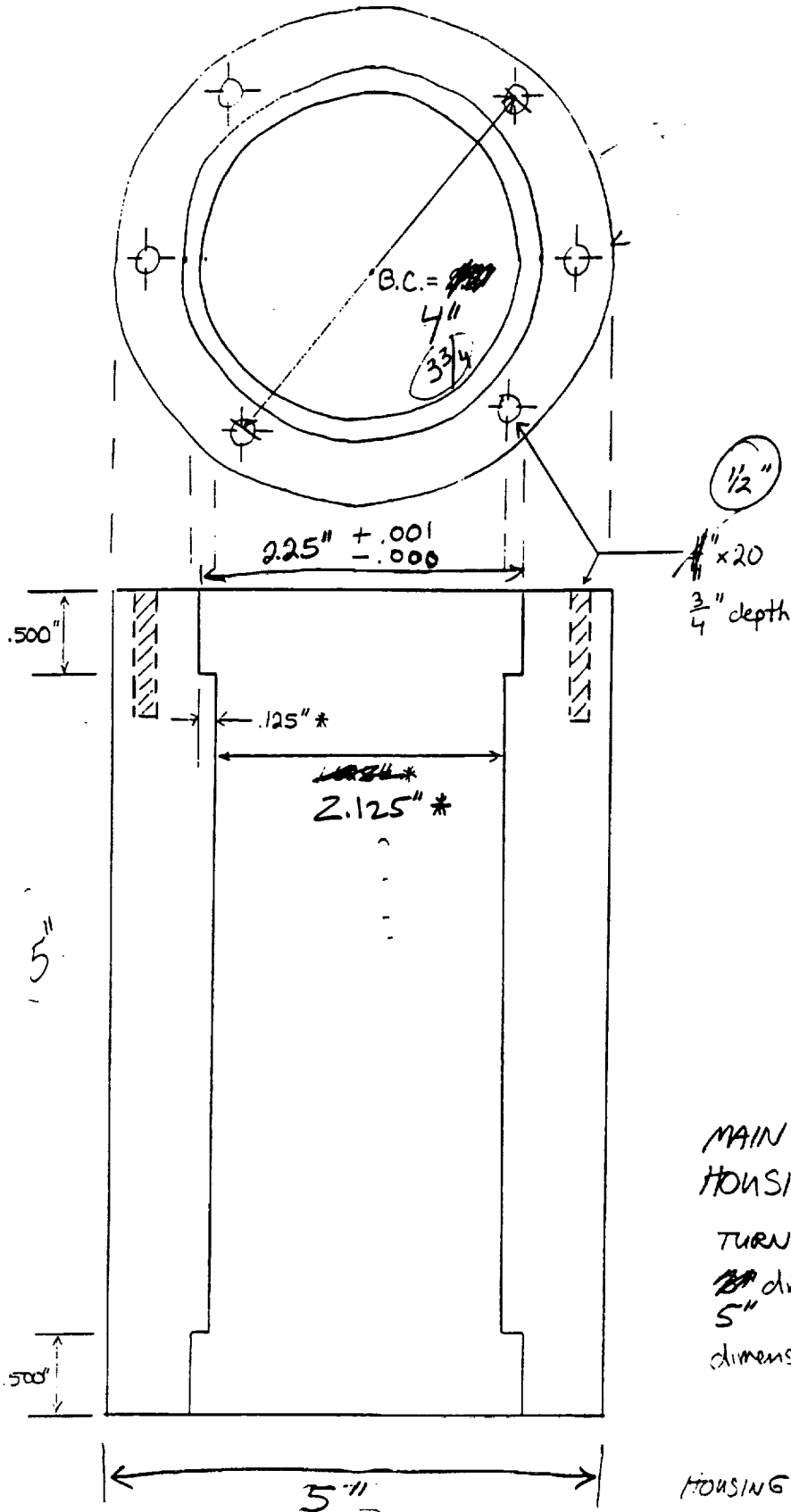


ART # 1

Appendix A

NOT to scale

has many holes  
has long part  
1.5" in  
5" ?



### MAIN BEARING HOUSING

TURN FROM ALUMINUM  
~~2 1/4"~~ dia stock cylinders  
 5"  
 dimensions ±.010"  
 \* ±.001"

HOUSING FOR use with  
 2 sealed bearings

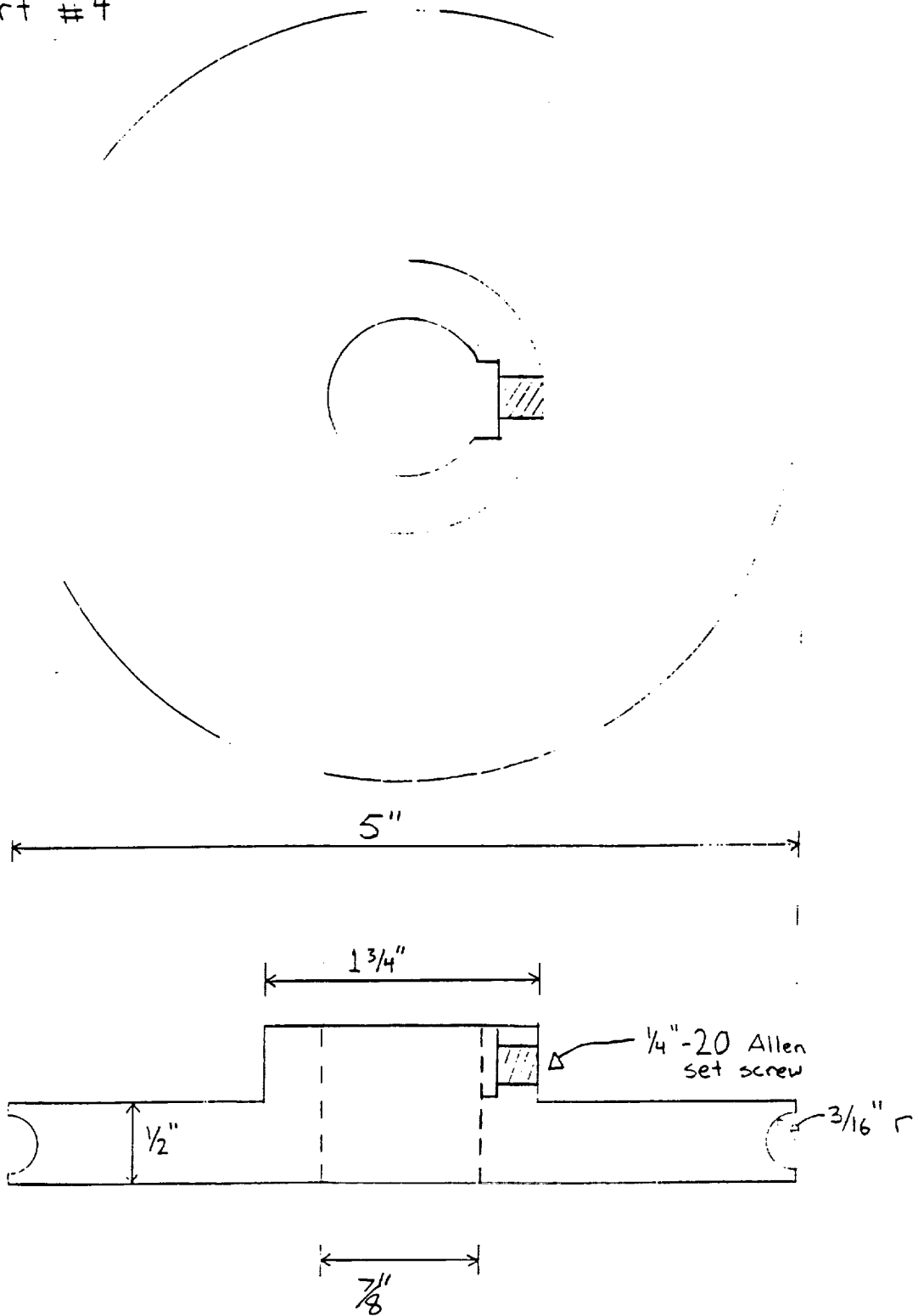
1 1/4" ~~2 1/4"~~ I.D.  
 2 1/4" ~~2 1/4"~~ O.D.  
 1/2" ~~1/2"~~ width

ORIGINAL PAGE IS OF POOR QUALITY

Feb. 15, 90

(INCOMPLETE)

Part #4



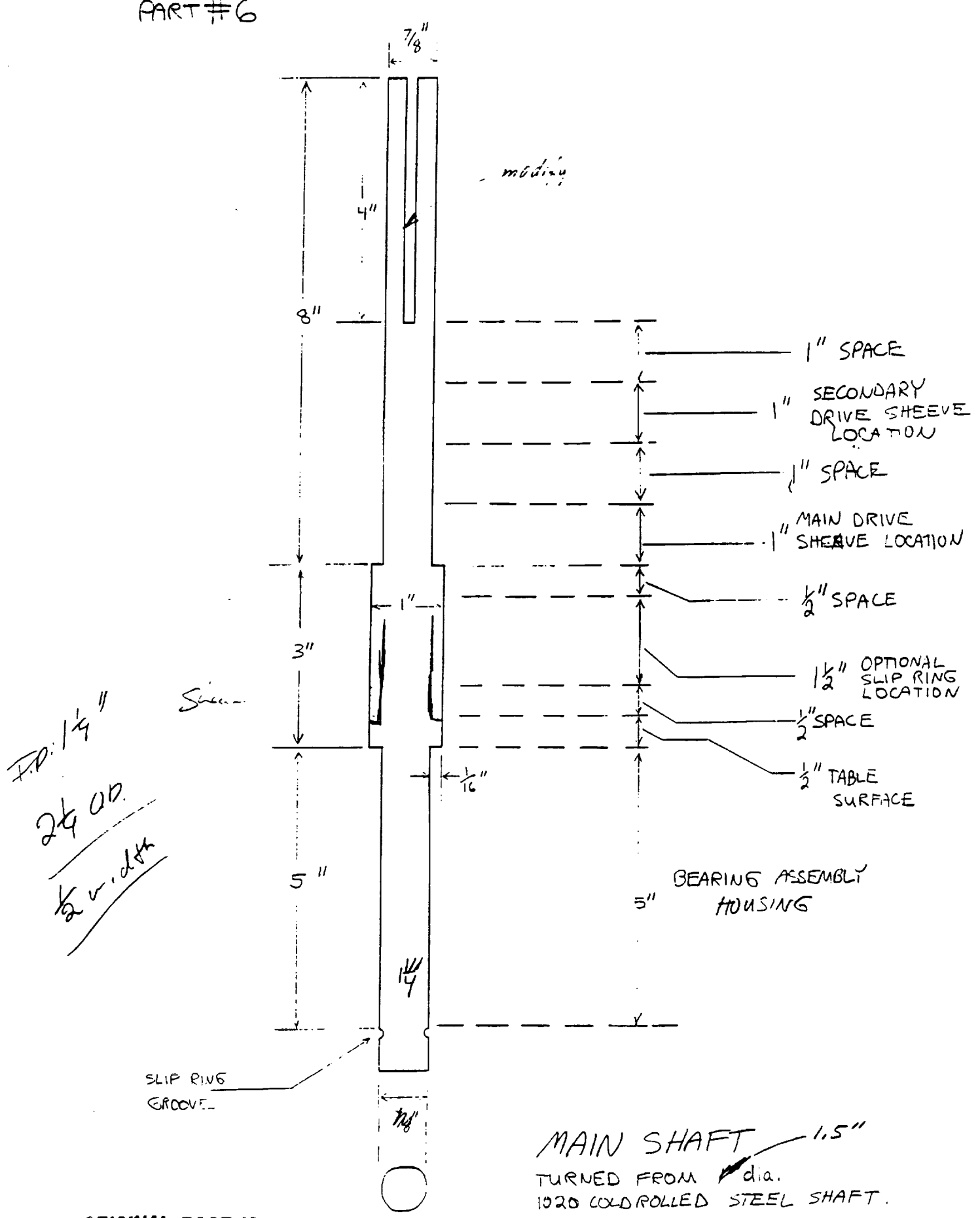
Aluminum Stock

(not to scale)

67

ORIGINAL PAGE IS  
OF POOR QUALITY

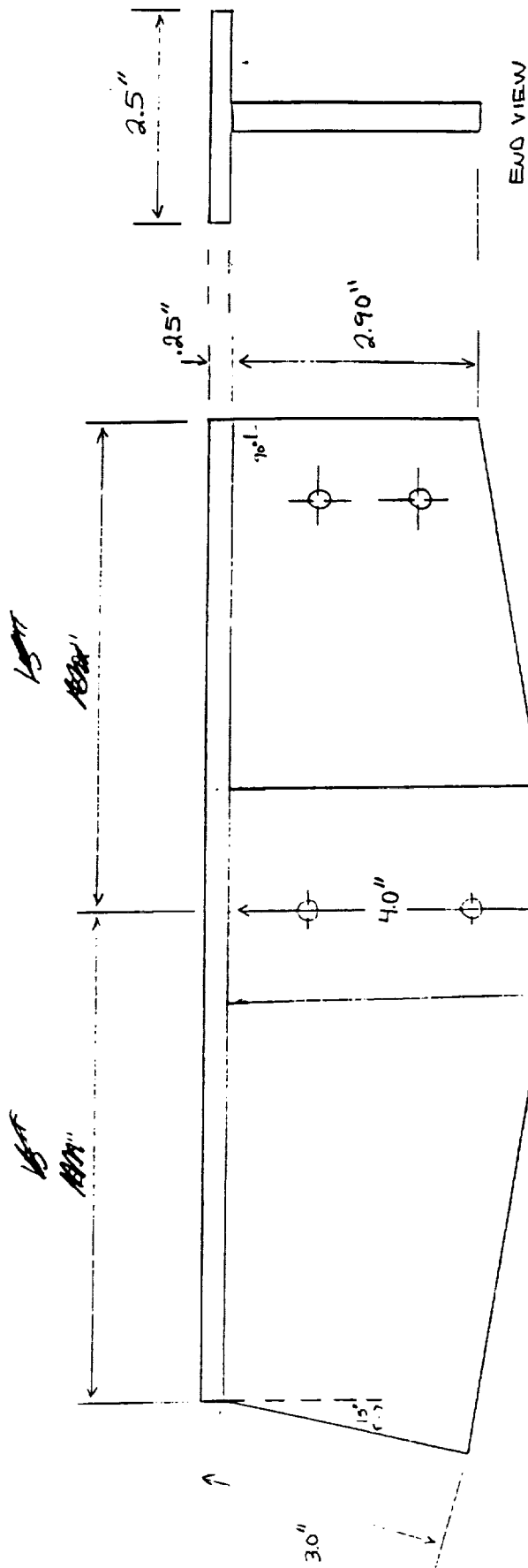
PART #6



F.P. 1 1/4"  
 2 1/4 O.D.  
 1/2 width

ORIGINAL PAGE IS OF POOR QUALITY

PART # 7

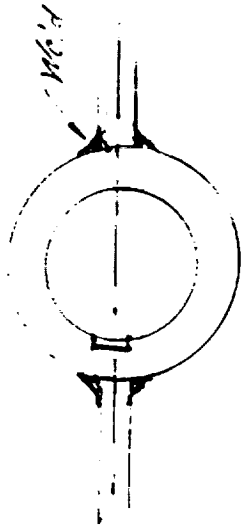


SIDE VIEW

END VIEW

Belt for attachment for shaft

Bottom View



CONTROL ARM  
 HELIARC WELD TO ALUMINUM  
 PLATES, ALSO WELD ARM TO  
 BEARING HOUSING. a.k.  
 DIMENSIONS ±.1"

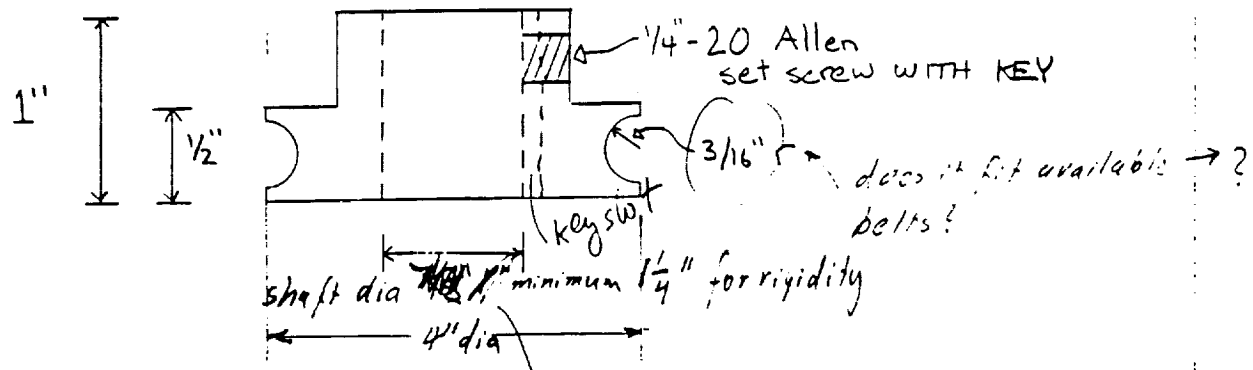
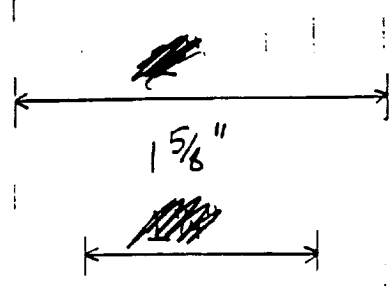
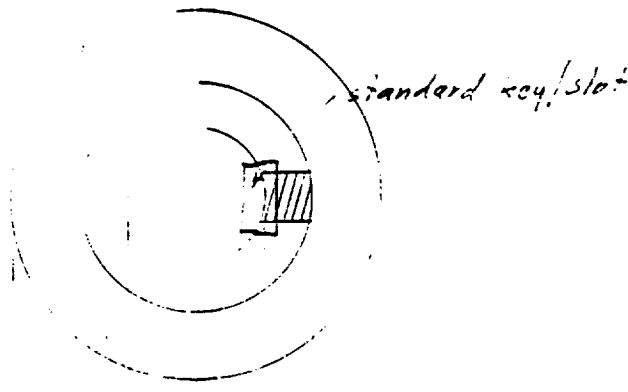
Feb 15 2

✓  
C. 100 10 10  
100 10 10  
100 10 10  
100 10 10  
100 10 10

Part #8

(INCOMPLETE)

22 20 15 10 5  
22 20 15 10 5  
22 20 15 10 5  
22 20 15 10 5  
22 20 15 10 5



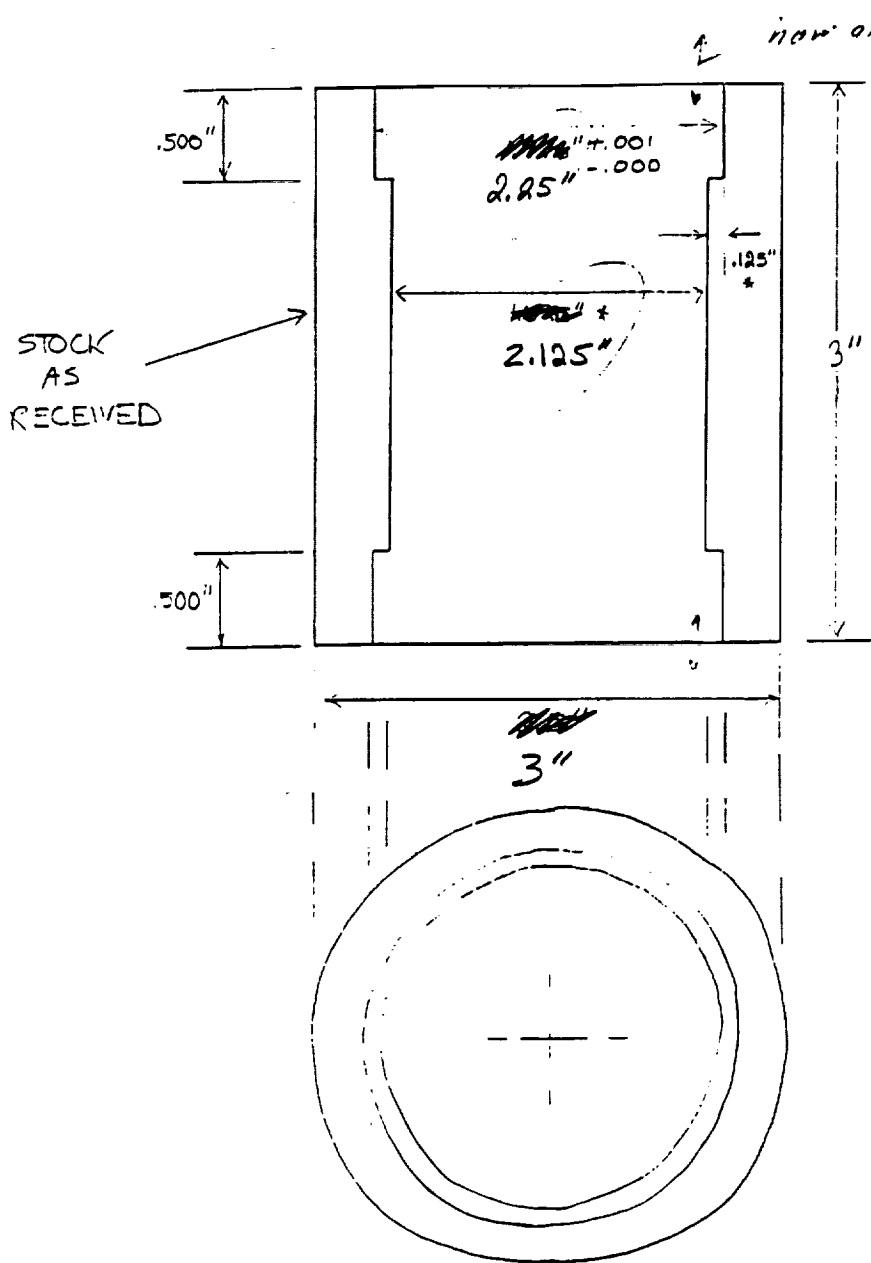
Aluminum Stock

$\frac{1}{4}''$

(Note)

ORIGINAL PAGE IS OF POOR QUALITY

PART # 9



now are bearings kept in place on nut, etc.

Housing # 9 attached to # 7. Consider slotted holes for tightening bolts.

BEARING HOUSING FOR FUEL TANK MOUNT

HOUSING FOR USE WITH 2 SEALED BEARINGS

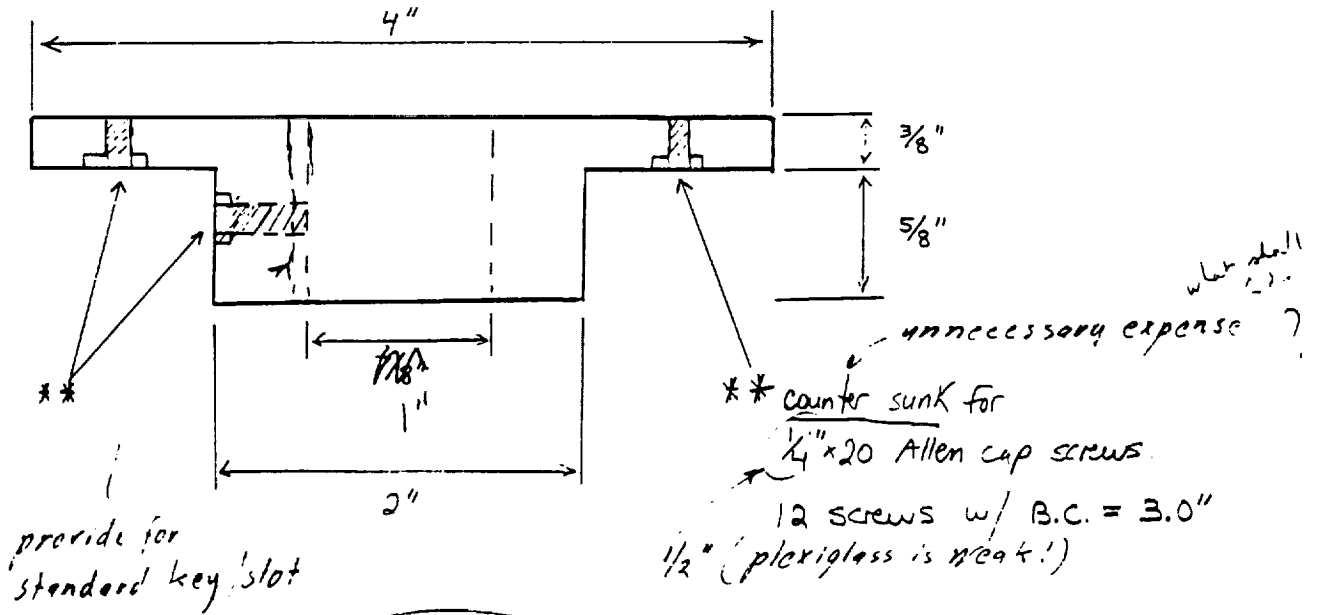
- ~~7/8" ID.~~ 1 1/4" ID.
- ~~1 1/8" ID.~~ 2 1/4" O.D.
- ~~1/2" width~~ 1/2" width.

TURNED FROM ~~2 1/8~~ dia. ALUMINUM CYLINDER.

ALL DIMENSIONS ± .010" \* ± .001

ORIGINAL PAGE IS OF POOR QUALITY

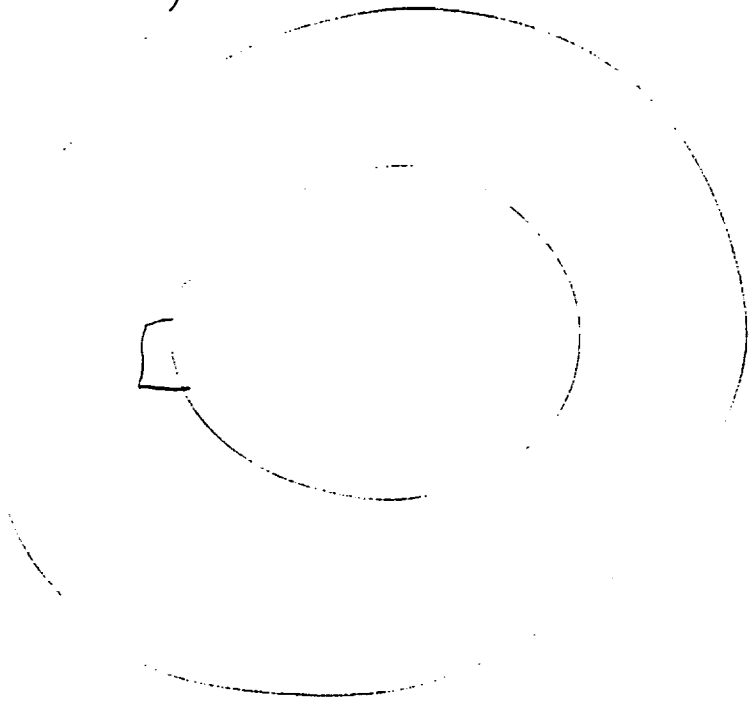
PART #10



\*\* provide for standard key slot

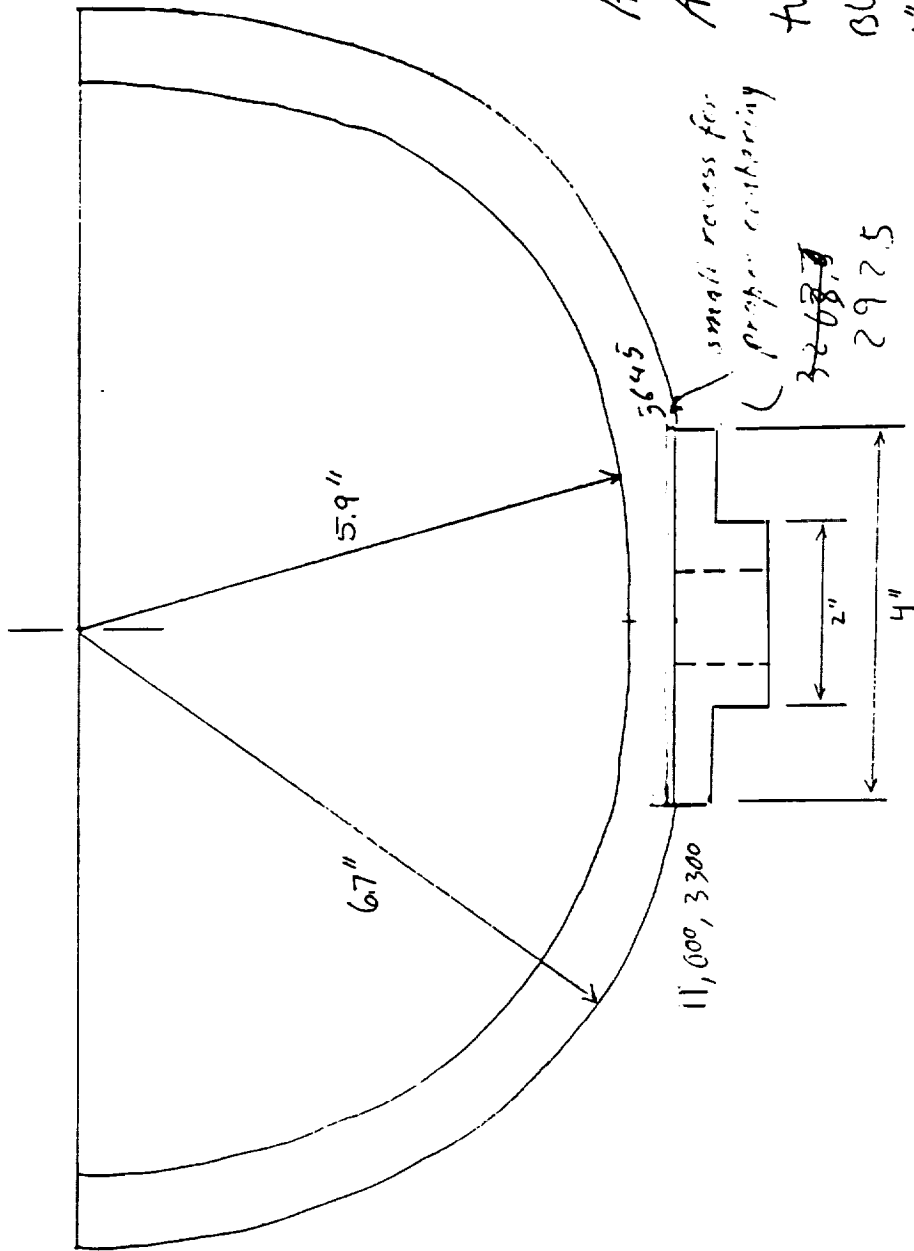
\*\* counter sunk for 1/4" x 20 Allen cap screws. 12 screws w/ B.C. = 3.0" 1/2" (plexiglass is neat!)

unnecessary expense?



FUEL TANK  
MOUNTING FLANGE  
turned from STAINLESS STEEL  
Stock cylinder  
All dimensions  $\pm .010$ "

PART #11

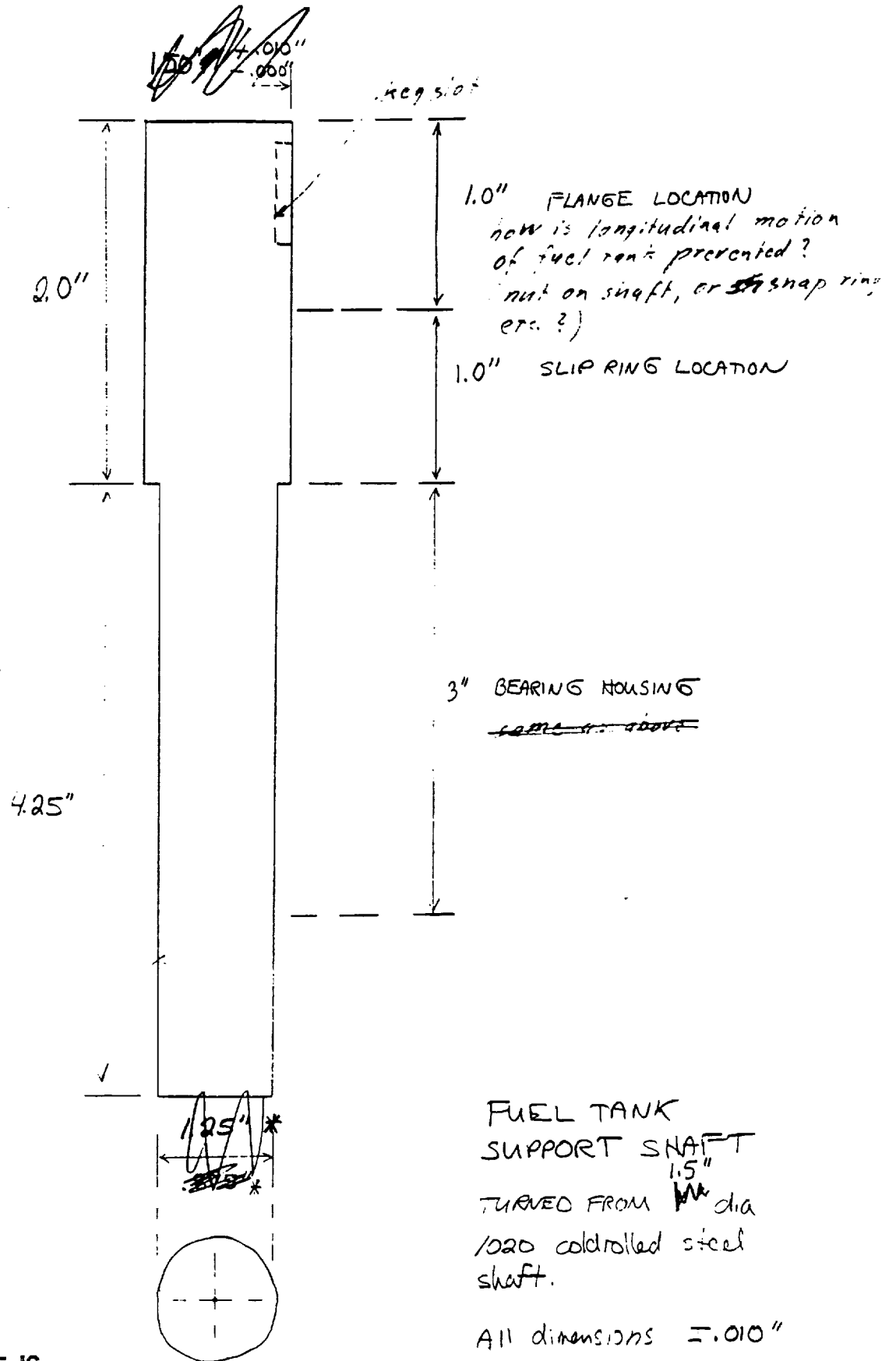


HEMISPHERICAL TANK  
AND FLANGE.

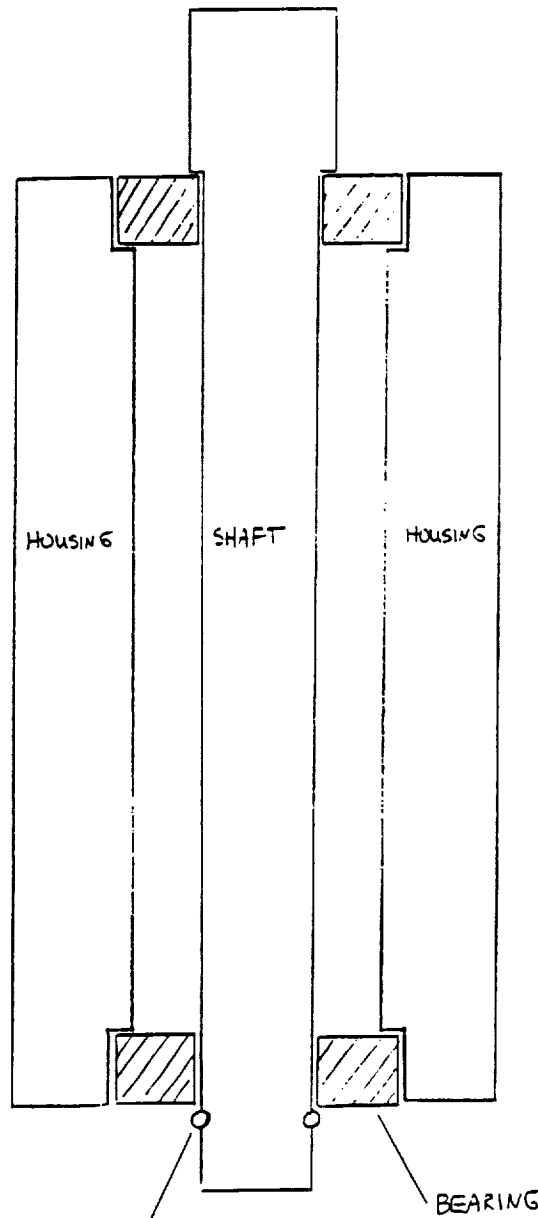
turned from Lucite  
Block - Block made from  
1" thick slabs.

TURN INSIDE AND OUTSIDE  
WITH CLEAR FINISH.

PART #12



ORIGINAL PAGE IS  
OF POOR QUALITY



SNAP RING  
 ↗ a.k.

BEARING

MAIN  
~~GENERAL~~ BEARING  
 ASSEMBLY

SIDE CUT VIEW

NOT DRAWN TO SCALE

# Appendix B.

Parameters of the modeled system

$$x := -15 \dots 15 \quad r_a := 15 \text{ cm} \quad r_c := 15 \text{ cm} \quad \omega_c := 80 \text{ rpm} \quad \omega_a := 40 \text{ rpm}$$

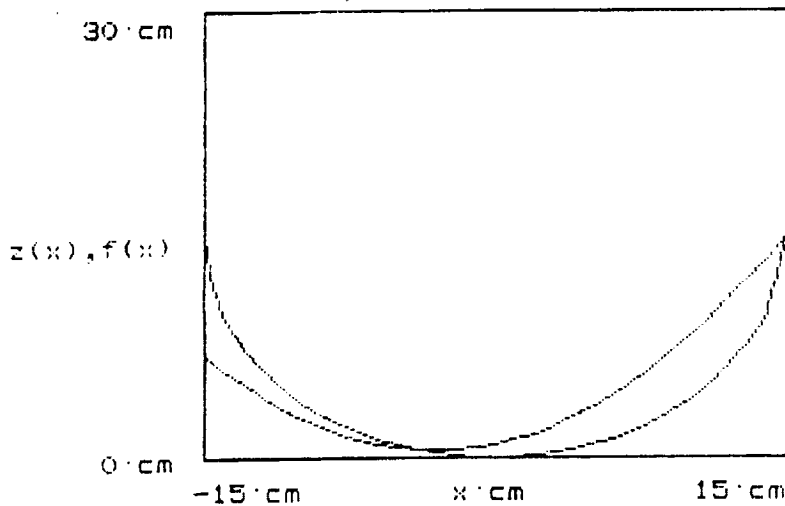
$$\text{CONST} := .91 \text{ cm}$$

"The equation representing the fluids' shape:"

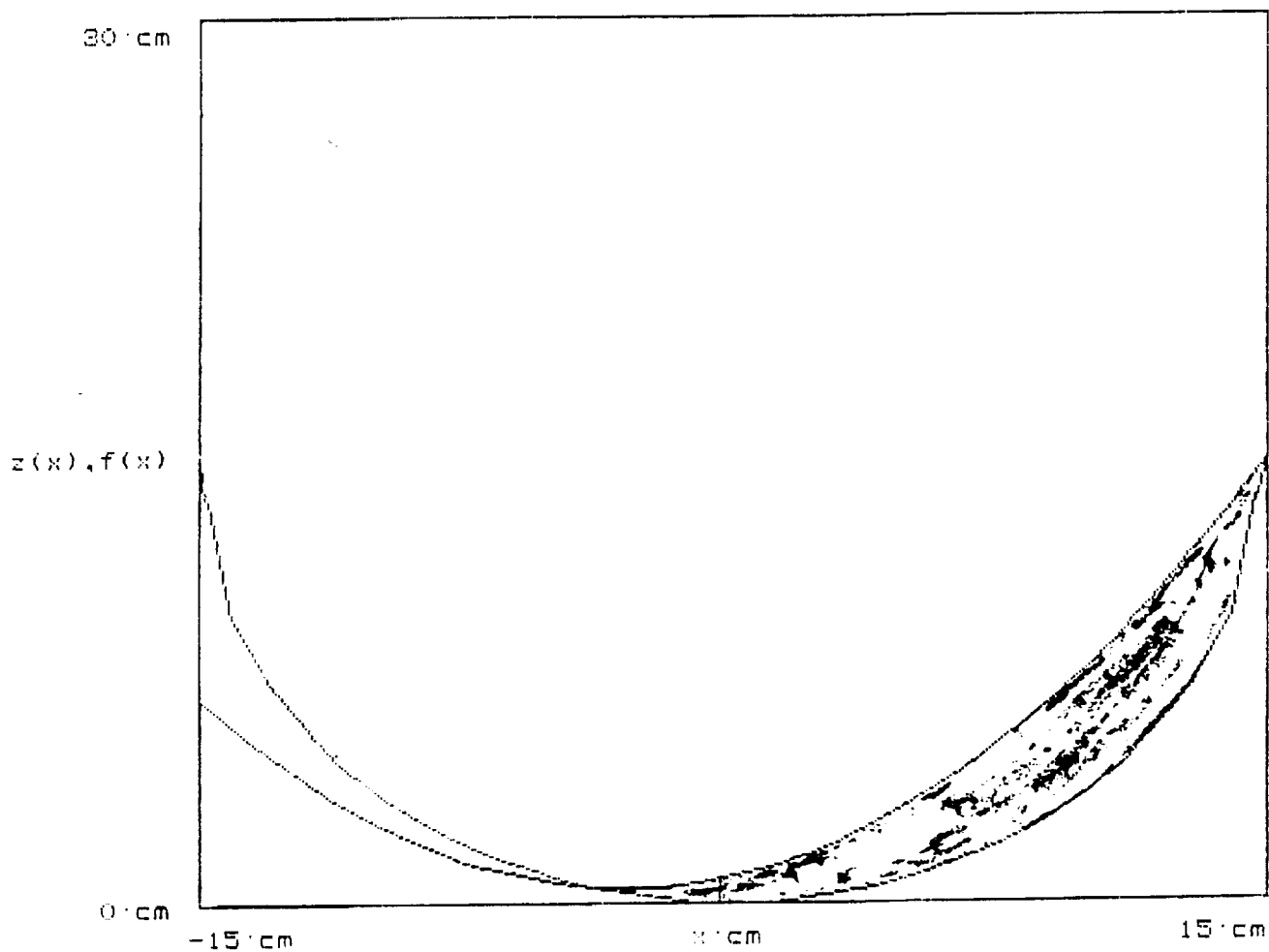
$$z(x) := \begin{bmatrix} 1 \\ - \\ g \end{bmatrix} \cdot \left[ \omega_a^2 r_a + \frac{\omega_a^2 + \omega_c^2}{2} x^2 \text{ cm} \right] x^2 \text{ cm} + \text{CONST}$$

"The equation representing the shape of the sphere:"

$$f(x) := -\sqrt{(r_c)^2 - (x \text{ cm})^2} + 15 \text{ cm}$$



GRAPH OF THE SPHERE AND FLUID SHAPE



~~Fluid~~ Fluid  
Sphere

ORIGINAL PAGE IS  
OF POOR QUALITY

*[Handwritten signature]*

Parameters of the modeled system

$\theta := 0, .08 .. 2 \cdot \pi$     $r_a := 15 \cdot \text{cm}$     $r_c := 15 \cdot \text{cm}$     $\omega_c := 80 \cdot \text{rpm}$     $\omega_a := 40 \cdot \text{rpm}$   
 $\text{CONST} := .91 \cdot \text{cm}$     $\phi := 0$     $R := r_c$

"The equation representing the fluids' shape:"

$$L(R, \phi, \theta) := \begin{bmatrix} 1 \\ - \\ g \end{bmatrix} \cdot \left[ \omega_a^2 \cdot r_a^2 + \frac{\omega_a^2 + \omega_c^2}{2} \cdot R \cdot \cos(\phi) \cdot \cos(\theta) \right] \cdot R \cdot \cos(\phi) \cdot \cos(\theta) \dots$$

$$+ (R \cdot \cos(\phi) \cdot \sin(\theta)) \cdot \frac{\omega_c^2}{2 \cdot g} + \text{CONST}$$

"The equation of a sphere:

$$P(R, \phi, \theta) := R$$

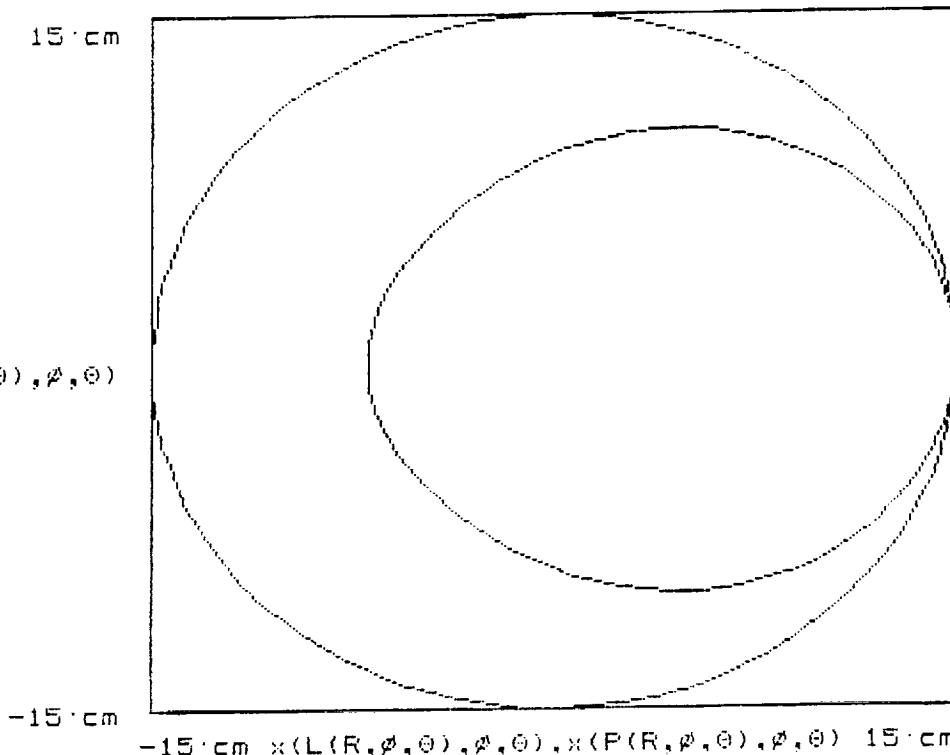
"Spherical Coordinates:"

$$x(R, \phi, \theta) \equiv R \cdot \cos(\phi) \cdot \cos(\theta)$$

$$y(R, \phi, \theta) \equiv R \cdot \cos(\phi) \cdot \sin(\theta)$$

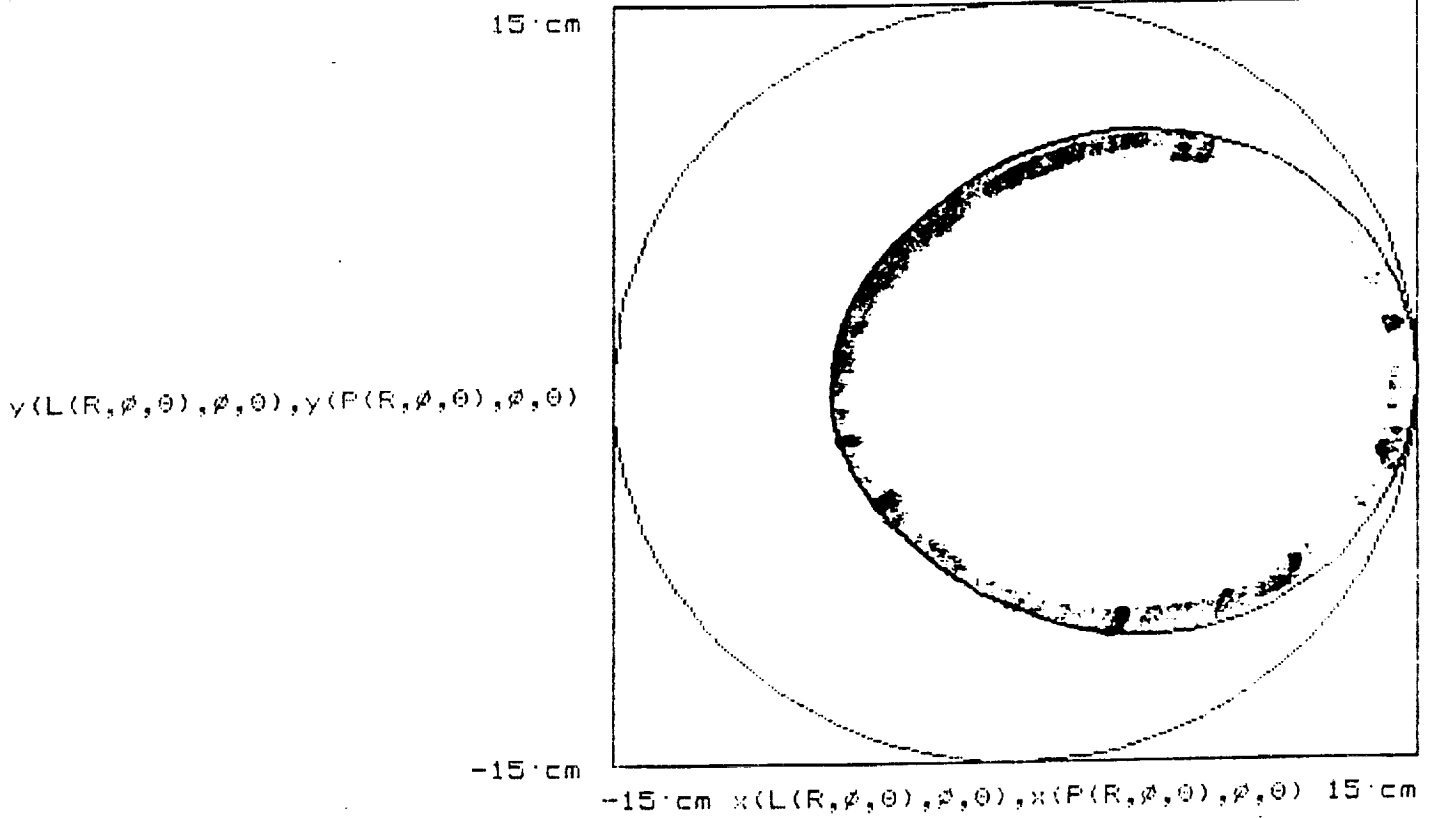
$$z(R, \phi, \theta) \equiv R \cdot \sin(\phi)$$

$v(L(R, \phi, \theta), \phi, \theta), y(P(R, \phi, \theta), \phi, \theta)$



ORIGINAL PAGE IS  
OF POOR QUALITY

TOP VIEW



ORIGINAL PAGE IS  
OF POOR QUALITY

# Appendix C

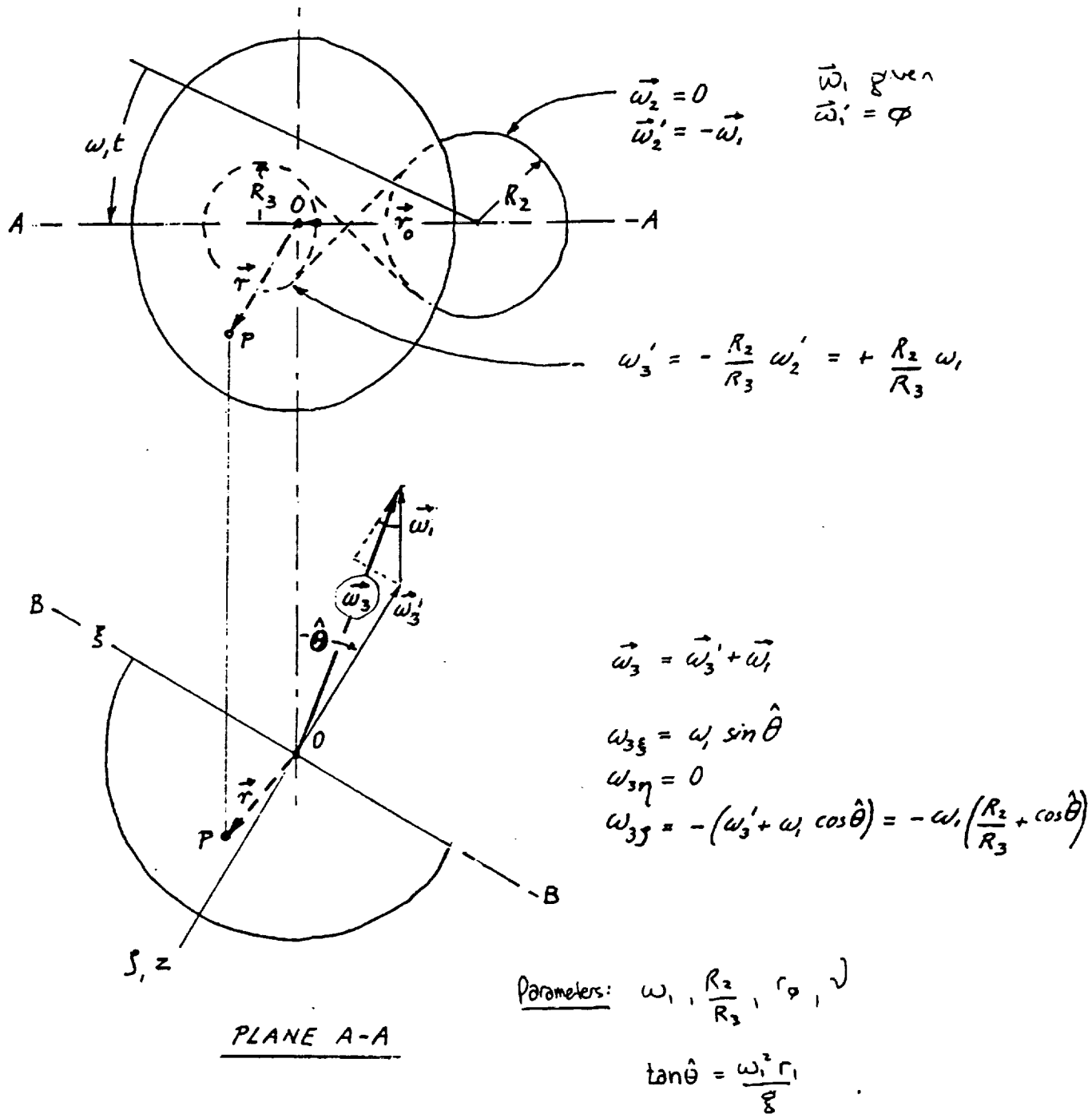
## Motion of Point Mass (P) in Spherical Container

### Kinematics:

#### Notation:

$\omega$  = angular velocity relative to laboratory ( $\approx$  inertial) reference.

$\omega'$ : " " " " rotating platform.



## \* MOTION of POINT MASS (P) in SPHERICAL CONTAINER

Governing Eqns:

$$\Theta_{tt} = (\Psi_t)^2 \sin \theta \cos \theta + \frac{1}{r} (g_\theta - a_{\theta\theta}) - \dot{\Psi} \Theta_t - \omega_{3r} (\omega_{3\theta} - 2\Psi_t \sin \theta) - (\omega_{3\psi})_t$$

$$\Psi_{tt} = \frac{1}{\sin \theta} \left[ -2\Theta_t \Psi_t \cos \theta + \frac{1}{r} (g_\psi - a_{\psi\psi}) - \dot{\Psi} \Psi_t \sin \theta - \omega_{3r} (\omega_{3\psi} + 2\Theta_t) + (\omega_{3\theta})_t \right]$$

note:  $( )_{tt} = \frac{d^2( )}{dt^2}$  ;  $( )_t = \frac{d( )}{dt}$

$$\omega_{3x} = \omega_1 \sin \theta \cos \left( \frac{R_2}{R_3} \omega_1 t \right) ; \omega_{3y} = \omega_1 \sin \theta \sin \left( \frac{R_2}{R_3} \omega_1 t \right) ; \omega_{3z} = -\omega_1 \left( \frac{R_2}{R_3} + \cos \theta \right)$$

$$\begin{aligned} \omega_{3r} &= \omega_{3x} \sin \theta \cos \psi + \omega_{3y} \sin \theta \sin \psi + \omega_{3z} \cos \theta \\ \omega_{3\theta} &= \omega_{3x} \cos \theta \cos \psi + \omega_{3y} \cos \theta \sin \psi - \omega_{3z} \sin \theta \\ \omega_{3\psi} &= -\omega_{3x} \sin \psi + \omega_{3y} \cos \psi \end{aligned}$$

$$(\omega_{3x})_t = -\omega_1^2 \frac{R_2}{R_3} \sin \theta \sin \left( \frac{R_2}{R_3} \omega_1 t \right) ; (\omega_{3y})_t = \omega_1^2 \frac{R_2}{R_3} \sin \theta \cos \left( \frac{R_2}{R_3} \omega_1 t \right) ; (\omega_{3z})_t = 0$$

$$\begin{aligned} (\omega_{3\theta})_t &= (\omega_{3x})_t \cos \theta \cos \psi + (\omega_{3y})_t \cos \theta \sin \psi - (\omega_{3z})_t \sin \theta \\ (\omega_{3\psi})_t &= -(\omega_{3x})_t \sin \psi + (\omega_{3y})_t \cos \psi \end{aligned}$$

$$g_x = -g \sin \hat{\theta} \cos \left( \frac{R_2}{R_3} \omega_1 t \right) ; g_y = -g \sin \hat{\theta} \sin \left( \frac{R_2}{R_3} \omega_1 t \right) ; g_z = g \cos \hat{\theta}$$

$$g_\theta = g_x \cos \theta \cos \psi + g_y \cos \theta \sin \psi - g_z \sin \theta ; g_\psi = -g_x \sin \psi + g_y \cos \psi$$

$$a_{\theta x} = -\omega_1^2 r_\theta \cos \theta \cos \left( \frac{R_2}{R_3} \omega_1 t \right) ; a_{\theta y} = -\omega_1^2 r_\theta \cos \theta \sin \left( \frac{R_2}{R_3} \omega_1 t \right) ; a_{\theta z} = -\omega_1^2 r_\theta \sin \theta$$

$$\begin{aligned} a_{\theta\theta} &= a_{\theta x} \cos \theta \cos \psi + a_{\theta y} \cos \theta \sin \psi - a_{\theta z} \sin \theta \\ a_{\theta\psi} &= -a_{\theta x} \sin \psi + a_{\theta y} \cos \psi \end{aligned}$$

## \* SOLVING SYSTEM of ODEs : HEUN'S METHOD

1) Linearize into system of 4 first order equations:

$$f_1 \equiv \frac{du_1}{dt} = u_2 \quad ;$$

$$u_1 \equiv \Theta \quad u_2 \equiv \Theta_t$$

$$f_2 \equiv \frac{du_2}{dt} = \Theta_{tt}$$

$$f_3 \equiv \frac{du_3}{dt} = u_4 \quad ;$$

$$u_3 \equiv \Psi \quad u_4 \equiv \Psi_t$$

$$f_4 \equiv \frac{du_4}{dt} = \Psi_{tt}$$

B.C.

$$u_1(t=0)$$

$$u_2(t=0)$$

$$u_3(t=0)$$

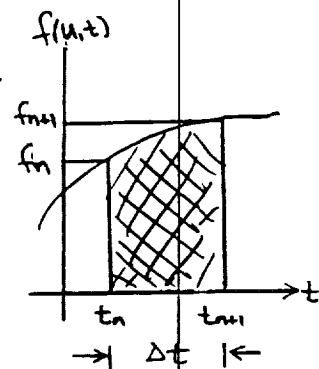
$$u_4(t=0)$$

$$J(f) \equiv \begin{bmatrix} \frac{\partial f_1}{\partial u_1} & \frac{\partial f_1}{\partial u_2} & \frac{\partial f_1}{\partial u_3} & \frac{\partial f_1}{\partial u_4} \\ \frac{\partial f_2}{\partial u_1} & \frac{\partial f_2}{\partial u_2} & \dots & \dots \\ \frac{\partial f_3}{\partial u_1} & \dots & \dots & \dots \\ \frac{\partial f_4}{\partial u_1} & \dots & \dots & \frac{\partial f_4}{\partial u_4} \end{bmatrix} \quad \{u\} \equiv \begin{Bmatrix} u_1 \\ u_2 \\ u_3 \\ u_4 \end{Bmatrix} \quad \{f\} \equiv \begin{Bmatrix} f_1 \\ f_2 \\ f_3 \\ f_4 \end{Bmatrix}$$

2) Now use trapezoidal rule to integrate each equation:

$$u' = f(u, t) \quad ; \quad h \equiv t_{n+1} - t_n = \Delta t \quad \left[ \begin{array}{l} \text{step} \\ \text{size} \end{array} \right]$$

$$u_{n+1} \approx u_n + \frac{h}{2} \left[ f(u_{n+1}^*, t_{n+1}) + f(u_n, t_n) \right]$$



3) Estimate  $u_{n+1}^*$  w/ forward Euler discretization:

$$u_{n+1}^* \approx u_n + h f(u_n, t_n)$$

now we have:

$$u_{n+1} \approx u_n + \frac{h}{2} \left[ f(u_n + h f(u_n, t_n), t_{n+1}) + f(u_n, t_n) \right]$$

## \* SOLVING SYSTEM of ODEs: HEUN'S METHOD (cont.)

4) Minimize this equation for iteration:

$$F(u_{n+1}) = u_{n+1} - u_n - \frac{h}{2} \left[ f(u_n + h f(u_n, t_n), t_{n+1}) + f(u_n, t_n) \right]$$

$= 0 \leftarrow$  want this to be true for soln.

5) Evaluate Jacobian of  $F(u_{n+1})$ :

$$J(F) = \delta_{ij} - \frac{h}{2} J(f) \quad ; \quad \delta_{ij} = \begin{cases} 1 & ; \quad i = j \\ 0 & ; \quad i \neq j \end{cases}$$

6) Solve system of linear equations:

$$J(F)(u_{n+1} - u_n) = -F$$

or, 
$$u_{n+1} = u_n - [J(F)]^{-1} F(u_{n+1})$$

now let 
$$\Delta u_i = -J(F) F(u_{n+1})$$

or, 
$$J(F) \Delta u_i = -F(u_{n+1}) \quad \leftarrow \text{Solve with Gauss Elimination}$$

$\begin{matrix} \uparrow & \uparrow & \uparrow \\ \text{known} & \text{unknown} & \text{known} \end{matrix}$

7) Update solution and iterate until convergence:

$$u_i^{n+1} = u_i^n + \Delta u_i^n \quad ; \quad \left[ \text{if } \Delta u_i^n > \epsilon, \text{ goto (4)} \right]$$

# \* ALGORITHM :

Common block dimension  $U(10)$

1) Read control flags:  $negns, maxit$

Read step size,  $h$  and tolerance,  $\epsilon$

Read initial data:  $(U_i(t=0); i=1, negns); t_a, t_b$

Read <sup>(given)</sup> parameters:  $RPM, r_1, r, R\theta, RZ, R3, \nu$  ← friction factor

2) Begin timestepping:

$$nsteps = \lfloor (t_b - t_a) / h \rfloor$$

DO  $n = 0, nsteps$

$$t = \left(\frac{n}{nsteps}\right) t_b$$

Evaluate all parameters:  $(\omega_{sr}, (\omega_{s0})_t, g_0, \text{etc.})$

Call  $heun(negns, maxit, h, \epsilon, t, U)$

if  $|\theta|$  or  $|\psi| > 2\pi$  rad,

subtract/add  $2\pi$  rad to keep  $-2\pi \leq \theta, \psi \leq 2\pi$

determine  $x, y, z$ :

$$x = r \sin \theta \cos \psi$$

$$y = r \sin \theta \sin \psi$$

$$z = r \cos \theta$$

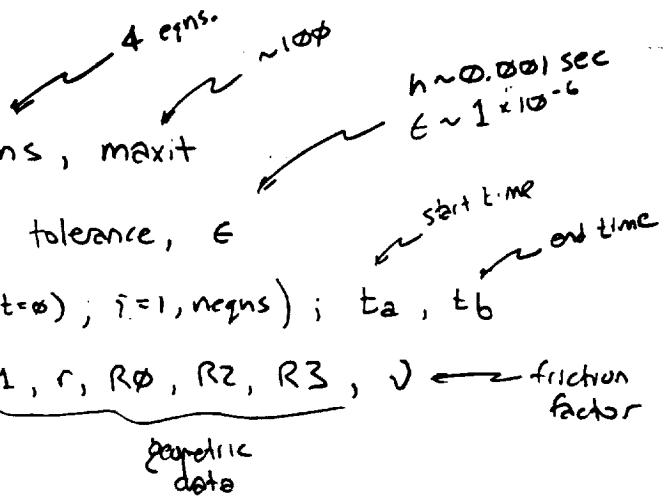
Print out results:  $n, t, x, y, z$   
(every 50<sup>th</sup> result or so)

if  $\theta > \frac{\pi}{2}$ , stop! marble flew out of tearup!!

repeat  $n$

function  $f(i, U, t)$   
Common block  
dimension  $U(10)$

subroutine Jacobn(I, U, t)  
Common block  
dimension  $I(10, 10), U(10)$



note:  
 $U(1) = \theta; U(2) = \frac{\partial \theta}{\partial t}$   
 $U(3) = \psi; U(4) = \frac{\partial \psi}{\partial t}$

note:  
 TGP uses  
 format (ix, eis.8, zx, eis.8)  
 for x, y data plots

## Appendix D

```
      program ball
C***** MAIN PROGRAM
C*****

      implicit double precision (a-z)
      parameter (pi = 3.141592654,neqns=4,eps = 1.0D-06)

      common wr,wthet,wpsi,wthett,wpsit,gthet,gpsi,athet,apsi
      dimension U(10)
      integer n,nsteps,maxit,i,j,npj

      open(15,file = 'xy.tgp')
      open(20,file = 'xyz.out')
      open(16,file = 'input.dat')
      read(16,*) rpm
      read(16,*) r1
      read(16,*) r
      read(16,*) r0
      read(16,*) r2
      read(16,*) r3
      read(16,*) nu
      read(16,*) u(1)
      read(16,*) u(2)
      read(16,*) u(3)
      read(16,*) u(4)
      read(16,*) ta
      read(16,*) tb
      print *, 'input maxit and h: '
      read *, maxit,h

      nsteps = abs((tb-ta)/h)
      w1=rpm*2.0*pi/60.0

      do 10,n=0,nsteps
         t=tb*n/nsteps

         print*, 'n,u(1),u(3): ',n,u(1),u(3)

         call Params(w1,r,r0,r1,r2,r3,U,t)
         call Heun(neqns,maxit,h,eps,t,U)

         the = U(1)
         psi = U(3)
         if (dabs(the).gt.2.0*pi) then
            npj = dint(the/2.0/pi)
            the = the-npj*2.0*pi
         endif

         if (dabs(psi).gt.2.0*pi) then
            npj = dint(psi/2.0/pi)
            psi = psi-npj*2.0*pi
         endif
         U(1) = the
         U(3) = psi
      enddo
```

```

        x = r*sin(U(1))*cos(U(3))
        y = r*sin(U(1))*sin(U(3))
        z = r*cos(U(1))
        if (MOD(n,50).eq.0) then
            write (15,1000) x,y
            write (20,1002) n,t,x,y,z
1000         format (e15.8,2x,e15.8)
1002         format (i6,2x,e10.5,2x,e15.8,2x,e15.8,2x,e15.8)
        endif
        if (U(1).gt.(pi/2.0)) then
            stop
        endif
        if (U(1).lt.(-pi/2.0)) then
            stop
        endif
10    continue
end

```

C\*\*\*\*\* THE VECTOR FUNCTION  
C\*\*\*\*\*

```

double precision function f(i,U,t)
implicit double precision (a-z)
common wr,wthet,wpsi,wthett,wpsit,gthet,gpsi,athet,apsi
integer i,npi
dimension U(10)

print *, 'func',U(1),U(3)

if (i.eq.1) then
    f = U(2)
else if (i.eq.2) then
    f = U(4)*U(4)*sin(U(1))*cos(U(1)) + (gthet - athet)/r -
%      nu*(2) - wr*(wthet - 2.0*U(4)*sin(U(1))) - wthett
else if (i.eq.3) then
    f = U(4)
else if (i.eq.4) then
    f = (-2.0*U(2)*U(4)*cos(U(1)) + (gpsi - apsi)/r -
%      nu*U(4)*sin(U(1)) - wr*(wpsi + 2.0*U(2))
%      + wthett)/sin(U(1))
endif
end

```

C\*\*\*\*\* THE FORMULAS FOR THE PARAMETERS  
C\*\*\*\*\*

```

subroutine Params(w1,r,r0,r1,r2,r3,U,t)
implicit double precision (a-z)
common wr,wthet,wpsi,wthett,wpsit,gthet,gpsi,athet,apsi
integer npi
dimension U(10)

```

```

print *, 'param',U(1),U(3)

g = 9.81
hat = atan(w1*w1*r1/g)
wx = w1*sin(U(1))*cos(r2*w1*t/r3)
wy = w1*sin(U(1))*sin(r2*w1*t/r3)
wz = -w1*(r2/r3+cos(U(1)))
wr = wx*sin(U(1))*cos(U(3)) + wy*sin(U(1))*sin(U(3)) +
%     wz*cos(U(1))
wthet = wx*cos(U(1))*cos(U(3)) + wy*cos(U(1))*sin(U(3)) -
%     wz*sin(U(1))
wpsi = -wx*sin(U(3)) + wy*cos(U(3))
wxt = -w1*w1*r2/r3*sin(hat)*sin(r2*w1*t/r3)
wyt = w1*w1*r2/r3*sin(hat)*cos(r2*w1*t/r3)
wzt = 0.0
wthett = wxt*cos(U(1))*cos(U(3)) + wyt*cos(U(1))*sin(U(3)) -
%     wzt*sin(U(1))
wpsit = -wxt*sin(U(3)) + wyt*cos(U(3))
gx = -g*sin(hat)*cos(r2*w1*t/r3)
gy = -g*sin(hat)*sin(r2*w1*t/r3)
gz = g*cos(hat)
gthet = gx*cos(U(1))*cos(U(3)) + gy*cos(U(1))*sin(U(3)) -
%     gz*sin(U(1))
gpsi = -gx*sin(U(3)) + gy*cos(U(3))
ax = -w1*w1*r0*cos(U(1))*cos(r2*w1*t/r3)
ay = -w1*w1*r0*cos(U(1))*sin(r2*w1*t/r3)
az = -w1*w1*r0*sin(U(1))
athet = ax*cos(U(1))*cos(U(3)) + ay*cos(U(1))*sin(U(3))
%     -az*sin(U(1))
apsi = -ax*sin(U(3)) + ay*cos(U(3))
end

```

```

C*****      SUBROUTINE JACOBN
C*****

```

```

subroutine Jacobn(J,U,t)
common wr,wthet,wpsi,wthett,wpsit,gthet,gpsi,athet,apsi
dimension J(10,10)
dimension U(10)
implicit double precision (a-z)
integer npi
print *, 'jaco', U(1),U(3)

J(1,1) = 0
J(1,2) = 0
J(1,3) = 0
J(1,4) = 0
J(2,1) = U(4)*U(4)*(cos(U(1))*cos(U(1))-sin(U(1))*sin(U(1)))
J(2,1) = J(2,1)+wr*(2*U(4)*cos(u(1)))
J(2,2) = -NU
J(2,3) = 0
J(2,4) = 2*U(4)*SIN(U(1))*COS(U(1))+2*wr*sin(U(1))
J(3,1) = 0
J(3,2) = 0

```

```

J(3,3) = 0
J(3,4) = 1
J(4,1) = -2*U(2)*U(4)*cos(U(1))+(gpsi-apsi)/r
J(4,1) = J(4,1)-nu*U(4)*sin(U(1))-wr*(wpsi+2*U(2))+wthett
J(4,1) = J(4,1)*cos(U(1))
J(4,1)=sin(U(1))*(2*U(2)*U(4)*sin(U(1))-nu*U(4)*cos(U(1)))-J(4,1)
J(4,1) = J(4,1)/(sin(U(1))*sin(U(1)))
J(4,2) = -2*U(4)*COS(U(1))/SIN(U(1))-(2*WR/sin(U(1)))
J(4,3) = 0
J(4,4) = (-2*U(2)*COS(U(1))/SIN(U(1)))-NU
RETURN
END

```

```

-----
c
c
c   MARBLE : finds the position of a marble placed in the TEACUP
c   =====
c
c   James Marcolesco
c   Winter 1990
c   MANE 199   Prof. Meyer
c
c   This routine drives the Heun subroutine
c
-----
c
c   maxit = maximum number of iterations
c   h     = step size
c   eps   = convergence tolerance
c   neqns = number of equations to be solved in system
c   F     = function vector
c   J     = Jacobian matrix of function vector
c   du    = vector to add to solution vector
c   U     = solution vector to be solved in HEUN
c   t     = current time at call to HEUN
c
-----
c234567
program main
implicit double precision (a-z)
integer maxit,neqns,nsteps,i,j,n,np1,rad,count,limit
common r,nu,gthe,gphi,athe,aphi,w3r,wthe,wphi,wphidt,wthedt
dimension u(10)

open (15, file = 'xy.tgp' , status = 'unknown')
open (16, file = 'x.out' , status = 'unknown')
open (17, file = 'y.out' , status = 'unknown')
c   open (18, file = 'z.out' , status = 'unknown')
open (19, file = 'xyz.out' , status = 'unknown')
open (20, file = 'input.dat', status = 'old')

c
c.....set control parameters
c
neqns = 4
g     = 9.80665d0
pi    = 3.141592654d0
pi2   = 2.d0 * pi
pi90  = pi / 2.d0
rtd   = 180.d0 / pi

write(*,1002)
print*, 'Enter max iterations:'
print*, '=====/'
write(*,1001)
print*, 'maxit = 1 is explicit Heun method'
print*, 'maxit > 1 is implicit trapezoidal method'
write(*,1001)
read*, maxit

```

```

write(*,1002)
print*, 'input convergence tolerance, eps:'
write(*,1001)
read*, eps

write (19,1002)
if (maxit.eq.1) write(19,*) '** Explicit Heun-s Method **'
if (maxit.gt.1) write(19,*) '** Implicit Trapezoidal Method **'
write (19,1002)

1001 format (/)
1002 format (//)

1 continue

count = 0

write(*,1002)
print*, 'input time step, h:'
write(*,1001)
read*, h
write(*,1002)
print*, 'for plot files, skip how many points?'
write(*,1001)
read*, limit
write(*,1002)

read(20,*) RPM
read(20,*) r1

w1 = RPM * 0.10472d0
THETA = datan(w1 * w1 * r1 / g)

read(20,*) r
read(20,*) R0
read(20,*) R2
read(20,*) R3

read(20,*) nu

c
c.....read in initial conditions
c
do 2, i = 1,4
  read(20,*) u(i)
2 continue

read(20,*) ta
read(20,*) tb

the = u(1)
phi = u(3)

write (19,1000) h,THETA*ntd,w1,r,r1,R0,R2,R3,nu,the,phi

1000 format (1x,'step size, h = ',f7.4,' sec',/)

```

```

.      1x,'THETA = ',f7.4,' deg',2x,'w1 = ',f7.4,' rad/s',
.      2x,'r = ',f6.4,' m',/,',r1 = ',f6.4,' m',
.      2x,'R0 = ',f6.4,' m',1x,'R2 = ',f6.4,' m',
.      2x,'R3 = ',f6.4,' m',2x,/,',nu = ',f6.4,
.      2x,'the(0) = ',f6.4,' rad',2x,'phi(0) = ',f6.4,' rad',/,/,
.      3x,'time step',5x,'time',9x,'x',12x,'y',14x,'z')
C
C.....(1) calc nsteps
C
      nsteps = dabs(tb-ta) / h + 1
      t = ta - h
C
C.....(2) begin time stepping
C      include t = ta
C      Calculate coefficients...
C
do 100, n = 1, nsteps

      t = t + h

      msin = dsin(the)
      mcos = dcos(the)

      psin = dsin(phi)
      pcos = dcos(phi)

      tsin = dsin(THETA)
      tcos = dcos(THETA)

      rsin = dsin(R2 / R3 * w1 * t)
      rcos = dcos(R2 / R3 * w1 * t)

      w3x = w1 * tsin * rcos
      w3y = w1 * tsin * rsin
      w3z = - w1 * (R2 / R3 * tcos)

      w3r   = w3x * msin * pcos + w3y * msin * psin + w3z * mcos
      w3the = w3x * mcos * pcos + w3y * mcos * psin - w3z * msin
      w3phi = - w3x * psin + w3y * pcos

      w3xdt = - w1 * w1 * R2 / R3 * tsin * rsin
      w3ydt = w1 * w1 * R2 / R3 * tsin * rcos
      w3zdt = 0.d0

      wthedt = w3xdt*mcos*pcos + w3ydt*mcos*psin - w3zdt*msin
      wphidt = - w3xdt * psin + w3ydt * pcos

      gx = - g * tsin * rcos
      gy = - g * tsin * rsin
      gz = g * tcos

      gthe = gx * mcos * pcos + gy * mcos * psin - gz * msin
      gphi = - gx * psin + gy * pcos

      a0x = - w1 * w1 * r0 * tcos * rcos

```

```

a0y = - w1 * w1 * r0 * tcos * rsin
a0z = - w1 * w1 * r0 * tsin

a0the = a0x * mcos * pcos + a0y * mcos * psin - a0z * msin
a0phi = - a0x * psin + a0y * pcos
c
c..... call solving subroutine
c
call heun(neqns,maxit,h,eps,t,U)

the = u(1)
phi = u(3)
c
c..... reduce to Order(2 pi)
c
if (dabs(the).gt.pi2) then
  npi = dint(the/pi2)
  the = the - npi * pi2
endif

if (dabs(phi).gt.pi2) then
  npi = dint(phi/pi2)
  phi = phi - npi * pi2
endif
c
c..... find x,y,z coords
c
x = r * dsin(the) * dcos(phi)
y = r * dsin(the) * dsin(phi)
z = r * dcos(the)
c
c.....(11) print out results
c
count = count + 1

if (count.gt.limit) then
  write(15,1102) x,y

  write(16,1101) x
  write(17,1101) y
  write(18,1101) z

  write(19,1105) n,t,x,y,z
  count = 0
endif

1101 format(1x,e15.8)
1102 format(1x,e15.8,2x,e15.8)
1105 format(4x,i5,7x,f6.3,3(2x,e12.4))
c
c..... stop if out of teacup
c
if (dabs(the).gt.pi90) then
  write(*,1000)
  print*, 'mangle flew out of teacup: THETA = ',the*ntd,' deg'

```

ORIGINAL PAGE IS  
OF POOR QUALITY

```

        stop
    endif

    u(1) = the
    u(3) = phi

100 continue

```

```

close(15)
close(16)
close(17)
close(18)
close(19)
close(20)

end

```

---

```

c functions

```

---

```

double precision function f(i,U,t)
implicit real*8(a-z)
integer i
common r,nu,gthe,gphi,athe,aphi,w3r,wthe,wphi,wphidt,wthedt
dimension u(10)

c1 = dcos(u(1))
c2 = c1 * c1
s1 = dsin(u(1))
s2 = s1 * s1

goto (10,20,30,40), i

10 f = u(2)
return

20 f = u(4) * u(4) * c1 * s1 + (gthe - athe) / r - nu * u(2)
    - w3r * (wthe - 2.d0 * u(4) * s1) - wthedt
return

30 f = u(4)
return

40 f = (-2.d0 * u(2) * u(4) * c1 + (gphi-aphi)/r - nu * u(4) * s1
    - w3r * (wphi + 2.d0 * u(2)) + wthedt) / s1
return

end

```

ORIGINAL PAGE IS  
OF POOR QUALITY

---

```

c Jacobian subroutine

```

---

```

subroutine Jacobn(J,U,t)
implicit real*8(a-z)
common r,nu,gthe,gphi,athe,aphi,w3r,wthe,wphi,wphidt,wthedt

```

```
dimension J(10,10),u(10)
```

```
c1 = dcos(u(1))
```

```
c2 = c1 * c1
```

```
s1 = dsin(u(1))
```

```
s2 = s1 * s1
```

```
J(1,1) = 0.d0
```

```
J(1,2) = 1.d0
```

```
J(1,3) = 0.d0
```

```
J(1,4) = 0.d0
```

```
J(2,1) = u(4) * u(4) * (c2 - s2) + 2.d0 * u(4) * w3r * c1
```

```
J(2,2) = - nu
```

```
J(2,3) = 0.d0
```

```
J(2,4) = 2.d0 * u(4) * c1 * s1 + 2.d0 * w3r * s1
```

```
J(3,1) = 0.d0
```

```
J(3,2) = 0.d0
```

```
J(3,3) = 0.d0
```

```
J(3,4) = 1.d0
```

```
J(4,1) = (2.d0 * u(2) * u(4) * s1 - nu * u(4) * c1) / s1  
- c1/s2 * (-2.d0 * u(2) * u(4) * c1 + (gphi - aphi) / r  
- nu * u(4) * s1 - w3r * (wphi + 2.d0 * u(2))  
+ wthedt)
```

```
J(4,2) = (-2.d0 * u(4) * c1 - 2.d0 * w3r) / s1
```

```
J(4,3) = 0.d0
```

```
J(4,4) = (-2.d0 * u(2) * c1 - nu * s1) / s1
```

```
return
```

```
end
```

```
-----  
c  
c  
c HUEN's METHOD  
c =====  
c  
c James Marcollesco  
c Fall 1989  
c MANE 192C Prof. McDonough  
c  
c This routine solves Initial Value Problems for ODE's  
c  
c-----
```

```
c m = number of final iterations
```

```
c maxit = maximum number of iterations
```

```
c h = step size
```

```
c a,b = time domain
```

```
c F = function vector
```

```
c J = Jacobian matrix of function vector
```

```
c du = vector to add to solution vector
```

```
c U = solution vector to be solved in NEWTON  
c  
c-----
```

```

subroutine heun(neqns,maxit,h,eps,t,U)
implicit double precision (a-h,j,o-z)

dimension Jf(10,10),JFF(10,10),FF(10),u(10),uold(10),du(10),
ustar(10),g(10)

double precision maxdif
integer delta,i,j,m,maxit,n,neqns,nsteps
external f,delta

c
c.....(3) begin Newton iterations
c
3   told = t - h
    m = 0

    do 80, m = 1, maxit
      if (m.gt.1) goto 6

c
c.....(4) Evaluate Ustar for use in
c      Huen's method
4   do 20, i = 1, neqns
      g(i) = f(i,u,told)
      ustar(i) = u(i) + h * g(i)
20  continue

c
c.....(5) Calculate initial guess for
c      trapezoidal rule from Huen's
c      method
5   do 30, i = 1, neqns
      uold(i) = u(i)
      u(i) = u(i) + 0.5 * h * (g(i) + f(i,ustar,t))
30  continue

      if (maxit.eq.1) return

c
c.....(6) Load J(f) for Newton iteration
c
6   call Jacobn(Jf,U,t)

c
c.....(7) Evaluate FF(Um) and J(F)
c
7   do 50, i = 1, neqns
      FF(i) = u(i) - 0.5*h*f(i,u,t) - (uold(i) + 0.5*h*g(i))
      do 40, j = 1, neqns
        JFF(i,j) = delta(i,j) - 0.5 * h * Jf(i,j)
40  continue
50  continue

c
c.....(8) Solve for du using Gauss
c
8   call GAUSS(neqns,JFF,du,FF)

c
c.....(9) Calculate max norm of du(i)
c      and increment U(i)

```

```

9      dumax = 0.d0
      do 60, i = 1, neqns
          if (dabs(du(i)).gt.dumax) dumax = dabs(du(i))
          u(i) = u(i) - du(i)
60     continue
c
c.....(10) Test convergence of Newton
c      iterations
c
10     if (dumax.lt.eps) return
c
80     continue

      print*, 'Newton iterations failed to converge at time step n + 1'

      return
      end

c
c.....define kroniker delta function
c
      function delta(i,j)
      implicit integer(a-z)

      if (i.eq.j) delta = 1
      if (i.ne.j) delta = 0

      return
      end

-----
c
c      GAUSS ELIMINATION SUBROUTINE
c      =====
c
c      James Marcolesco
c      MANE 192C
c      Fall 1989 Prof. McDonough
c
-----
c234567
      subroutine gauss(n,A,X,B)
      implicit real*8 (a-h,m,o-z)
      dimension A(10,10),X(10),B(10),M(10,10)
c
c.....forward elimination
c
      do 100, k = 1, n-1
c
c.....row pivoting
c
          imax = k
          amax = dabs(A(k,k))

```

```

do 10, i = k + 1, n
  if (dabs(A(i,k)).gt.amax) then
    amax = dabs(A(i,k))
    imax = i
  endif
10  continue

  if (imax.eq.k) go to 30
do 20, j = k, n
  atemp = A(k,j)
  A(k,j) = A(imax,j)
  A(imax,j) = atemp
20  continue

  btemp = b(k)
  b(k) = b(imax)
  b(imax) = btemp

30  do 60, i = k + 1, n
    M(i,k) = A(i,k) / A(k,k)
    b(i) = b(i) - M(i,k) * b(k)

    do 40, j = k + 1, n
      A(i,j) = a(i,j) - M(i,k) * A(k,j)
40  continue

60  continue
100 continue
c
c.....back substitution (solve stage)
c
  x(n) = b(n) / A(n,n)

do 200, i = n - 1, 1, -1
  x(i) = 0.d0

  do 210, j = i + 1, n
    x(i) = x(i) + A(i,j) * x(j)
210  continue

  x(i) = (b(i) - x(i)) / A(i,i)
200  continue

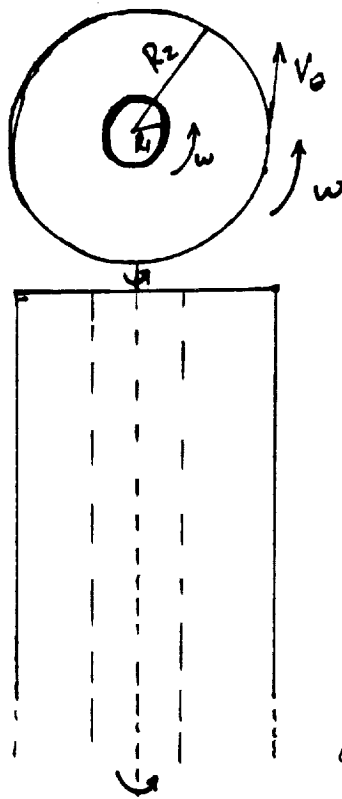
  return
end

```

## APPENDIX E

### Calculation of velocity of sloshing fluid around wire

Assume two concentric cylinders. The inner cylinder is fixed to the outer one, and both of them are rotating with the same angular velocity about their common axis of symmetry. Moreover, assume that the velocity of the fluid around the inner cylinder is only a function of the distance  $r$  from the center of this cylinder (wire). For simplicity no flow in the direction of the axis of symmetry is assumed (this is not a very good assumption), and the cylinders are very long in their axial direction. Also, as it will be shown, the main problem with this analysis is the Boundary Conditions.



From the Navier-Stone's Eq.:

$$\frac{V_\theta}{r} \frac{\partial V_\theta}{\partial \theta} = \mu \left[ \frac{\partial^2 V_\theta}{\partial r^2} + \frac{1}{r} \frac{\partial}{\partial r} V_\theta - \frac{V_\theta}{r^2} \right] \quad (A)$$

but  $V_\theta$  is a function only of  $r$ ,  $V_\theta(r)$ .

So:

$$\frac{\partial^2 V_\theta}{\partial r^2} + \frac{1}{r} \frac{\partial V_\theta}{\partial r} - \frac{V_\theta}{r^2} = 0$$

or:

$$r^2 V_\theta'' + r V_\theta' - V_\theta = 0 \quad (B)$$

Integration of (B) gives: (substituting)

$$V_\theta = r^x \quad \text{into (B)} \therefore$$

$$(x(x-1)r^{x-2})r^2 + r x r^{x-1} - r^x = 0 \quad (C)$$

or:

$$r^x(x^2-1) = 0 \quad \therefore x = \pm 1$$

So, substitution into  $V_\theta$  form gives:

$$V_\theta = C_1 r + C_2 \left(\frac{1}{r}\right) \quad (D)$$

Now, to evaluate (D), Two Boundary conditions are needed.

$$\text{B.C. 1: } V_{\theta}(r=R_1) = \omega R_1$$

$$\text{B.C. 2: } ?$$

If B.C.2 is taken as  $V_{\theta}(r=R_2) = \omega R_2$ , from the concept of "non-slip condition" the following is obtained,

$$V_{\theta 1} = \omega R_1 = C_1 R_1 + \frac{C_2}{R_2} \Rightarrow C_1 = \omega - \frac{C_2}{R_1^2} \quad (E_1)$$

$$V_{\theta 2} = \omega R_2 = C_1 R_2 + \frac{C_2}{R_2} \Rightarrow C_1 = \omega - \frac{C_2}{R_2^2} \quad (E_2)$$

Subtracting (E<sub>2</sub>) from (E<sub>1</sub>), we get:

$$R_1^2 = R_2^2 \quad (E_3)$$

How ever (E<sub>3</sub>) is impossible since  $R_1$  and  $R_2$  were defined to be different.

hence,  $V_{\theta 2} = \omega R_2$  is NOT a Boundary condition.

So, Assuming that the outer cylinder is now fixed,

$V_{\theta}(r=R_2) = 0$ , and eq. (D) becomes:

$$w = C_1 + \frac{C_2}{R_1^2} \quad \therefore$$

$$C_1 = w - \frac{C_2}{R_1^2} \quad (D-1)$$

and,

$$C_2 = -C_1 R_2^2 \quad \therefore$$

$$C_1 = -\frac{C_2}{R_2^2} \quad (D-2)$$

Combination of eq. (D-1) & (D-2) give:

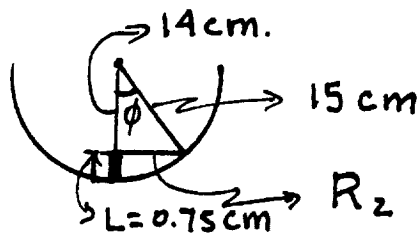
$$C_2 = \frac{-w R_1^2 R_2^2}{R_1^2 - R_2^2} \quad \text{and,} \quad (E)$$

$$C_1 = -\frac{w R_1}{R_1^2 - R_2^2}$$

Substitution of eqs. (E) into eq. (D) give:

$$V_{\theta} = \frac{w}{r} \left[ R_1^2 \right] \frac{r^2 - R_2^2}{R_1^2 - R_2^2} \quad (F)$$

Evaluating (F) at a time when the wire is fully submerge in water give.



So, if:

$$R_2 = 4.6837 \text{ cm.}$$

$$r = 1.00 \text{ cm}$$

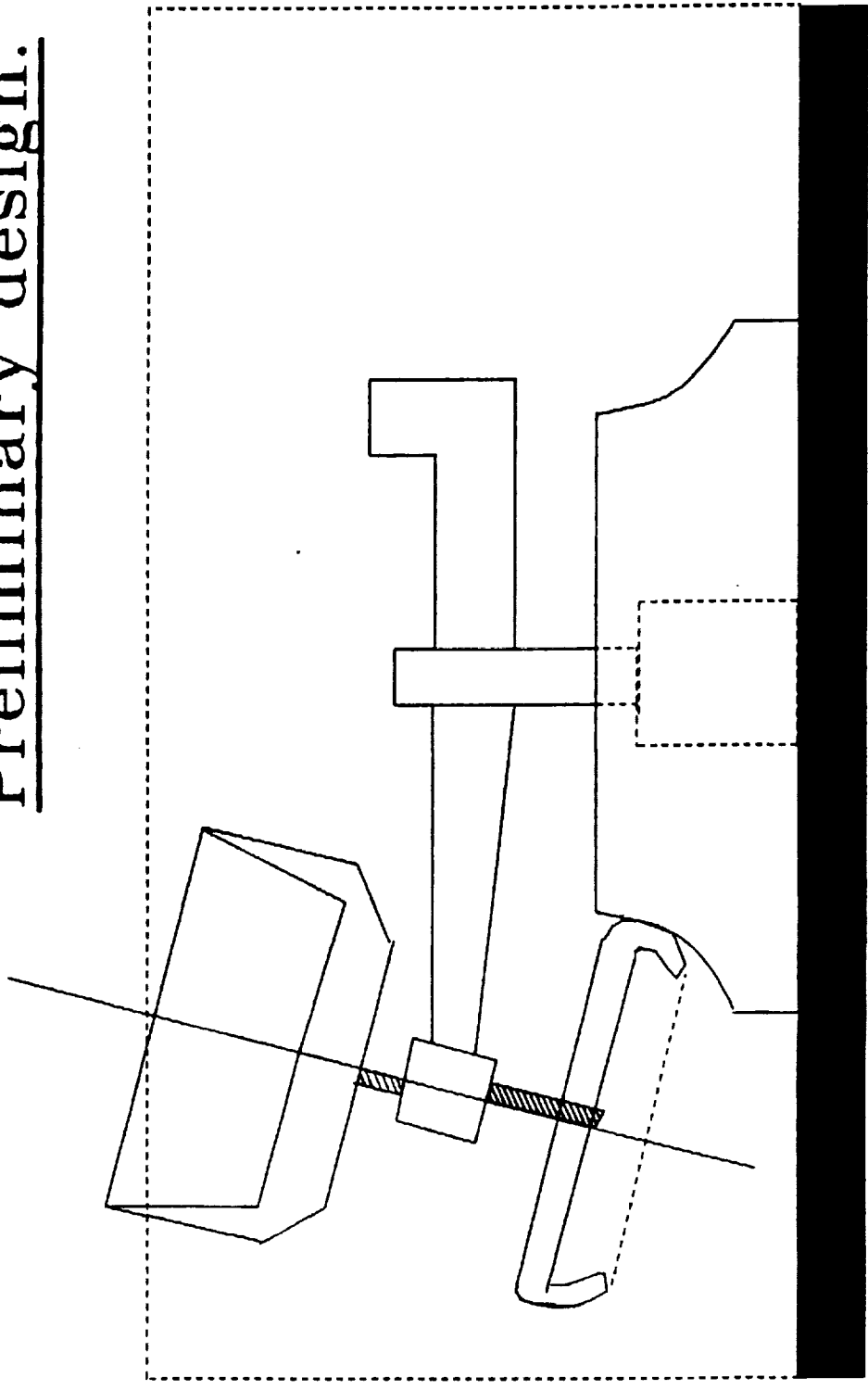
$$\omega = 40 \text{ rpm}$$

$$V_{\theta} = \frac{40 \text{ RPM}}{0.01 \text{ m}} \frac{2\pi}{60 \text{ sec}} \left( \frac{1.27 \times 10^{-4} \text{ m}}{2} \right)^2 \times \left[ \frac{0.01^2 - (4.6837 \times 10^{-2} \text{ m})^2}{\left( \frac{1.27 \times 10^{-4}}{2} \right)^2 - (4.6837 \times 10^{-2} \text{ m})^2} \right]$$

$$V_{\theta} = 1.612 \times 10^{-6} \text{ m/sec.}$$

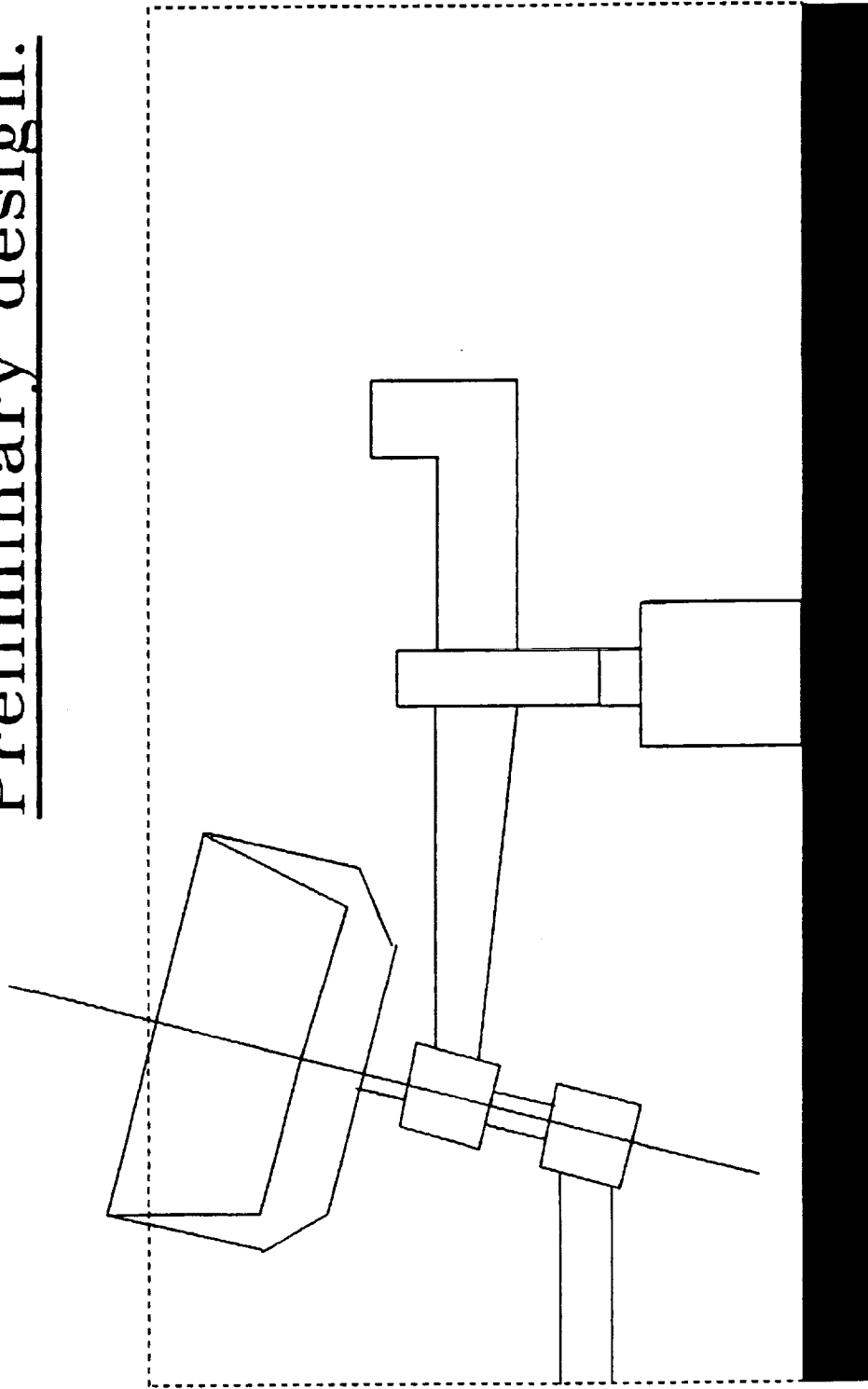
(Too slow to cause any significant forced convection heat transfer to the wire.)

Rig for the study of fluid sloshing.  
Preliminary design.



Miguel Falcon-Martin  
MANE 199, Dr. Meyer  
Winter 90

Rig for the study of fluid sloshing.  
Preliminary design.



## REFERENCES

1. Meyer, R.X., "Stability Tests of Spin-Stabilized Spacecraft in the Presence of Thrust," Journal of Guidance and Controls, August 1990.
2. Personal communication between N. Furumoto and J.P. Vanyo.
3. Vanyo, J.P. and P.W. Likins, "Measurement of Energy Dissipation in a Liquid-Filled, Precessing, Spherical Cavity," Transactions of the ASME, September 1971.
4. Garg, S.C., N. Furumoto, and J.P. Vanyo, "Spacecraft Nutational Instability Prediction by Energy-Dissipation Measurements," Journal of Guidance, Control, and Dynamics, May-June 1986.
5. Mingori, D.L. and Y. Yam, "Nutational Stability of a Spinning Spacecraft with Internal Mass Motion and Axial Thrust," AIAA Paper 86-2271, 1986.
6. Handout by James Marcolesco.

## BIBLIOGRAPHY

- Agriwal, Brij N., Design of Geosynchronous Spacecraft, Prentice-Hall, Inc., New Jersey, 1986.
- Brown, R.C., P. Andreussi, and S. Zanelli, "The Use of Wire Probe for the Measurement of Liquid Film Thickness in Annular Gas-Liquid Flows," *The Canadian Journal of Chemical Engineering*, Dec. 1978.
- Garg, S.C., N. Furumoto, and J.P. Vanyo, "Measurement of Energy Dissipation in Forced Precession Compared to Flight Data," AIAA Guidance and Control Conference, August 1984.
- Garg, S.C., N. Furumoto, and J.P. Vanyo, "Spacecraft Nutational Instability Prediction by Energy-Dissipation Measurements," *Journal of Guidance, Control and Dynamics*, May-June 1986.
- Harrison, J.A., S.C. Garg, N. Furumoto, "A Free-Fall Technique to Measure Nutation Divergence, and Applications," AAS/AIAA Astrodynamics Specialist Conference, August 1983.
- Incropera, F.D., and D.P. DeWitt, Fundamentals of Heat and Mass Transfer, John Wiley and Sons, 1985.
- Kaplan, Marshall H., Modern Spacecraft Dynamics and Control, John Wiley and Sons, 1976.
- Lomas, C.G., Fundamentals of Hot Wire Anemometry, Cambridge University Press, 1986.
- Martin, Ernesto R., "Fuel Slosh and Dynamic Stability of Intelsat IV," AIAA Guidance, Control and Flight Mechanics Conference, August 1971.
- Meyer, Rudolf X., "Stability Tests of Spin-Stabilized Spacecraft in the Presence of Thrust," *AIAA Journal of Guidance and Control*, August 1990.
- Nunn, R.H., Intermediate Fluid Mechanics, Hemisphere Publishing Corporation, 1989.
- Perry, A.E., Hot-Wire Anemometry, Clarendon Press, Oxford, 1982.
- Vanyo, J.P. and P.W. Likins, "Measurement of Energy Dissipation in a Liquid-Filled, Precessing, Spherical Cavity," *Transactions of the ASME*, September 1971.

Vanyo, J.P., "An Energy Assessment for Liquids in a Filled  
Precessing Spherical Cavity," Journal of Applied  
Mechanics, December 1973.